COMPUTER SIMULATION OF COMBINED MICROWAVE AND WATER

HEATING PROCESSES FOR PACKAGED FOODS USING FINITE

DIFFERENCE TIME DOMAIN METHOD

By

HAO CHEN

A dissertation submitted in partial fulfillment of
the requirements for the degree of

DOCTOR OF PHILOSOPHY

WASHINGTON STATE UNIVERSITY
Department of Biological Systems Engineering

May 2008

To the Faculty of Washington State University:

The members of the Committee appointed to examine the dissertation of HAO CHEN find it satisfactory and recommend that it be accepted.

_____

Chair

_____

_____

_____

ACKNOWLEDGMENT

COMPUTER SIMULATION OF COMBINED MICROWAVE AND WATER

HEATING PROCESSES FOR PACKAGED FOODS USING FINITE

DIFFERENCE TIME DOMAIN METHOD

Abstract

By Hao Chen, Ph.D.
Washington State University
May 2008

Chair: Dr. Juming Tang

A microwave sterilization system was developed at Washington State University (WSU) that allows development of High-Temperature-Short-Time (HTST) processes for packaged foods. This system combines microwave and hot water heating. A major challenge of this novel technique is possible non-uniform heating created from the non-even electromagnetic distribution. The objective of this research is to develop an efficient and reliable numeric model to simulate the microwave sterilization process and provide the prediction of temperature profiles and distributions. Various conditions such as different dielectric properties, different physical configurations and different operation parameters were investigated to study their influences on heating uniformity in packaged foods. The simulation results were applied to predict system performance and obtain parameters for process optimization.

Before the numeric model can be applied to analyze and optimize the system, it has to be validated. In this study, the simulation model was validated by comparing the

numeric results with experimental measurements under both stationary and moving conditions. The heating patterns were measured by using a computer vision method developed by the microwave sterilization group at WSU. This method uses a chemical marker M-2 as an indicator of heat intensity inside the food packages, the marker intensity is converted to colour image for visualization purpose.

The numeric model was then used to investigate the heating patterns under various conditions to improve the heating uniformity and reduce heating time. A sophisticate algorithm was developed to provide the set of operational parameters or physical configurations so that optimal performance can be achieved. Finally, future researches were suggested.

TABLE OF CONTENTS

LIST OF TABLES

LIST OF FIGURES

Chapter 1 Fundamentals of Microwave Heating

Introduction

Microwaves generate heat by directing electromagnetic waves into a dielectric material. The electromagnetic wave with frequency between 0.3GHz and 300 GHz is denoted as microwave (Metaxas and Meredith, 1993). A dielectric material is one with dominant negative and positive charges in atoms and molecules which are not allowed to travel. However, when an electrical field is present, the centroids of negative and positive charges slightly shift in position to each other, creating electrical dipoles. This formation of dielectric dipole is referred to as orientation polarization, which differs from induced polarization inside electric conductors. Whenever an electrical field is applied, the dielectric materials having permanent dipoles such as water will reorient due to orientation polarization (Curtis, 1999). This reorientation provides the dielectric materials the ability to store electric energy, and causes volumetric heat generation for microwave applications (Balanis, 1989). It should be noticed that the electric conductors can also be heated because of the induced polarization. However, in this research, we focused on the microwave heating investigation for dielectric materials.

Compared to conventional heating methods, microwave heating has several advantages. It can be used in High Temperature Short Time (HTST) processes since microwave heating can provide high power into dielectric materials with great penetration and hence reduce the heating time. In addition, heating uniformity is improved further when combining microwave heating method with traditional heating such as hot water surface heating. In the meantime, it is relatively straightforward to

operate and control microwave heating. This chapter presents fundamentals of electromagnetics, rectangular waveguide and cavity, electromagnetic power generation, temperature response as well as microwave heating applications especially in the area of food sterilization.

Maxwell's equations

The theoretical concepts of electromagnetics are described by a set of basic equations formulated through various experiments conducted by numerous researchers and then combined into a final form of vector equations by Maxwell around 1873 (Guan, 2003). These equations have either differential or integral form. The differential form is used to govern the relations and variations of the electric and magnetic fields at any point any time. For these equations to be valid, it is assumed that the field vectors be continuously derivative and they are single-valued, bounded and continuous function of time and space (Balanis, 1989). To completely define an electromagnetic field, boundary conditions need to be incorporated to take into account the discontinuous charges and currents along the interface between different medians into consideration. The differential form of Maxwell's equations is given in the following equations (Balanis, 1989):

$$\nabla \times E = -\mu_r \mu_0 \frac{\partial H}{\partial t} \tag{1}$$

$$\nabla \times H = \sigma E + \varepsilon_r \varepsilon_0 \frac{\partial E}{\partial t} \tag{2}$$

$$\nabla \bullet D = q \tag{3}$$

$$\nabla \bullet B = 0 \tag{4}$$

where E is electric field vector (Volt/m), H is magnetic field vector (Ampere/m). D is electric flux density (coulombs/m^2), related to E by D=$\varepsilon_r\varepsilon_0$E. B is magnetic flux density (webers/m^2), related to H by B=$\mu_r\mu_0$H. ε_0 and ε_r denote the dielectric permittivity in free space and the value relative to free space, respectively. μ_0 and μ_r denote the dielectric permeability in free space and relative value, respectively. q is electric charge density per unit volume (coulombs/m^3). Equation (1) is called Faraday's law, indicating that the circulation of electric field strength surrounded by a closed contour is determined by the rate of change of the magnetic flux density. Equation (2) is referred to as Ampere's law, indicating the circulation of magnetic field strength enclosed by a closed contour is equal to the net current through the surface. Equation (3) presents Gauss's electric law, which requires net electric flux equal to the charges contained within the region. Equation (4) presents Gauss's magnetic law, which requires net magnetic flux out of a region to be zero.

Boundary conditions

As mentioned above, field discontinuities along the interface between different medians need to be examined physically from field vectors instead of their derivatives in the differential form of Maxwell's equations. The behaviour of field vectors is determined by the boundary conditions. The boundary conditions can be derived from Gauss's electric and magnetic law along the median interface:

$$\hat{n} \times (E_2 - E_1) = 0 \tag{5}$$

$$\hat{n} \times (H_2 - H_1) = 0 \tag{6}$$

$$\hat{n} \bullet (D_2 - D_1) = 0 \tag{7}$$

$$\hat{n} \bullet (B_2 - B_1) = 0 \tag{8}$$

where $\hat{n}$ is normal unit component of the interface, the subscripts 1 and 2 denote the regions with different medium for each field vector. They depict how the field vectors relate to each other across the boundary. Equations (5) and (6) state that the tangential components on an interface between two medians are continuous for electrical field and magnetic field, respectively. Equations (7) and (8) show the continuity of normal component across the boundary for electric flux density and magnetic flux density, respectively. It should be pointed out that equation (7) holds only if there is no impress magnetic current density along the boundary, which is always true for microwave heating applications. These boundary conditions are not independent. In fact, we can combine the equations (5) and (7) to solve the electrical fields across the boundary or combine the equations (6) and (8) to solve the magnetic fields.

Dissipated power inside dielectric material

For microwave heating applications, electromagnetic power is dissipated inside the dielectric material to heat the product. Therefore, it is necessary to calculate the energy associated with electromagnetic waves. The dissipated power can be derived from time average Pointing vector over one period (Balanis, 1989):

$$\psi_{av} = \frac{1}{2} \text{Re}\left[E \times H^* \right] \tag{9}$$

By taking the volume integral and applying divergence theorem, the dissipated real power is achieved in the following:

$$P_d = \frac{1}{2} \iiint_V \sigma |E|^2 \, dv \tag{10}$$

4

where P_d is electromagnetic power dissipated inside a volume V. σ denotes electrical conductivity of media inside a volume V, which depends on microwave frequency and dielectric loss. Once the power dissipation is calculated, it is then used as a source to heat the food product.

Temperature response

It is critical for microwave heating applications to obtain the temperature response due to dissipated microwave power. That is, the spatial variant of temperature is desired inside the medium. The temperature profile can be determined by applying the energy conservation requirement on a differential control volume (Incropera and DeWitt, 2001). The law of energy conservation states that for a unit volume in the medium, the rate of energy transfer by conduction plus the volumetric rate of thermal energy generation must be equal to the rate of change of thermal energy stored within the volume, which is mathematically represented in the following equation:

$$\rho c_p \frac{\partial T}{\partial t} = \nabla(K(T) \bullet \nabla T) + \dot{q} \tag{11}$$

where ρ is mass density (Kg/m^3), c_p is specific heat (KJ/Kg·K), $\dot{q}$ is the thermal energy per unit volume, K(T) is thermal conductivity (W/m^2K). For microwave heating, $\dot{q}$ is provided by electromagnetic power.

Temperature distribution can be determined by solving equation (11) with appropriate boundary and initial conditions. Three types of boundary conditions are encountered in heat transfer equation (11): Dirichlet condition, Neumann condition and Convective surface condition. Dirichlet corresponds to a situation that the surface is maintained at a fixed temperature T_s; Neumann condition requires that the heat flux on

the boundary be fixed; and Convective surface condition is obtained by exchanging thermal energy between different mediums (Incropera and DeWitt, 2001).

Temperature measurement and distribution

Temperature is one of the most important indicators for the microwave heating applications. As a standard scientific index, temperature is quantitatively recorded by different kinds of thermometers or sensors (Guan, 2003). In practice, temperature is measured by numerous electronic sensors such as resistance temperature detectors (RTDs), Integrated Circuits (IC) sensors, thermistors, and thermocouples. The first three types use either metal or semi-conducting materials relying correlationships between electric resistance of the material with temperature. A thermocouple has two electrical conductors made from different materials at one end, while connecting the conductors to the measurement unit at the other end. Of all these methods, thermocouples are widely used in the temperature sensing field to monitor processing temperatures (Desmarais and Breuereis, 2001). However, when exposed in a high electromagnetic field environment, the metal parts of the electronic sensors may result in electromagnetic interference (EMI). Because of this reason, fiber optic sensors have been developed to measure temperature during microwave heating. The fiber optic sensor uses photons as its signal propagation element, which effectively eliminates the effect of EMI. The fiber optic sensors have several advantages: (1) high chemical resistance; (2) measuring accuracy (1°C) independent of the presence of severe EMI; (3) small response time (1.5-1.8 sec); (4) the probes can be placed either in a solid or a liquid material; (5) flexible length (up to 5km). During microwave processing, fiber optic sensors can be directly placed at selected points inside the material to record temperature changes.

In addition to temperature changes of particular points, overall temperature distribution is also critical to measure the heating performance. Several indirect methods have been developed, including using infrared camera to take pictures at selected layer of food package after heating process. Another popular method to determine heating pattern uses chemical marker M-2 (Pandit, et al., 2007a; Pandit, et al., 2007b). This method measures color changes as a result of formation of chemical compound (M-2) due to the Millard reaction between amino acids of proteins and a reducing sugar, ribose. The color response depended upon heat intensity at temperatures beyond 100°C and, therefore, served as an indicator of temperature distribution during microwave heating for food sterilization that calls for product temperature to be above 100˚C. Detailed information about the kinetics of M-2 formation with temperature could be found elsewhere (Lau, et al., 2003; Pandit, et al., 2006). After microwave processing, the heating pattern inside whey protein gels are checked with computer vision software IMAQ (National instrument, TX, USA) using a chemical marker M-2 and computer vision method.

Challenges for microwave heating

Microwave energy can be used to sterilize the food product in a short time period because it offers the potential to overcome the limitation of conventional heating method (Burfoot, et al., 1988; DeCareau, 1985; Harlfinger, 1992; Meredith, 1998). When properly designed, the electromagnetic power provides sharply reduced heating time to obtain the required temperature for thermal process. Because of the short process time, the heating quality can be improved compared to the traditional methods (Giese, 1992; Guan, et al., 2003; O'Meara, et al., 1977; Ohlsson, 1987, 1991; Stenstrom, 1974).

In despite of the advantages that microwave provides, industrial applications of microwave heating are not as popular as its home applications because of a lack of the method to determine the food dielectric properties and temperature during process for safety issues as well as costly equipment and electricity (Mudgett and Schwartzberg, 1982). Fortunately, recently commercial systems such as impedance analyzer and network analyzer (Hewlett-Packard Company, CA, USA) became available to measure the dielectric properties with an open coaxial cable; and temperature can be measured using fiber optical sensors with accuracy of $\pm 1^{\circ}$C. In addition, the cost for microwave equipment has been continuously reduced over the years.

There are several other major challenges which hinder the industrial microwave heating applications, including design of a high efficient system, prediction of heating distribution after a thermal process, as well as online monitor of temperature change for sterilization purpose. Firstly, it is difficult to design the electromagnetic waveguide and cavity which are well matched with the microwave source and provides low power reflection. Because of the discontinuity of the electromagnetic field components on the boundary between food packages and surrounding medium, the reflection and refraction phenomena of electromagnetic wave produce non-uniform distribution of the microwave energy within the food packages (Ayoub, et al., 1974; DeCareau, 1985; Ruello, 1987; Schiffmann, 1990; Stanford, 1990). Sever corner and edge heating are resulted from the non-uniform distribution (Ohlsson, 1991). Many techniques have been developed to improve heating uniformity. Instead of air, water is used as surrounding medium of food packages to minimize the non-uniform heating effects (Guan, 2003; Guan, et al., 2002; Lau, 2000; Ohlsson, 1992; Stenstrom, 1972). For microwave heating purposes, two

frequencies are allocated by the US Federal Communications Commission (FCC): namely 915 MHz and 2450MHz. 2450MHz is widely used in domestic ovens. However, the high operating frequency produces multi-mode electromagnetic field inside the cavity, which makes heating patterns untraceable for each different process. Recent studies (Chen, et al., 2007a; Guan, 2003) have indicated that a 915 MHz microwave heating system can provide relative uniform heating and more stable heating pattern within food products both in pouches and trays.

Secondly, it is a tough task to predict the heating pattern as well as the hot and cold spots inside the package after microwave heating processes. Kim and Taub (1993) conducted a non-invasive assessment of heating uniformity within food packages for microwave sterilization process by developing an intrinsic chemical marker technology (Kim, et al., 1996; Prakash, et al., 1997). However, it is still unclear how the marker yield is directly related with temperature value inside the food package. There are other popular methods used to determine the temperature distribution including preliminary inoculated pack studies as well as computer simulations. Inoculated pack studies is very time consuming and costly since it uses the amount of survivor bacteria to predict the heating pattern. Computer simulation is an effective and economic way with the development of computer technology and consistently reduced hardware cost (Chen, et al., 2007a). Nevertheless, due to the complex nature of microwave interference with food products and lack of reliable computer model designed for microwave heating applications, the computer simulation method has not been widely used until recent studies (Chen, et al., 2007a; Ma, et al., 1995).

Thirdly, online control of temperature response becomes challenging for the high power short time processes. The applied voltage stress may result in voltage break down even though the high dissipated power can be achieved (Meredith, 1998). Therefore, a stable microwave heating system is required for sterilization purpose, which is only available recently.

Other challenges for microwave sterilization applications include design of packages as well as the optimization of process conditions for homogeneous or inhomogeneous food packages. Despite of these challenges of microwave heating technology, it still provides a very promising way for industrialized sterilization purpose.

References

Ayoub, J., Berkowitz, D., Kenyon, E., & Wadsworth, C. (1974). Continuous microwave sterilization of meat in flexible pouches. *Journal of food science* 39, 303-313.

Balanis, C. A. (1989). *Advanced engineering electromagnetics*, John Wiley & Sons,

Burfoot, D., Griffin, W., & James, S. (1988). Microwave pasteurization of prepared meals. *Journal of Food Engineering*, 8, 145-156.

Chen, H., Tang, J., & Liu, F. (2007). Coupled simulation of an electromagnetic heating process using the Finite Difference Time Domain method *Journal. of Microwave Power and Electromagnetic Energy*, 41(3), 50-68.

Curtis, J. M. (1999). Experimental verification for microwave processing of materials in a single mode rectangular resonant cavity. Virginia Polytechnic Institute and State University, USA.

DeCareau, R. (1985). *Microwaves in the food processing industry,* Academic Press, Inc. NY. USA.,

Desmarais, R., & Breuereis, J. (2001). How to select and use the right temperature sensor. *Sensor*, 18(1).

Giese, J. (1992). Advances in microwave food processing. *Food Technol.*, 46, 118-123.

Guan, D. (2003). Thermal processing of hermetically packaged low-acid foods using microwave-circulated water combination (MCWC) heating technology. Thesis (Ph. D.): Washington State University, Pullman, WA, USA

Guan, D., Plotka, V., Clark, S., & Tang, J. (2002). Sensory evaluation of microwave treated macaroni and cheese. *Journal of Food Process. Preserv.*, 26, 307-322.

Harlfinger, L. (1992). Microwave sterilization. *Food Technol.*, 46(12), 57-60.

Incropera, F. P., & DeWitt, D. P. (2001). *Introduction to heat transfer, 4th*, John Wiley & Sons, New York.

Kim, H. J., & Taub, I. A. (1993). Intrinsic chemical markers for Aseptic processing of particulate foods. *Food Technol*, 47(1), 91-97.

Kim, H. J., Taub, I. A., Choi, Y. M., & Prakash, A. (1996). Principles and applications of chemical markers of sterility in high-temperature-short-time processing of particular foods, American Chemical Society, Washington, D.C. 54-69.

Lau, M. H. (2000). Microwave heating uniformity in model food systems. From Microwave pasteurization and sterilization of food products. *Ph.D. Dissertation*, Washington State University. Pullman, WA, USA.

Lau, M. H., Tang, J., Taub, I. A., Yang, T. C. S., Edwards, C. G., & Mao, R. (2003). Kinetics of chemical marker formation in whey protein gels for studying microwave sterilization. *Journal of Food Engineering*, 60(4), 397-405.

Ma, L. H., Paul, D. L., Pothecary, N., Railton, C., Bows, J., Barratt, L., Mullin, J., & Simons, D. (1995). Experimental Validation of a Combined Electromagnetic and Thermal Fdtd Model of a Microwave-Heating Process. *IEEE Transactions on Microwave Theory and Techniques*, 43(11), 2565-2572.

Meredith, R. (1998). *Engineer's handbook of industrial microwave heating*, The Institution of Electrical Engineers, London, UK.

Metaxas, A. C., & R.J., M. (1993). *Industrial Microwave Heating*, London, UK.

Mudgett, R., & Schwartzberg, H. G. (1982). Microwave food processing: Pasteurization and sterilization: A review. *AIChe Symposium Series*, 78(218), 1-11.

O'Meara, J., Farkas, D., & Wadsworth, C. (1977). Flexible pouch sterilization using combined microwave-hot water hold simulator. *Contact No. (PN) DRXNM 77-120*, U.S. Army Natick Research & Development Laboratories, Natick, MA 01760.

Ohlsson, T. (1987). Sterilization of foods by microwaves. *International Seminar on New Trends in Aseptic Processing and Packaging of Food stuffs*, 22 Oct. 1987;Munich. SLK Report nr 564. Goteborg, Sweden: The Swedish Institute for Food and Biotechnology.

Ohlsson, T. (1991). Microwave heating uniformity. *AICHE Conference on Food Engineering*, Chicago. March 11-12.

Ohlsson, T. (1992). Development and evaluation of microwave sterilization process for plastic pouches. *Paper presented at the AICHE Conference on Food Engineering*, March 11-12, Chicago.

Pandit, R. B., Tang, J., Liu, F., & Mikhaylenko, M. (2007a). A computer vision method to locate cold spots in foods in microwave sterilization processes. *Pattern Recognition*, 40, 3667-3676.

Pandit, R. B., Tang, J., Liu, F., & Pitts, M. (2007b). Development of a novel approach to determine heating pattern using computer vision and chemical marker (M-2) yield. *Journal of Food Engineering*, 78(2), 522-528.

Pandit, R. B., Tang, J., Mikhaylenko, G., & Liu, F. (2006). Kinetics of chemical marker M-2 formation in mashed potato - A tool to locate cold spots under microwave sterilization. *Journal of Food Engineering*, 76(3), 353-361.

Prakash, A., Kim, H. J., & Taub, I. A. (1997). Assessment of microwave sterilization of foods using intrinsic chemical markers. *Journal of Microwave Power and Electromagnetic Energy*, 32(1), 50-57.

Ruello, J. H. (1987). Seafood and microwaves: some preliminary observations. *Food Technol.in Australia.*, 39, 527-530.

Schiffmann, R. (1990). Problems in standardizing microwave over performance. *Microwave World*, 11(3), 20-24.

Stanford, M. (1990). Microwave oven characterization and implications for food safety in product development. *Microwave World*, 11(3), 7-9.

Stenstrom, L. (1972). Taming microwaves for solid food sterilization. *IMPI symposium*, Ottawa, Canada, May 24-26.

Chapter 2 Solutions to Maxwell's Equations

Theorems

To better understand the fundamentals of electromagnetic wave, including its generation, propagation as well as reception, the set of Maxwell's equations needs to be solved and the obtained field component is analyzed according to the nature of the problem under consideration. There are numerous theorems and principles which facilitate the solution of Maxwell's equations such as duality, uniqueness, image, reciprocity, reaction, volume equivalence, surface equivalence, induction, and physical equivalent (Balanis, 1989; Harrington, 1961).

Duality theorem: when an equation has been solved, another equation with identical mathematic form of previous solved equation has the same solution construction. Duality theorem is a good tool to predict the solutions of complex mathematic equations.

Uniqueness theorem: it is always desired that the solution found for an equation has a unique mathematic form and under what conditions the unique solution can be achieved. Theoretical studies have shown that once the boundary condition is specified over the boundary of a lossy region, the unique solution is obtained. For lossless material, uniqueness theorem breaks down in general, however, according to the particular nature of individual problem; it may be treated as a special case of lossy solution.

Image theory: the scattering parameters of electromagnetic wave are significantly affected by the presence of obstacle. Generally speaking, when an obstacle is present, the solution at any point in problem space can be obtained by computing two independent solutions s1 and s2. s1 is contributed directly from the source, while s2 is generated from

the source image due to the appearance of obstacle. The source image is symmetric to the source point with respect to the tangential line of the obstacle. Using this way, the solution at point p can be constructed by adding the solution s1 and s2 as if the obstacle does not exist.
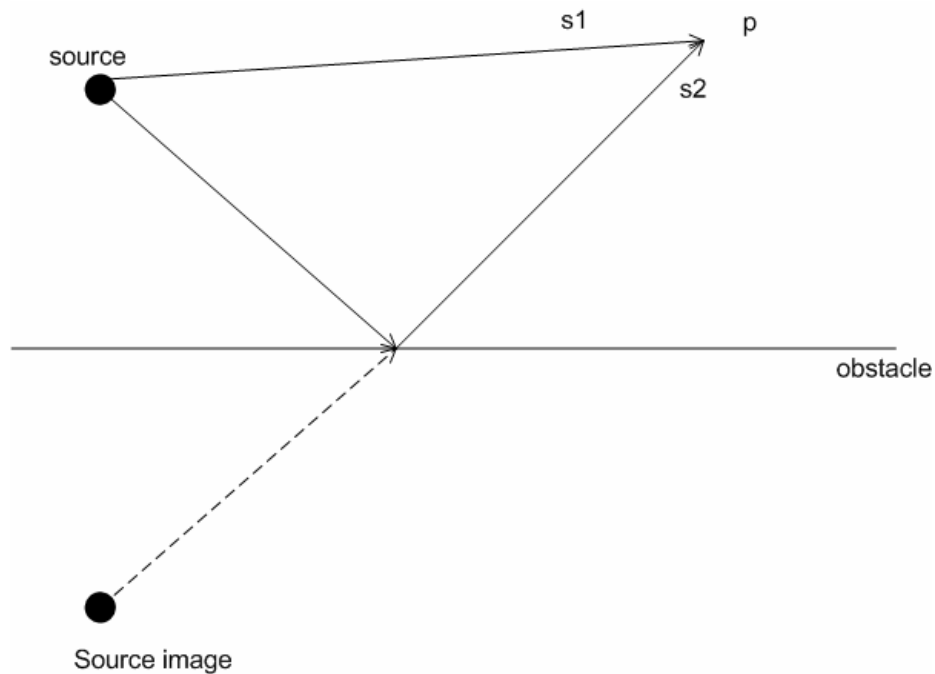
Fig 2.1 illustration of image theory

Reciprocity theorem: in classical electromagnetism, reciprocity theorem states that the electrical field is unchanged when interchanging the points where the current source is placed and where the field is measured (Carson, 1929; Hayt and Kimmerly, 1978). It is very useful when calculating the scattering matrix due to transmitted and reflected electromagnetic wave (Balanis, 1982).

Volume equivalence theorem: when a material is introduced to a free space where a complete solution has been reached, we can assume that the electromagnetic field inside the material is resulted from an equivalent electric and current density and the field

outside the obstacle stays untouched. This is called volume equivalence theorem, which is very helpful to find the scattered field by a dielectric material.

Surface equivalence theorem: the surface equivalence theorem is applied mostly when only the solution inside a specific region is required. By using a imaginary source S, we can replace the original source with an equivalent one which has current electric and magnetic density over the boundary, producing identical electrical and magnetic field inside the solution region (Huygens, 1690; Kraus and Carver, 1973; Schelkunoff, 1936). The surface equivalence theorem is illustrated by the following Fig 2.2.
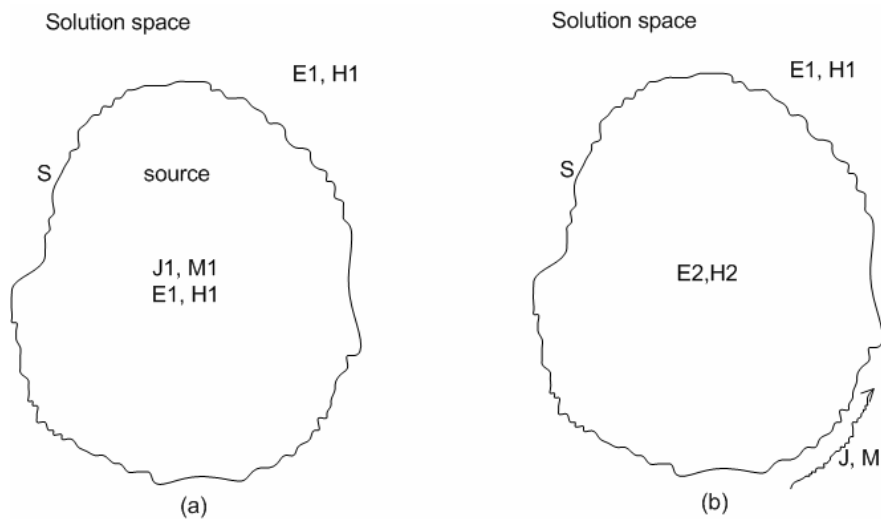
Fig 2.2 (a) original source; (b) equivalent model to produce identical fields inside the solution region

Induction theorem: the induction theorem uses a magnetic and electric equivalent current density to replace physical obstacles.   This theorem is similar to surface equivalent theorem, though it is applied more for scattering problem instead of radiation problem.

Physical equivalent: physical equivalent is another alternative method to calculate scattering problem for a perfect electric conductor (PEC), which yields identical solution

as induction theorem for some special cases. However in general, it provides different approximations from induction theorem (Harrington, 1959, 1961).

Wave equations and analytical solutions

Equations (1)-(4) in Chapter 1 give the differential form of Maxwell's equations, which are first order partial differential equations. However, they are coupled partial differential equations, with at least two unknown variables in each equation. To uncouple these equations, only one unknown variable can appear inside the equation, while the other needs to be eliminated, leading to second order partial differential equations. We also assume the time-harmonic electric and magnetic fields in a source-free region, equations (1) and (2) in Chapter 1 can then be written respectively (Balanis, 1989):

$$\nabla^2 E = j\omega\mu\sigma E - \omega^2\mu\varepsilon E = \gamma^2 E \tag{1}$$

$$\nabla^2 H = j\omega\mu\sigma H - \omega^2\mu\varepsilon H = \gamma^2 H \tag{2}$$

$$\nabla \bullet E = 0 \tag{3}$$

$$\nabla \bullet B = 0 \tag{4}$$

where σ is electrical conductivity for a lossy material. In practice, we usually introduce a variable γ called propagation constant with $\gamma^2 = j\omega\mu\sigma - \omega^2\mu\varepsilon$. Equation (3) and (4) indicate the source-free region and are required to reduce Maxwell's equations to wave equations.

The electromagnetic fields can be obtained by solving wave equations (1) and (2) with appropriate boundary conditions. For many practical problems, the wave equations can be reduced to a set of scalar equations each having solutions to be combined to construct the general solutions. One of the most popular methods to solve the Helmholtz

equations is known as separation of variables (Hilderbrand, 1962; Wylie, 1960). In this method, the solution of a scalar function, e.g. $E_x(x, y, z)$ in rectangular coordinator system, is assumed to be a multiplication of three different scalar functions each having only one independent variable. Therefore, the field component $E_x(x, y, z)$ can be written in the following form:

$$E_x(x, y, z) = f(x)g(y)h(z) \qquad (5)$$

where f(x), g(y) and h(z) are function to be determined from wave equations. They represent the behaviour of electromagnetic waves in each of the three directions. Here we will briefly discuss the solutions in classical 3-D orthogonal coordinator system (rectangular, cylindrical, spherical system), depending on the nature of the propagation wave while the detailed procedure has been presented in numerous literatures (Balanis, 1989; Harrington, 1961; Sadiku, 2001).

Rectangular coordinator system

In rectangular coordinator system, a general solution for electrical field E can be written as:

$$E(x, y, z) = \hat{a}_x E_x(x, y, z) + \hat{a}_y E_y(x, y, z) + \hat{a}_z E_z(x, y, z) \qquad (6)$$

where $\hat{a}_x$, $\hat{a}_y$ and $\hat{a}_z$ are unit vector in x, y, and z direction, respectively. Substituting equation (6) into wave equation (1), we reduce the general equation into three scalar equations and solve them by using separation of variables equation (5). Depending on the natures of the problem, different structures of function are used to represent distinct wave propagations. For example, standing waves are represented using sinusoidal functions while travelling waves are constructed by exponential functions. As an

example, an electromagnetic wave is assumed to propagate inside a rectangular geometry, which has rectangular cross section with infinite length on the wave propagation direction. This is illustrated in Fig 2.3.
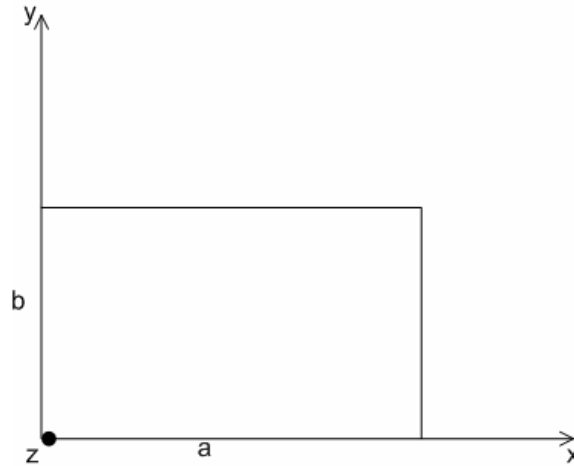
Fig 2.3 rectangular geometry for wave propagation

By following the procedures of separation of variable method, one can derive electrical field component E_x as:

$$E_x(x,y,z) = \left[A_1 \cos(\beta_x x) + A_2 \sin(\beta_x x)\right]\left[B_1 \cos(\beta_y y) + B_2 \sin(\beta_y y)\right]$$
$$\left[C_1 e^{-j\beta_z z} + C_2 e^{+j\beta_z z}\right]$$

(7)

where A_1, A_2, B_1, B_2, C_1, and C_2 are constants and determined by applying proper boundary conditions. Since the waveguide is bounded in x and y directions, the wave propagations in these directions are obtained using sinusoidal functions. In z direction, the electromagnetic wave propagates into infinite, producing travelling wave in both +z and −z directions. These are shown in equation (7). For other components, due to the symmetric merits of Maxwell's equations, the general solutions can be constructed similarly by applying duality or reciprocity theorem mentioned above.

Cylindrical coordinator system

19

In a cylindrical coordinator system, solutions for Maxwell's equations can be constructed as in a rectangular coordinator system except cylindrical coordinators are advisable. The general solution under a cylindrical coordinator system can be written as:

$$E(x, y, z) = \hat{a}_\rho E_\rho(x, y, z) + \hat{a}_\phi E_\phi(x, y, z) + \hat{a}_z E_z(x, y, z) \tag{8}$$

where $\hat{a}_\rho$, $\hat{a}_\phi$ and $\hat{a}_z$ are unit vector in cylindrical coordinators.
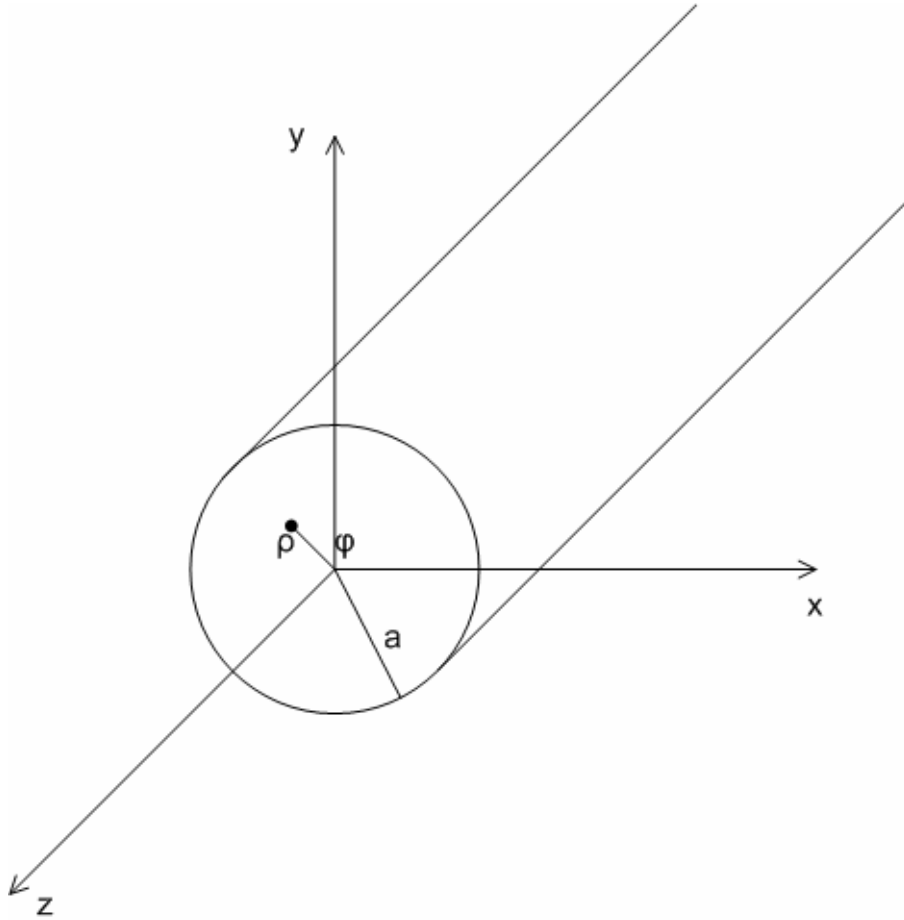
Fig 2.4 cylindrical coordinator system

Fig 2.4 shows a cylindrical coordinator system which has circular cross section in x-y plane and infinite length in z direction. Its general solution can be constructed by using separation of variable method, depending on the nature of the problem.

$$\psi(\rho,\phi,z) = \left[A_1 J_m(\beta_\rho\rho) + A_2 Y_m(\beta_\rho\rho)\right]\left[B_1\cos(m\phi) + B_2\sin(m\phi)\right]$$
$$\left[C_1 e^{-j\beta_z z} + C_2 e^{+j\beta_z z}\right] \tag{9}$$

where $\psi(\rho,\phi,z)$ is the solution for any field in cylindrical coordinator system.
$J_m(\beta_\rho\rho)$ is the first kind of Bessel function, while $Y_m(\beta_\rho\rho)$ is the second kind. A_1, A_2,
B_1, B_2, C_1, and C_2 are constants and determined by applying proper boundary conditions.
In the cylindrical coordinator system, $J_m(\beta_\rho\rho)$ and $Y_m(\beta_\rho\rho)$ represent a standing waves.
Therefore, equation (9) indicates a general field solution for an electromagnetic wave
which is bounded by a cylindrical waveguide and propagates into infinite in z direction.
For most radiation problem, it is required to calculate the field patterns outside cylinder.
For these cases, the first and second kind of Bessel functions is replaced by Hankel
function, which represents a travelling wave. Its solution is shown in the following
equation:

$$\psi(\rho,\phi,z) = [A_1 H_m^{(1)}(\beta_\rho\rho) + A_2 H_m^{(2)}(\beta_\rho\rho)][B_1\cos(m\phi) + B_2\sin(m\phi)][C_1 e^{-j\beta_z z} + C_2 e^{+j\beta_z z}] \tag{10}$$

Spherical coordinator system

The spherical coordinators are desirable when a spherical geometry is involved in
computing the electromagnetic field. The spherical coordinator system is shown in the
Fig 2.5:
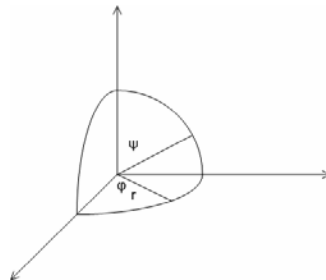
Fig 2.5 Spherical coordinator system

The general solutions are constructed by solving the following vector wave equations in the spherical coordinator system.

$$E(r,\varphi,\psi) = \hat{a}_r E_r(r,\varphi,\psi) + \hat{a}_\varphi E_\varphi(r,\varphi,\psi) + \hat{a}_\psi E_\psi(r,\varphi,\psi) \tag{11}$$

Similar to the solution of the rectangular and cylindrical coordinator system, the wave equation (11) is solved by using separation of variable technique.

$$\begin{aligned} E(r,\varphi,\psi) = &[A_1 j_n(\beta r) + A_2 y_n(\beta r)][B_1 P_n^m(\cos\psi) + B_2 Q_n^m(\cos\psi)] \\ &[C_1 \cos(m\varphi) + C_2 \sin(m\varphi)] \end{aligned} \tag{12}$$

where $j_n(\beta r)$ and $y_n(\beta r)$ which indicate the standing wave along the radius direction are spherical Bessel functions of the first and second kind, respectively. P_n^m and Q_n^m are referred to as the associated Legendre functions of the first and second kind, respectively. A_1, A_2, B_1, B_2, C_1, and C_2 are constants to be determined by appropriate boundary conditions. For the travelling wave outside the sphere along the radius direction, $j_n(\beta r)$ and $y_n(\beta r)$ are replaced respectively by $h_n^{(1)}(\beta r)$ and $h_n^{(2)}(\beta r)$ that denote as the Hankel functions of the first and second kind.

Dissipated electromagnetic power

The dissipated electromagnetic power inside dielectric materials plays an important role in the interaction of a dielectric with microwave energy. The dissipated power for microwave heating can be derived from the conversion of electromagnetic energy to heat. The power passing through a close surface can be determined from the integration of the Poynting vector (Metaxas and Meredith, 1993):

$$\zeta = E \times H^* \tag{13}$$

By taking the real part of Poynting vector and integrating it over a closed surface, the average power is computed as the following:

$$P_{av} = -\frac{1}{2}\int_S \operatorname{Re} al(\zeta) \cdot dS = \frac{1}{2}\omega\varepsilon_0\varepsilon_r'' \int_V (\mathrm{E} \cdot \mathrm{E}^*)dV \tag{14}$$

Equation (14) shows the dependency of microwave heating applications on dielectric loss at various industrially allocated frequencies such as 27.12MHz, 433.9MHz, 896/915MHz and 2450MHz. Assuming the dielectric loss and required average MW power are constant, the higher is the frequency, the smaller is the electrical field required.

Propagation factor and skin depth

Many problems in microwave heating involve the calculation of the dissipated MW power inside the dielectric materials, which can be derived from the wave equations (1) and (2). The solution attains the form:

$$\mathrm{E} = \mathrm{E}_0 e^{j\omega t} e^{-\gamma z} \tag{15}$$

where E_0 is the magnitude of electric field, $\gamma = \alpha + j\beta$ is denoted as propagation factor, which has real part representing the attenuation constant due to lossy characteristics and imaginary part representing the phase accumulation. The attenuation constant and phase accumulation are described in the following functions, respectively.

$$\alpha = \frac{2\pi f \sqrt{\mu_r \varepsilon_r'}}{\sqrt{2}c}\left[\sqrt{1+\left(\frac{\varepsilon_r''}{\varepsilon_r'}\right)^2} - 1\right]^{1/2} \tag{16}$$

$$\beta = \frac{2\pi f \sqrt{\mu_r \varepsilon_r'}}{\sqrt{2}c}\left[\sqrt{1+\left(\frac{\varepsilon_r''}{\varepsilon_r'}\right)^2} + 1\right]^{1/2} \tag{17}$$

23

where c=3.0*10^8 m/sec is the speed of light in free space, f is the frequency of electromagnetic waves (Hz), ε_r' and ε_r'' are dielectric constant and loss factor of the material. Due to the presence of attenuation constant, the strength of the electromagnetic wave decreases during the transmission inside the product. The degree of reduction is described by skin depth, which is defined as the distance where the magnitude of electromagnetic wave reduces to e^{-1} of its original value on the surface of the material (Buffler, 1993).

$$\delta = \frac{1}{\alpha} = \frac{\sqrt{2}c}{2\pi f \sqrt{\mu_r \varepsilon_r'} \left[\sqrt{1 + \left(\varepsilon_r'' / \varepsilon_r' \right)^2} \right]^{1/2}}$$ (18)

where δ is skin depth, which is a function of σ, ω and ε. Equation (18) can be simplified depending on the value of σ/ωε: if σ/ωε<<1, the media is referred as good dielectrics because the displacement current density is much greater than the conduction current density; if σ/ωε>>1, the media is referred as good conductor because the conduction current density is much greater than displacement current density. Therefore, the skin depth is reduced to:

$$\delta = \begin{cases} \dfrac{1}{\pi \varepsilon_0 \varepsilon_r''} \sqrt{\dfrac{\varepsilon_r'}{\mu}} & \text{good dielectric} \\[4mm] \dfrac{1}{2\pi f} \sqrt{\dfrac{2}{\mu \varepsilon_0 \varepsilon_r''}} & \text{good conductor} \end{cases}$$ (19)

Because of the nature of microwave heating problems, another concept for penetration depth that is given from the viewpoint of power absorption is defined as power penetration depth, which measures the depth from the incident surface to the location where the power intensity of an incident electromagnetic wave diminishes to 1/e (37%) of its original amplitude at the surface.

$$D_p = \frac{c}{2\pi f \sqrt{2\varepsilon_r'} \left[\sqrt{1 + \left(\dfrac{\varepsilon_r''}{\varepsilon_r'} \right)^2} - 1 \right]^{1/2}} \qquad (20)$$

where D_p is power penetration depth. Equation (20) shows that power penetration depth is one half of the skin depth for the same case.

From equations (18) and (20), the penetration depths are inversely proportional to the frequency of electromagnetic wave, which makes it possible to choose package size based on desired power absorption and working frequency. However, the penetration depth is not an exactly linear function of 1/f since the dielectric properties also vary with frequency. The influence of dielectric properties is very complicated. As an example, for those products with high dielectric loss such as salty foods, the penetration depth can be very small and temperature can be significantly increased with enhanced dielectric loss, leading to the phenomenon of *thermal runway heating*. In general, because the dielectric loss increases with temperature, the part of a product with higher temperature absorbs more heat than the rest part of the product, aggravating the non-uniformity of microwave heating. Numerous effective ways can be used to minimize the *runway* heating such as choosing distinct initial temperatures at different locations, for multiple materials in a food tray (Meredith, 1998).

Numeric solution to Maxwell's equations

We have discussed the analytical solutions to Maxwell's equations, including electromagnetic fundamentals, wave equations for classic geometries as well as the MW induced power dissipated inside the dielectric materials. However, for complex geometries, there exist no closed-form solutions so that numeric solutions are pursued

with acceptable accuracy and reasonable simulation time. The fundamental concept of numerically solving complex equations such as Maxwell's equations and thermal equations is to discretize the interested geometry into numerous cells with specified cell sizes. The numeric approach employs linear or polynomial approximations for each cell, thus reducing complex partial differential equations to sets of simple linear or polynomial equations. The numeric method allows the actual work to be conducted without investigating tedious mathematics and physics, leading to significant reduction of expensive and time-consuming experimental work. Starting from mid-1960s, considerable efforts has been explored to numerically solve practical EM-related problems by taking advantage of modern powerful computers (Sadiku, 2000). Researchers have developed numerous numeric methods such as Finite Difference Method (FDM), Method of Moment (MoM), Finite Element Method (FEM) as well as Transmission Line Method (TLM).

Finite difference method

The FDM was first developed by Thom (Thom and Apelt, 1961) to solve hydrodynamic problems. This technique permits applying finite difference approximations in algebraic form to replace the differential equations, which calculate the value of dependent variable at one point based on those values at its neighboring points. Basically, the FDM follows the following three steps to obtain the numeric solutions:

Discretize the geometry into numeric grid lines with specified cell size.

Replace the differential equations with finite difference equations by proper approximations in their algebraic form.

Solve the linear equations along with boundary and initial conditions.

Detailed procedures are slightly different depending upon the nature of the problems, their solution regions, as well as boundary conditions. For EM related problems, the finite difference technique was deployed to solve the time differentiated Maxwell's curl equations (Okoniewski, 1993; Taflove, 1980; Taflove and Brodwin, 1975b; Taflove and Umashankar, 1980, 1981, 1990; Umashankar and Taflove, 1982; Yee, 1966). Thus, this technique is usually called finite difference time domain method (FDTD). In brief, FDTD method is a time-marching procedure that simulates the continuous EM waves in a finite spatial region while time-stepping continues until desire simulation time is achieved or the interested stable field pattern is established (Taflove, 1998). Obviously, only finite computational grids can be stored in a computer data space though the modeled region extends to infinity in reality. As a result, absorbing boundary conditions (ABC) are employed to terminate the computational grids which permits all the out-going waves propagates into infinity with negligible reflections. Another factor to be considered in employing FDTD technique is to ensure the simulation accuracy by well-resolved spatial and temporal variations using time and space sampling process. The sampling in space is determined by following the Nyquist theorem that requires at least 10 cells per wavelength (Taflove, 1998). The sampling in time is dependent of the selection of spatial sampling size to ensure the overall stability of the algorithm.

Yee algorithm

The FDTD algorithm was originated by Kane Yee in 1966 to simulate wave propagation inside a lossless material by solving a set of finite-difference equations for the time-dependent Maxwell's curl equations (Yee, 1966). The Yee algorithm simultaneously calculates the coupled E and H fields instead of computing each one alone.

From the Yee algorithm, in a three-dimensional network, the E component in each direction is surrounded by four H components of its vertical counterpart, while each H component is surrounded by four E components in a similar fashion. The interlinked E and H field components intrinsically maintain the validity of Farady's Law and Ampere's Law. The algorithm naturally ensures the continuity of the tangential E and H fields across the interfaces of distinct media, making no special efforts required to satisfy the boundary conditions along the interfaces. The explicit second-order central-difference equations are employed in Yee algorithm, which intuitively guarantees the two Gauss's Law relations. The Yee algorithm calculates all of E field components based on the latest H fields and saved in the internal memory at a particular simulation time step, and then all of H field components are calculated from the newly obtained E fields. The whole process is looped until the required simulation time is reached. Due to the arrangement of E and H field as well as the explicit differential equation, the time-stepping process completely eliminates the matrix inversion that requires lengthy computation time and large computer memory. It also naturally simulates a wave propagation without spurious decay due to artificial non-physical wave resulted from the algorithm. For the sake of illustration, 1D and 2D FDTD algorithms are presented in this chapter while the fully detailed three-dimensional generalization is described in the next chapter.
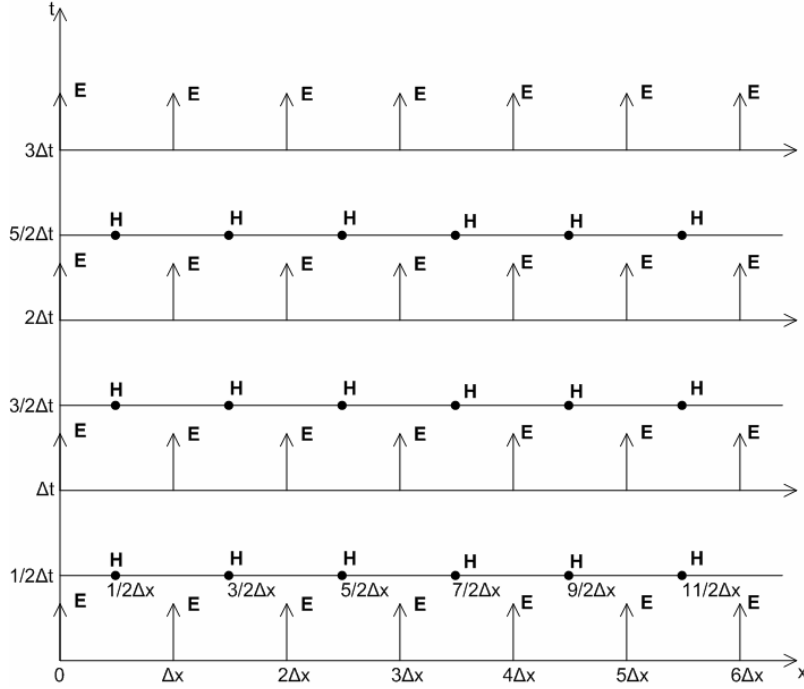
Fig 2.6 E and H field arrangement of FDTD algorithm for one-dimensional wave

propagation using central difference time stepping procedures

Fig 2.6 shows how the FDTD simulation approaches in time (t) and space (x). The electromagnetic wave is propagated into x+ direction, while only E_y and H_z are assumed to exist according to *Right Thumb Rule*. For one-dimensional wave propagation problem, the Maxwell's equations are reduced to (Taflove, 1998):

$$\frac{\partial E_y}{\partial t} = \frac{1}{\varepsilon}\left(-\frac{\partial H_z}{\partial x} - \sigma E_y\right) \tag{21}$$

$$\frac{\partial H_z}{\partial t} = \frac{1}{\mu}\left(-\frac{\partial E_y}{\partial x} - \rho' H_z\right) \tag{22}$$

where μ and ε are permeability and permittivity, respectively. σ is electrical loss and ρ' is magnetic loss, which are set to 0 for simplification. Equations (21) and (22) denote an electromagnetic wave propagates in TE mode, indicating that the electrical field is

29

vertical to wave propagation direction. The finite difference form for equation (21) is obtained using approximation as the following:

$$\frac{E_y^{n+1}[i\Delta x] - E_y^n[i\Delta x]}{\Delta t} = \frac{1}{\varepsilon}\left(-\frac{H_z^{n+1/2}[(i+1/2)\Delta x] - H_z^{n+1/2}[(i-1/2)\Delta x]}{\Delta x} - \sigma E_y^{n+1/2}[i\Delta x]\right) \quad (23)$$

where Δx is space resolution, i is spatial index and n is time step. Here n+1/2 is used because H_z is placed half-time step delayed from corresponding E_y from equation (23). The term $E_y^{n+1/2}$ is estimated using semi-implicit approximation:

$$E_y^{n+1/2} = \frac{E_y^{n+1} + E_y^n}{2} \quad (24)$$

Rearranging equation (23) with equation (24) and wipe out Δx for simplification:

$$E_y^{n+1}[i] = \left(\frac{1 - \frac{\sigma\Delta t}{2\varepsilon}}{1 + \frac{\sigma\Delta t}{2\varepsilon}}\right)E_y^n[i] - \frac{\frac{\Delta t}{\varepsilon\Delta x}}{1 + \frac{\sigma\Delta t}{2\varepsilon}}\left\{H_z^{n+1/2}[i+1/2] - H_z^{n+1/2}[i-1/2]\right\} \quad (25)$$

Similar procedures are followed to compute H_z in equation (22), except that H_z at time step n exists due to magnetic loss. From (22), the magnetic field H_z is supposed to be placed half time-step away from electrical field so that only H_z at time step n-1/2 and n+1/2 is stored in computer memory available for computation. As a result, to estimate the magnetic field H_z used in (22), a semi-implicit approximation is employed:

$$H_z^n = \frac{H_z^{n+1/2} + H_z^{n-1/2}}{2} \quad (26)$$

With equation (25), we obtain the explicit finite difference equation for H_z.

$$H_z^{n+1/2}[i] = \left(\frac{1 - \dfrac{\rho' \Delta t}{2\mu}}{1 + \dfrac{\rho' \Delta t}{2\mu}} \right) H_z^{n-1/2} - \frac{\dfrac{\Delta t}{\mu \Delta x}}{1 + \dfrac{\rho' \Delta t}{2\mu}} \left\{ E_y^n[i+1] - E_y^n[i] \right\} \qquad (27)$$

Equation (25) and (27) can be conveniently programmed for E and H field calculation. Their generalization to 3-dimensional problem will be discussed in the next chapter.

Numerical dispersion

Numerical dispersion is unavoidable whenever a numeric approach is employed to solve the continuous wave equation. Numerical dispersion is defined as the variation of numeric wavelength with frequency f since the wavelength is represented in terms of cell size. In this section, the 1-dimensional scalar wave equation is obtained first, followed by an asymptotic study for numeric accuracy.

For simplification, assume the non-existence of electric and magnetic loss, decoupling the E_y and H_z in equations (21) and (22), and the second order partial differential equation is obtained as the following:

$$\frac{\partial^2 H_z}{\partial t^2} = \frac{\partial}{\partial t}\left(\frac{\partial H_z}{\partial t} \right) = \frac{\partial}{\partial t}\left(-\frac{1}{\mu}\frac{\partial E_y}{\partial x} \right) = -\frac{1}{\mu}\frac{\partial^2 E_y}{\partial t \partial x} \qquad (28)$$

Similarly, according to (21), with the assumption of σ=0:

$$\frac{\partial^2 E_y}{\partial t \partial x} = -\frac{1}{\varepsilon}\frac{\partial^2 H_z}{\partial x^2} \qquad (29)$$

Combining equation (28) and (29),

$$\frac{\partial^2 H_z}{\partial t^2} = \frac{1}{\mu\varepsilon}\frac{\partial^2 H_z}{\partial x^2} = u^2 \frac{\partial^2 H_z}{\partial x^2} \qquad (30)$$

31

where $u = \sqrt{1/\mu\varepsilon}$ is the speed of light inside the material under consideration. Equation (30) is one-dimensional scalar wave equation for H_z. Following the similar procedures, wave equations for E_y are obtained as:

$$\frac{\partial^2 E_y}{\partial t^2} = u^2 \frac{\partial^2 E_y}{\partial x^2} \tag{31}$$

Obviously, both E_y and H_z vary as the same function of time and space. The solution of one field component leads to another. From now on, we replace E_y and H_z with a more general function f(x, t). The solution for f leads to both solution for E_y and H_z. In Yee algorithm, the partial differential equations in equation (30) and (31) are differentiated using second order central difference equations. In detail, by Taylor's expansion, at space point x_i with space increment Δx and fixed time point t_n:

$$f(x_i + \Delta x, t_n) = f(x_i, t_n) + \Delta x \frac{\partial f(x_i, t_n)}{\partial x} + \frac{(\Delta x)^2}{2} \frac{\partial f^2(x_i, t_n)}{\partial x^2} + O[(\Delta x)^2] \tag{32}$$

$$f(x_i - \Delta x, t_n) = f(x_i, t_n) - \Delta x \frac{\partial f(x_i, t_n)}{\partial x} + \frac{(\Delta x)^2}{2} \frac{\partial f^2(x_i, t_n)}{\partial x^2} + O[(\Delta x)^2] \tag{33}$$

where $O[(\Delta x)^2]$ is a notation for the remaining higher order terms that approach to zero much faster than the lower order of Δx. Combing equations (32) and (33) yields:

$$f(x_i + \Delta x, t_n) + f(x_i - \Delta x, t_n) = 2f(x_i, t_n) + (\Delta x)^2 \frac{\partial f^2(x_i, t_n)}{\partial x^2} + O[(\Delta x)^2] \tag{34}$$

With Δx small enough, $O[(\Delta x)^2]$ can be neglected without significant loss of accuracy. Therefore, the second order partial differential equation can be represented as:

$$\frac{\partial^2 f(x_i, t_n)}{\partial x^2} = \frac{f(x_i + \Delta x, t_n) + f(x_i - \Delta x, t_n) - 2f(x_i, t_n)}{(\Delta x)^2} \tag{35}$$

Similarly, the second order partial derivatives with respect to time are obtained as:

$$\frac{\partial^2 f(x_i, t_n)}{\partial t^2} = \frac{f(x_i, t_n + \Delta t) + f(x_i, t_n - \Delta t) - 2f(x_i, t_n)}{(\Delta t)^2} \tag{36}$$

For simplification, we write $f(x_i, t_n) = f_i^n$, $x_{i+1} = x_i + \Delta x$ and $t_{n+1} = t_n + \Delta t$. With these shorthand notations, combining equations (35) and (36), the wave equations in (30) and (31) can be reduced to:

$$\frac{f_i^{n+1} + f_i^{n-1} - 2f_i^n}{(\Delta t)^2} = u^2 \frac{f_{i+1}^n + f_{i-1}^n - 2f_i^n}{(\Delta x)^2} \tag{37}$$

Rearranging the terms in equation (37) to obtain the explicit expression of latest value at specified space point based on its previous value, the current value of itself and its neighbouring points.

$$f_i^{n+1} = \left(\frac{u\Delta t}{\Delta x}\right)^2 \left(f_{i+1}^n + f_{i-1}^n - 2f_i^n\right) + 2f_i^n - f_i^{n-1} \tag{38}$$

Equation (38) is the numeric dispersion relationship of the finite difference estimation for one-dimensional scalar wave equation (Taflove, 1998). It uses the current and previous values stored in the computer memory to calculate the latest value. For example, when evaluating the sinusoidal travelling wave in a one-dimensional finite difference scheme:

$$f_i^n = e^{j(\omega\Delta t - k_1 \Delta x)} \tag{39}$$

where $\omega = 2\pi f$ is angular frequency. k_1 is a numeric wave number that differs from the continuous wave number $k = \omega/u$ due to the numeric approximations. This can be observed by substituting equation (39) into equation (38) and factoring out the common terms on both sides of resulted equation. Finally, the implicit form of dispersion relation is obtained as the following (Taflove, 1998):

$$\frac{e^{j\omega\Delta t} + e^{-j\omega\Delta t}}{2} = \left(\frac{u\Delta t}{\Delta x}\right)^2 \left(\frac{e^{jk_1\Delta x} + e^{-jk_1\Delta x}}{2} - 1\right) + 1 \tag{40}$$

By using Euler identity, equation (40) can be reduced to:

$$\cos(\omega \Delta t) = \left(\frac{u\Delta t}{\Delta x}\right)^2 \left[\cos(k_1 \Delta x) - 1\right] + 1 \tag{41}$$

The difference between k_1 and k results in the numeric errors, which we need to depress to develop a reliable simulation algorithm. Based on equation (41), two cases will be considered:

a) $\Delta t \to 0$, $\Delta x \to 0$: for very small arguments, one-term Taylor's series is applied to approximate the cosine functions in equation (41):

$$1 - \frac{(\omega \Delta t)^2}{2} = \left(\frac{u\Delta t}{\Delta x}\right)^2 \left[1 - \frac{(k_1 \Delta x)^2}{2} - 1\right] + 1 \tag{42}$$

Simplifying equation (42) to $k_1 = \omega/u$. This is equal to continuous wave number. Therefore, when the time and space increment approach to infinite small, the numeric results converge to analytical solutions.

b) $u\Delta t = \Delta x$: this is another special case, by which equation (42) again is reduced to $k_1 = \omega/u$. It indicates that if the specified time and space steps are scaled by speed of light in the material u, numeric error does not exist.

While the two special cases are considered above, the general formulation for numeric wave number is:

$$k_1 = \frac{1}{\Delta x} \cos^{-1}\left\{ \left(\frac{\Delta x}{u\Delta t}\right)^2 \left[\cos(\omega \Delta t) - 1\right] + 1 \right\} \tag{43}$$

Equation (43) can be used to analyze the numeric error due to finite difference by solving the numeric wave number within distinct cell sizes in terms of wavelength.

For example, with cell size $\Delta x = \lambda_0/10$ and $\Delta t = \Delta x/2u$, equation (43) leads to $k_1 = 0.636/\Delta x$. Following the similar definition to the analogue phase velocity of the

continuous wave equation as $v_p = \omega/k$, where v_p is defined as phase velocity for the continuous wave equation, the numeric phase velocity is denoted as $\tilde{v}_p = \omega/\tilde{k}$. Therefore with the previous case, $\tilde{v}_p = 0.9873u$, indicating that for a continuous wave propagating into $10\lambda_0$, the simulate numeric wave only propagates over a distance of $9.873\lambda_0$. This discrepancy results in a phase error of $45.72°$. When the cell size is reduced to be $\Delta x = \lambda_0/20$, the phase velocity is changed to be $0.997u$. Accordingly, the phase error is reduced by three quarters to $10.8°$.

Numeric Stability

With Δx and Δt selected to reduce the numeric error, Δt needs to be bounded to avoid numeric instability, which spuriously increases the simulated results without limit as time-stepping approaching.

One convenient method to analyze the numeric stability is to use eigen-value method, which separates the space and time derivative part of original wave equation for analysis purpose. By setting the stable range for the complete spectrum of spatial eigen-values, it is guaranteed that all possible numeric modes in the grid are stable. The detailed procedure for eigen value problem is presented in the following equations:

$$\frac{\partial^2}{\partial t^2} f_i^n = \Pi f_i^n \tag{44}$$

where Π denotes the operator of second order time derivatives for wave functions. Combining the left side of equation (37) and right side of equation (44):

$$\frac{f_i^{n+1} + f_i^{n-1} - 2f_i^n}{(\Delta t)^2} = \Pi f_i^n \tag{45}$$

The numeric stability requires that the absolute value of f_i^{n+1}/f_i^n be less than one for all possible wave propagation modes. To take this requirement into consideration, rearrange equation (45):

$$\left(\frac{f_i^{n+1}}{f_i^n}\right)^2 - [2 + \Pi(\Delta t)^2]\left(\frac{f_i^{n+1}}{f_i^n}\right) + 1 = 0 \tag{46}$$

Solve the equation (46) to get:

$$\frac{f_i^{n+1}}{f_i^n} = \frac{[2 + \Pi(\Delta t)^2] \pm \sqrt{[2 + \Pi(\Delta t)^2]^2 - 4}}{2} \tag{47}$$

To guarantee $\left|f_i^{n+1}/f_i^n\right| \leq 1$, we need to have $[2 + \Pi(\Delta t)^2]^2 - 4 \leq 0$, which reduces to:

$$\frac{-4}{(\Delta t)^2} \leq \Pi \leq 0 \tag{48}$$

Following the similar procedure, the eigen value Π can be bounded by spatial resolution:

$$\frac{-4u^2}{(\Delta x)^2} \leq \Pi \leq 0 \tag{49}$$

For any spatial grid inside the computational domain, numeric stability requires that the eigen values of spatial mode fall completely into the range of eigen values based on time-stepping equations, i.e. equation (49) should be completely contained inside equation (48). For this reason, the time step can be bounded by a predetermined cell size Δx.

$$\Delta t \leq \frac{\Delta x}{c} \tag{50}$$

Equation (50) gives the bound for time increment selection for one-dimensional scalar wave equation. The extension of (50) to two-dimensional and three-dimensional cases is very straightforward (Taflove, 1998).

Finite element method

Another popular method to numerically solve electromagnetic problem is Finite Element Method (FEM). This method is very powerful for very complicated and inhomogeneous geometries. The FEM has a capability of providing a generic computer program for a broad range applications such as waveguide problems, absorption of EM energy by biological bodies (Sadiku, 2000). Basically there are four steps involved in FEM:

dividing the solution region into multiple sub-regions or elements,

obtaining the partial differential equation in each element,

integrating the solutions of all sub-regions into the solution for the entire solution space,

and solving the obtained linear equations.

These procedures are explained using the following Fig 2.7:
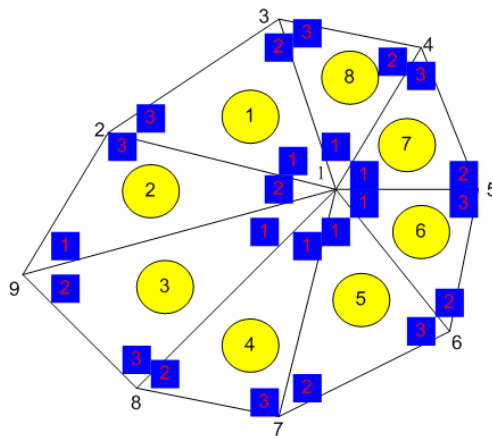
Fig 2.7 FEM discretization for irregular geometry

Usually, in FEM method, the computational domain is divided into numerous elements, each having a triangular or other simple shape. For each element, there are three vertices (number dependent on the elements), which are indexed by integer numbers. To illustrate the principle of FEM, we calculate the potential distribution inside an irregular geometry shown in Fig 2.7. Basically, the potential in each triangular element is assumed to be constant V_e and the overall distribution of potential is assumed equal to the summation of the potential in each element.

$$V(x,y) \approx \sum_{e=1}^{N} V_e(x,y) \tag{51}$$

where N is the number of elements, V(x,y) is the desired potential distribution. Since the element is triangular, V_e(x,y) is represented by a linear equation with three constants to be determined (Sadiku, 2001).

$$V_e(x,y) = a + bx + cy \tag{52}$$

where a, b, and c are constants that are calculated from the potentials at each vertice. From equation (52), we denote the potential at zenith i as Vei (i = 1, 2, 3), the value of a, b, and c can be computed using matrix manipulation:

$$\begin{bmatrix} a \\ b \\ c \end{bmatrix} = \begin{bmatrix} 1 & x_1 & y_1 \\ 1 & x_2 & y_2 \\ 1 & x_3 & y_3 \end{bmatrix}^{-1} \begin{bmatrix} V_{e1} \\ V_{e2} \\ V_{e3} \end{bmatrix} \tag{53}$$

Combining equations (52) and (53), the potential at any point in the element is obtained as:

$$V_e(x,y) = \begin{bmatrix} 1 & x & y \end{bmatrix} \begin{bmatrix} 1 & x_1 & y_1 \\ 1 & x_2 & y_2 \\ 1 & x_3 & y_3 \end{bmatrix}^{-1} \begin{bmatrix} V_{e1} \\ V_{e2} \\ V_{e3} \end{bmatrix} \tag{54}$$

Having considered the potential in each element, the potential distribution is obtained by assembling all elements in the solution region. The detailed procedures are documented in numerous literatures. We briefly list the equations as the following:

$$W = \frac{1}{2}\varepsilon[V]^T[C][V]$$

(55)

where W is the energy associated with the solution region, ε is dielectric permittivity.

$$[V] = [V_1 \quad V_2 \quad \cdots \quad V_n]^T$$

(56)

$$[C] = \begin{bmatrix} C_{11} & C_{12} & C_{13} & C_{14} & C_{15} & C_{16} & C_{17} & C_{18} & C_{19} \\ C_{21} & C_{22} & C_{23} & C_{24} & C_{25} & C_{26} & C_{27} & C_{28} & C_{29} \\ C_{31} & C_{32} & C_{33} & C_{34} & C_{35} & C_{36} & C_{37} & C_{38} & C_{39} \\ C_{41} & C_{42} & C_{43} & C_{44} & C_{45} & C_{46} & C_{47} & C_{48} & C_{49} \\ C_{51} & C_{52} & C_{53} & C_{54} & C_{55} & C_{56} & C_{57} & C_{58} & C_{59} \\ C_{61} & C_{62} & C_{63} & C_{64} & C_{65} & C_{66} & C_{67} & C_{68} & C_{69} \\ C_{71} & C_{72} & C_{73} & C_{74} & C_{75} & C_{76} & C_{77} & C_{78} & C_{79} \\ C_{81} & C_{82} & C_{83} & C_{84} & C_{85} & C_{86} & C_{87} & C_{88} & C_{89} \\ C_{91} & C_{92} & C_{93} & C_{94} & C_{95} & C_{96} & C_{97} & C_{98} & C_{99} \end{bmatrix}$$

(57)

where [C] is a global coefficient matrix which has each element denoting the coupling between different nodes, i.e. C_{ij} is the coupling between node i and j. The C_{ij} is calculated based on the continuity of potential distribution across the boundary of neighbouring elements. For example, we want to calculate C_{12} in Fig 2.7. There are totally 9 global nodes and 8 elements to represent the solution region. Each element has three local nodes indexed in counter-clockwise direction:

$$C_{12} = C_{13}^{[1]} + C_{23}^{[2]}$$

(58)

where $C_{13}^{[1]}$ is the coupling coefficient between local nodes 1 and 3 in local element 1. $C_{23}^{[2]}$ is the coupling efficient between local nodes 2 and 3 in local element 2. After obtaining the global coefficient matrix from equation (58), physical conditions are applied in equation (55) to solve the desired potential. For example, to solve the Laplace's equation, we require that the associated energy W be minimum. Therefore, the first partial derivatives of W are set to zero:

$$\frac{\partial W}{\partial V_1} = \frac{\partial W}{\partial V_2} = \cdots = \frac{\partial W}{\partial V_n} = 0 \qquad (59)$$

Substituting equation (55) into equation (59), we obtain a set of linear equations. These equations are then solved by several popular methods such as iteration method and band matrix method (Sadiku, 2001).

FEM has been applied to solve a wide range of problems due to its capability of handling complex geometry and relative easy extension for general purpose. However, there are several disadvantages for this method, including intensive memory usage for matrix inversion and tedious data pre-processing.

Method of moment

The Method of Moment (MoM) is another popular numeric approach applied to a wide range of EM problems. This method takes moments with corresponding weighing functions; discretizes the differential or integral equations for each of these moments; solves the obtained matrix for interested parameters (Harrington, 1967, 1968, 1992). The fully development of MoM are described in numerous literatures (Mittra(Ed.), 1973; Moore and Pizer, 1984; Richmond, 1965; Tsai, 1978), while the briefly procedures are presented here. For illustration purpose, we use the MoM to calculate the dissipate power

due to EM radiation. The primary concern of biological response of EM field is the specific absorption rate (SAR), which is defined as:

$$SAR = \frac{\sigma |E|^2}{\rho} \tag{60}$$

where σ is electrical conductivity, ρ is mass density and E is the electrical field inside a biological body (Kastner and Mittra, 1983). From equation (60), SAR can be calculated after the electrical field E is obtained. Because of the complex geometry of biological body, E is derived by representing Maxwell's curl equations using a tensor integral equation (TIE) (Kong, 1981; Livesay and Chen, 1974). Following the procedures developed by (Livesay and Chen), the solution of E is obtained as:

$$E(r) = -j\omega\mu_0 \int G_0(r,r') \cdot J_{eq}(r')dv' \tag{61}$$

Where $G_0(r, r')$ is free-space Green's function, indicating the electrical field at space point r due to infinitesimal source at space point r'. $J_{eq}(r')$ is equivalent current density, which is a singular function at each direction:

$$J_{eq}(r,r') = \delta(r - r') \tag{62}$$

The TIE is then obtained as:

$$E(r) = \frac{PV}{1 + \frac{\chi(r)}{3j\omega\varepsilon_0}} \int_v \chi(r')E(r) \cdot G(r,r')dv' + \frac{E^i(r)}{1 + \frac{\chi(r)}{3j\omega\varepsilon_0}} \tag{63}$$

Where PV is principle value (Sadiku, 2000), $E^i(r)$ is incident electrical field that is already known. E(r) is electrical field to be determined by MoM.

The next step is to discretize the equation (63) and write it into matrix form, which is suitable for programming.

41

$$[G][E] = -[E^i]\tag{64}$$

The electrical field E is then determined from (64) as

$$[E] = -[G]^{-1}[E^i]\tag{65}$$

A computer program was developed by (Guru and Chen, 1976) to compute the SAR inside a biological body using MoM following equation (60) to equation (65).

It is obvious from equation (65) that matrix inversion, elimination, and iteration are involved during the computation. This usually requires large memory consumption and lengthy computation time as does the FEM method mentioned in the last section. Due to these reasons, the application of MoM is limited to solve the scattered and irradiated problems with geometry that is electrically large enough to the order of λ^3.

Conclusions

In this chapter, we discussed the analytical and numeric methods to solve the Maxwell's equations. While analytical solution is available only for standard geometry, numerical solution is necessary and desirable for most of the practical problems. Many concerns have been discussed for constructing a reliable and accurate computer aided solution to solve the EM problems such as the selection of spatial and time increments, numeric dispersion, and numeric stability. Several state-of-art techniques including FDTD, FEM, and MoM are briefly discussed in this chapter. Among these methods, FDTD employs a finite difference equation to solve Maxwell's curl or integral equations; FEM solves the partial differential equations of each element and take the summations to obtain the global solution; MoM discretizes the integral equation and carries out the matrix manipulations for interested parameters. To minimize the numeric error and substantially improve the accuracy, large computational grids are required so as the

computer memory. Therefore, the advantages of FDTD over the FEM and MoM are that it eliminates the matrix inversion and solve the time domain field components explicitly, which significantly reduces the memory consumption and simulation time. Due to these reasons, FDTD is usually preferred for large and complicated problems such as industrial MW heating simulation. Starting from next chapter, a FDTD model will be developed to solve the MW scattered problem, then followed by a coupled model to conduct MW heating simulation for stationary and moving obstacles.

References

Balanis, C. A. (1982). *Antenna theory: analysis and design*, Wiley, New York,

Balanis, C. A. (1989). *Advanced engineering electromagnetics*, John Wiley & Sons,

Buffler, C. R. (1993). *Microwave cooking and processing*, Van Nostrand Reinhold, NY. USA.

Carson, J. R. (1929). Reciprocal theorems in radio communication. *Proc. IRE*, 17, 952-956.

Guru, B. S., & Chen, K. M. (1976). A computer program for calculating the induced EM field inside an irradiated body. *Dept. of Electrical Engineering and System Science*, Michigan State Univ., East Lansing, MI 48824.

Harrington, R. F. (1959). On Scattering by large conducting bodies. *IRE Trans. Antennas Propagat*, AP-7(2), 150-153.

Harrington, R. F. (1961). *Time-Harmonic Electromagnetic Fields*, McGraw-Hill, New York.

Harrington, R. F. (1967). Matrix methods for field problems. *Proc. IEEE*, 55(2), 136-149.

Harrington, R. F. (1968). *Field Computation By Moment Methods* Macmillan, New York.

Harrington, R. F. (1992). *Origin and development of the method moments for field computation*, Computational electromagnetics, New York: IEEE Press.

Hayt, W. H., & Kimmerly, J. E. (1978). *Engineering Circuit Analysis*, 3rd ed., McGraw-Hill, New York,

Hilderbrand, F. B. (1962). *Advanced Calculus for Applications*, Prentice-Hall, Englewood Cliffs, N. J.

Huygens, C. (1690). Traite de la lumiere. Translated into English by Thompson, S. P., London, 1919 and reprinted by the University of Chicago press.

Kastner, R., & Mittra, R. (1983). A new stacked two-dimensional spectral iterative technique (SIT) for analyzing microwave power deposition in biological media. *IEEE Trans Micro. Theo. Tech.*, MTT-31(1), 898-904.

Kong, J. A. (1981). *Research Topics in Electromagnetic Theory*, New York: John Wiley. pp: 290-355.

Kraus, J. D., & Carver, K. R. (1973). Electromagnetics. 464-467. McGraw-Hill, New York.

Livesay, D. E., & Chen, K. M. (1974). Electromagnetic fields induced inside arbitrary shaped biological bodies. *IEEE Trans Micro. Theo. Tech.*, MTT-22(12), 1273-1280.

Meredith, R. (1998). *Engineer's handbook of industrial microwave heating*, The institution of Electrical Engineers,

Metaxas, A. C., & Meredith, R. J. (1993). *Industrial Microwave Heating*, London, UK.

Mittra(Ed.), R. (1973). *Computer Techniques for Electromagnetics*, Pergamon, New York.

Moore, J., & Pizer, R. (1984). *Moment Methods in Electromagnetics*, Wiley, New York.

Okoniewski, M. (1993). Vector wave equation 2D-FDTD method for guided wave equation. *IEEE Micro. Guided Wave Lett.*, 3(9), 307-309.

Richmond, J. H. (1965). Digital computer solutions of the rigorous equations for scattering problems. *Proc. IEEE*, 53, 796-804.

Sadiku, M. N. O. (2000). *Numerical Techniques in Electromagnetics*, 2 ed., CRC, NYC.

Sadiku, M. N. O. (2001). *Elements of Electromagnetics*, 3 ed., Oxford University Press, New York.

Schelkunoff, S. A. (1936). Some equivalence theorems of electromagnetics and their application to radiation problems. *Bell System Tech. J.*, 15, 92-112.

Taflove, A. (1980). Application of the finite-difference time-domain method to sinusoidal steady-state electromagnetic-penetration problems. *IEEE Trans. EM Comp.*, EMC-22(3), 191-202.

Taflove, A. (1998). Computational electrodynamics : the finite-difference time-domain method, Artech House, Boston.

Taflove, A., & Brodwin, M. E. (1975). Numerical solution of steady-state electromagnetic scattering problems using the time-dependent Maxwell's equations. *IEEE Micro. Theo. Tech.*, MTT-23(8), 623-630.

Taflove, A., & Umashankar, K. (1980). A hybrid moment method/finite-difference time-domain approach to electromagnetic coupling and aperture penetration into complex geometries. *IEEE Trans. Ant. Prop.*, AP-30(4), 617-627.

Taflove, A., & Umashankar, K. (1981). Solution of complex electromagnetic penetration and scattering problems in unbounded regions. *Computational methods for infinite domain media-structure interaction*, Washington, D.C: ASME, 46, 83-113.

Taflove, A., & Umashankar, K. (1990). The finite-difference time-domain method for numerical modeling of electromagnetic wave interactions. *Electromagnetics*, 10, 105-126.

Thom, A., & Apelt, C. J. (1961). *Field Computations in Engineering and Physics*, D.Van Nostrand, London.

Tsai, L. L. (1978). Moment methods in electromagnetics for undergraduates. *IEEE Trans. on Education*, E-21(1), 14-22.

Umashankar, K., & Taflove, A. (1982). A novel method to analyze electromagnetic scattering of complex objects. *IEEE Trans. EM Comp.*, EMC-24(4), 397-405.

Wylie, C. R. (1960). *Advanced Engineering Mathematics*, McGraw-Hill, New York.

Yee, K. S. (1966). Numerical solution of initial boundary-value problems involving Maxwell's equations in isotropic media. *IEEE Trans. Ant. Prop.*, AP-14, 302-307.

Chapter 3 Analysis of the Steady-State Electromagnetic Fields inside Food Package using Finite Different Time Domain Method

Abstract

A computer simulation model was developed to calculate the electromagnetic field inside a food package by using a finite difference time domain method. The model treated the food package as a scatter object and its irradiation as an initial value problem. The plane-wave source was turned on at t = 0 and kept on until the steady-state was reached. The envelope of electrical field in the last half-wave cycle was then recorded as the steady-state scatter field. For illustration and simplification, a two-dimensional problem was presented. The calculated results were compared with analytical solution with good agreement. The model was then used to calculate the scatter field inside food packages with different dielectric constant and loss factor.

Introduction

The effect of microwave heating on lossy dielectric foods has gained more research interest since it has been involved in many aspects of food processing such as cooking, pasterization and sterilization. Compared with conventional heating methods, microwave energy generates volumetric heating and reduces process time (Chen, et al., 2007a, 2007b). To better design microwave-drived food process systems, it is necessary to understand the mechanism of interaction between electromagnetic field and food

packages, as well as the field response to dielectric properties of foods. However, due to the complexity of Maxwell's equations and its interaction with dielectric foods, the analytical solutions are only available for the objects with regular shape such as rectangular, cylinder and sphere. For more realistic problems with regular and irregular boundaries, numeric techniques such as Finite Difference Time Domain (FDTD) method, Finite Element Method(FEM) and Mothod of Moment (MoM) are needed to solve complete partial differential equations.

Several early papers (McDonald and Wexler, 1972; Spiegel, 1984; Wu and Tai, 1974) summarize the computational methods to study electromagnetic field distribution. In (Wu and Tai, 1974), a coupled integral equation was developed to solve a two-dimensional scattering problem for an arbitrary dielectric cylinder. They employed a pair of the electrical fields and their normal derivatives at the surface of the scattering objects and then solved the resulted complete set of linear equations by using MoM. In (McDonald and Wexler, 1972), a FEM was employed to solve Helmholtz equations within computational region for a two-dimensional radiating antenna with a dielectrical object. In Spiegel (1984), the FDTD method was reviewed for medical applications. FDTD method has several advantages over other numeric methods since this method maitains continuities on the boundaries between differernt dielectric medias and does not require the formulation of integral equations as well as the inversion of large matrix. Due to these merits, FDTD method has been increasingly used to solve realistic problems such as the temperature response to microwave-irradiated human eye (Taflove and Brodwin, 1975a) and response of military crafts to electromagnetic pulses (Kunz and Lee, 1978). In addition, the electromagnetic effects on biological tissues exposed to microwave energy

were explored in several studies (Cook, 1952; Guy, et al., 1974; Livesay and Chen, 1974; Michaelson, 1969; Schwan, 1972), including the induced heating response.

Although many studies were carried out to investigate the electromagnetic (EM) effects on biological tissues, most of those studies focused on the response of human bodies. Until now, few studies were conducted to explore EM effects on microwave-irradiated food packages. Dielectric food has a very unique feature when exposed to microwave. Its dielectric properties largely depend on its residence time inside electromagnetic fields. On one hand, dielectric properties vary with the induced temperature response to microwave irradiation; on the other hand, the changed dielectric properties significantly affect the electromagnetic field. Due to this feature, it is important to explore the coupling effects between food packages and electromagnetic fields. In Ma (1995), a three-dimensional FDTD model was developed to obtain the microwave heating pattern of gels placed inside a domestic microwave oven. In Chen (2007a), an industrial-scale microwave sterilization system was simulated by a combination of EM and thermal model, both employing FDTD method and its validity was tested by experiment measurements. Though heating patterns were presented in both studies, there were not explicit interactive presentations of dielectric properties with microwave irradiation.

In this paper, a FDTD model was implemented to calculate the electrical field inside a food package. Its validity was then illustrated by computing the numeric solutions inside a two-dimensional cylinder and comparing them with analytical results. The model was then applied to investigate the variation of dielectric properties under electromagnetic effect and its reaction on the electromagnetic field.

FDTD Method

The Maxwell's equations in rectangular coordinator system can be presented in a time harmonic form (Taflove, 1998):

$$\frac{\partial H_x}{\partial t} = \frac{1}{\mu_t}\left(\frac{\partial E_y}{\partial z} - \frac{\partial E_z}{\partial y}\right) \qquad (1)$$

$$\frac{\partial H_y}{\partial t} = \frac{1}{\mu_t}\left(\frac{\partial E_z}{\partial x} - \frac{\partial E_x}{\partial z}\right) \qquad (2)$$

$$\frac{\partial H_z}{\partial t} = \frac{1}{\mu_t}\left(\frac{\partial E_x}{\partial y} - \frac{\partial E_y}{\partial x}\right) \qquad (3)$$

$$\frac{\partial E_x}{\partial t} = \frac{1}{\varepsilon_t}\left(\frac{\partial H_z}{\partial y} - \frac{\partial H_y}{\partial z} - \sigma_t E_x\right) \qquad (4)$$

$$\frac{\partial E_y}{\partial t} = \frac{1}{\varepsilon_t}\left(\frac{\partial Hx}{\partial z} - \frac{\partial H_z}{\partial x} - \sigma_t E_y\right) \qquad (5)$$

$$\frac{\partial E_z}{\partial t} = \frac{1}{\varepsilon_t}\left(\frac{\partial H_z}{\partial x} - \frac{\partial H_x}{\partial y} - \sigma_t E_z\right) \qquad (6)$$

where μ_t, ε_t and σ_t denote dielectric permeability, permittivity and conductivity, respectively. The subscripts t emphasizes that these constitutive parameters inside dielectric food are dependent of time.

To numerically solve equations (1)-(6), Yee (1966) proposed the class FDTD method, which discretized the computational region into unit cells and estimate the derivatives by second-order central finite-different approximation. To achieve second-order accuracy, electrical field component and magnetic field component were placed half cell size away from each other, as shown in Fig 3.1.
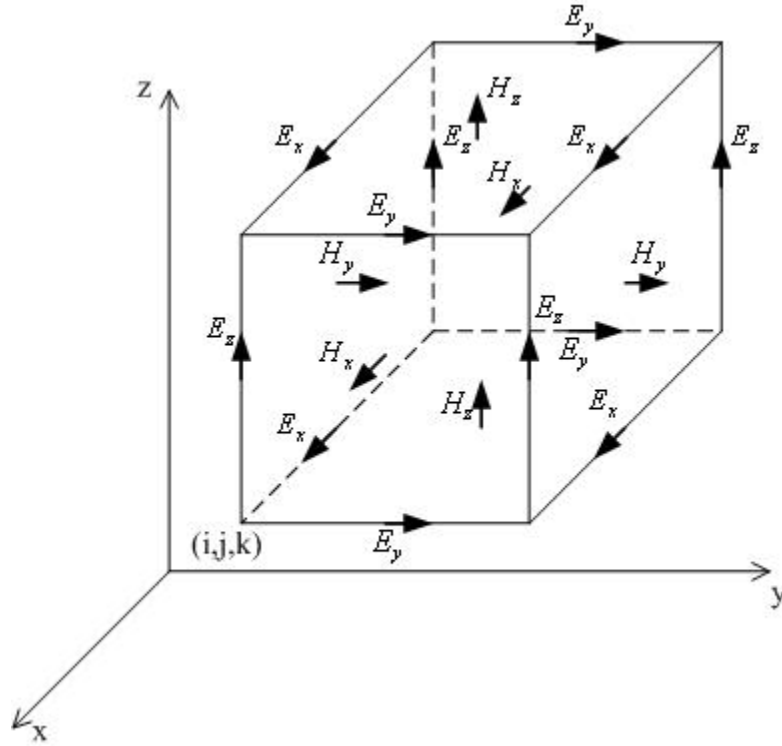
Fig 3.1 Layout of field components for FDTD algorithm

In problem space, a grid point can be expressed as:

$$(i, j, k) = (i * \delta x, j * \delta y, k * \delta z) \tag{7}$$

where δx, δy and δz are cell size in x-, y- and z-direction, respectively. For a function having space and time dependence, it can be expressed as:

$$g(x, y, z, t) = g(i * \delta x, j * \delta y, k * \delta z, n * \delta t) = g^n(i, j, k) \tag{8}$$

where $g(x, y, z, t)$ is a generic function and δt is a time step.

From these notations, the second order central finite-difference forms for equations (1)-(6) were derived to be suitable for computer programming (Lau and Sheppard, 1986; Taflove and Brodwin, 1975b).

$$H_x^{n+1/2}(i, j+1/2, k+1/2) = H_x^{n-1/2}(i, j+1/2, k+1/2)$$
$$+ \frac{\delta t}{\mu * \delta_{i,j+1/2,k+1/2}} \begin{bmatrix} E_y^n(i, j+1/2, k+1) - E_y^n(i, j+1/2, k) \\ + E_z^n(i, j, k+1/2) - E_z^n(i, j+1, k+1/2) \end{bmatrix} \tag{9}$$

$$H_y^{n+1/2}(i+1/2, j, k+1/2) = H_y^{n-1/2}(i+1/2, j, k+1/2)$$
$$+ \frac{\delta t}{\mu * \delta_{i+1/2,j,k+1/2}} \begin{bmatrix} E_z^n(i+1, j, k+1/2) - E_z^n(i, j, k+1/2) \\ + E_x^n(i+1/2, j, k) - E_x^n(i+1/2, j, k+1) \end{bmatrix} \tag{10}$$

$$H_z^{n+1/2}(i+1/2, j+1/2, k) = H_z^{n-1/2}(i+1/2, j+1/2, k)$$
$$+ \frac{\delta t}{\mu * \delta_{i+1/2,j+1/2,k}} \begin{bmatrix} E_x^n(i+1/2, j+1, k) - E_x^n(i+1/2, j, k) \\ + E_y^n(i, j+1/2, k) - E_y^n(i+1, j+1/2, k) \end{bmatrix} \tag{11}$$

$$E_x^{n+1}(i+1/2, j, k) = \left(1 - \frac{\sigma_{i+1/2,j,k}\delta t}{\varepsilon_{i+1/2,j,k}}\right) E_x^n(i+1/2, j, k)$$
$$+ \frac{\delta t}{\varepsilon_{i+1/2,j,k} * \delta_{i+1/2,j,k}} \begin{bmatrix} H_z^{n+1/2}(i+1/2, j+1/2, k) - H_z^{n+1/2}(i+1/2, j-1/2, k) \\ + H_y^{n+1/2}(i+1/2, j, k-1/2) - H_y^{n+1/2}(i+1/2, j, k+1/2) \end{bmatrix} \tag{12}$$

$$E_y^{n+1}(i, j+1/2, k) = \left(1 - \frac{\sigma_{i,j+1/2,k}\delta t}{\varepsilon_{i,j+1/2,k}}\right) E_y^n(i, j+1/2, k)$$
$$+ \frac{\delta t}{\varepsilon_{i,j+1/2,k} * \delta_{i,j+1/2,k}} \begin{bmatrix} H_x^{n+1/2}(i, j+1/2, k+1/2) - H_x^{n+1/2}(i, j+1/2, k-1/2) \\ + H_z^{n+1/2}(i-1/2, j+1/2, k) - H_z^{n+1/2}(i+1/2, j+1/2, k) \end{bmatrix} \tag{13}$$

$$E_z^{n+1}(i, j, k+1/2) = \left(1 - \frac{\sigma_{i,j,k+1/2}\delta t}{\varepsilon_{i,j,k+1/2}}\right) E_z^n(i, j, k+1/2)$$
$$+ \frac{\delta t}{\varepsilon_{i,j,k+1/2} * \delta_{i,j,k+1/2}} \begin{bmatrix} H_y^{n+1/2}(i+1/2, j, k+1/2) - H_y^{n+1/2}(i-1/2, j, k+1/2) \\ + H_x^{n+1/2}(i, j-1/2, k+1/2) - H_x^{n+1/2}(i, j+1/2, k+1/2) \end{bmatrix} \tag{14}$$

From equations (9)-(14), the six field components are calculated from their corresponding previous values as well as the previous values of their neighboring field components. The computation approaches one grid at each time step and is terminated after reaching a steady state. We also assumed that the permeability was isotropic and time independent,

but the dielectric constant and electrical conductivity were dependent on both time and space.

It is well known that a least ten cells are needed in one wavelength to keep FDTD algorithm valid (Chen, et al., 2007a). In addition, for accuracy and stability, the time step δt is bounded by a value determined by local media and cell size in three directions.

$$\delta t \le \frac{1}{c} \sqrt{\frac{(\varepsilon_t)_{min}}{(\delta x)_{max}^{-2} + (\delta y)_{max}^{-2} + (\delta z)_{max}^{-2}}} \tag{15}$$

where c is the speed of light in free space. We also explicitly denote the subscript t of dielectric constant to emphasize its time dependent in food applications. To ensure the stability of the program everywhere and anytime in the problem space, (15) has to be satisfied.

Absorbing boundary condition

When dealing with microwave irradiated food, it is assumed that microwave stroke the food package from infinity, part of its energy is absorbed by food and part is scattered to infinity. Therefore, it is necessary for the model to be able to terminate the computation at particular space grids while, in the same time, keeping the scatter field effectively approaching into infinity. Due to this requirement, the lattice boundary needed to permit outgoing numeric waves and suppress the artifactitious reflected waves from all directions. This lattice truncation is theoretically called Absorbing Boundary Condition (ABC). The formulations of ABC were developed in Taflove (1998) by using Taylor series approximation.

Based on Taylor series expansion, there are first-order, second-order and higher order ABC. The second-order ABC was employed in our numeric model because of its

relative higher accuracy compared with first-order ABC and moderate computation burdens compared with higher order ABCs. Since second-order ABC was used, every node on the lattice boundary needed a two dimensional array to keep its past value and the current value of interior nodes to facilitate calculations. In a three dimensional lattice, there are six faces, each having two tangential fields so that total 72 2D array are needed to facilitate the calculations. For the sake of illustration, assume there is E_z field component tangential to the boundary x=0, the second-order ABC was implemented in the following formulation:

$$
\begin{aligned}
E_z^{n+1}(0,j,k) &= \frac{2-s-1/s}{2+s+1/s}\left[E_z^{n+1}(2,j,k) + E_z^{n-1}(0,j,k)\right] \\
&+ \frac{2(1/s-s)}{2+s+1/s}\left[E_z^n(0,j,k) + E_z^n(2,j,k) - E_z^{n+1}(1,j,k) - E_z^{n-1}(1,j,k)\right] \\
&+ \frac{4(1/s+s)}{2+s+1/s} E_z^n(1,j,k) - E_z^{n-1}(2,j,k)
\end{aligned}
\tag{16}
$$

where $s = \delta t / \sqrt{\mu\varepsilon}\,\delta_{0,j,k}$. Here we only present the update equation for E_z on the lattice boundary, for the other components tangential to the boundary, the update equations are pretty similar. The complete set of update equations for ABC is presented in (Taflove, 1998).

Source specification

Since this study mainly focuses on FDTD applications on microwave irradiated food packages, the plane wave excitation instead of pulse excitation was found to be more suitable for this type of problem (Ma, et al., 1995). Therefore, in this paper, we used a sinusoidal plane wave with a prescribed energy as an excitation source. In numeric modeling, to radiate the desired plane wave in computation lattice, a simple approach is

to place the excitation plane on the lattice boundary. However, it does not consider any possible outgoing fields scattered by the object, hence introducing undesired reflected wave which distorts the final results. As a result, in practice, the excitation source was placed on a reference plane which was several cells away from lattice boundary. This placement introduced the desired plane wave propagating through the FDTD grids and, in the meantime, the reflected fields propagated into infinity through the lattice boundary without any reflection presented. As an example, assuming a sine wave with the dominant TE_{10} mode of a rectangular waveguide far away from the modeled object, it only has E_y field component and propagates into z-direction. We then set up the excitation plane at k=3:

$$E_y^n(i,j,3) \leftarrow E_0 \sin(2\pi f n \delta t) + E_y^n(i,j,3) \tag{17}$$

where E_0 is determined by specified source power. In the numeric simulation, the sinusoidal wave was activated at time step n = 1 and left on until steady-state was established, which usually needs four or five wave cycles.

Model validation

Any numeric model is not useful until it is validated. To check the correctness of the FDTD technique proposed in previous sections, the electrical field inside a cylindrical food model was calculated and compared with the analytical results. The cylindrical model is shown in the following figure:
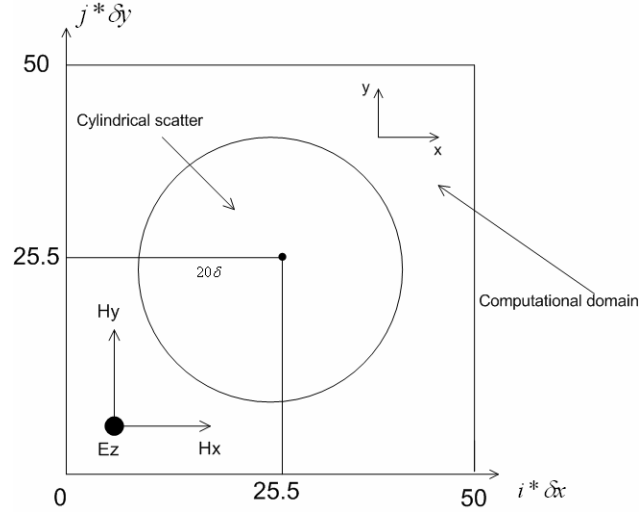
Fig 3.2 cylindrical food model for verifying FDTD algorithm

The cylinder was assumed to have an infinite length in z-direction and circular cross section in x-y plane. For simplification purpose, it was assumed that the cell size was uniform in the whole computational lattice, i.e. $\delta x = \delta y = \delta$. The cylinder had a radius of 20δ. The incident wave was assumed to be a sinusoidal wave with operating frequency of f_0. In this verification, we investigated two cases when $f_0 = 0.915 GHz$ and $f_0 = 2.45 GHz$, which are FCC allocated frequencies for microwave applications. Because the cylinder was infinite in z-direction, there was no variation in this direction with respect to the geometry and incident fields. Thus, this problem could be treated as a two-dimensional scattering problem. In addition, we assumed that the incident wave was a +y-directed TM wave. Therefore, it only had three field components involved in this simulation: E_z, H_x, H_y.

Based on the above analysis, we built a two-dimensional computational lattice consisting of 50 grids in either direction. Each of them contained a media with dielectric

parameters dependent on its location. The center of the cylinder was assumed to be the central point of the lattice $\left(25\frac{1}{2}, 25\frac{1}{2}\right)$, the geometry function to describe this object was:

$$\sqrt{\left(i - 25\frac{1}{2}\right)^2 + \left(j - 25\frac{1}{2}\right)^2} \leq 20 \tag{18}$$

Thus, for each pair (i, j), if it satisfied equation (18), we assigned dielectric parameters for specified food package, otherwise, the dielectric properties for free space was used. Due to the two-dimensional lattice, the plane wave source was specified as the following according to (17):

$$E_z(i,3) \leftarrow E_z(i,3) + 1000 * \sin(2\pi f n \delta t) \tag{19}$$

Another interesting feature of this problem was that the modeled structure was symmetric over the center line. The dielectric properties were also assumed to be symmetric over the same line. In addition, since the incident wave was in +z direction, the field components which were normal to propagation direction were symmetric naturally, i.e.

$$E_z^n\left(26, j\right) = E_z^n(25, j) \tag{20}$$

$$H_y^n(26, j) = H_y^n(25, j) \tag{21}$$

Therefore, we truncated the computational lattice on the center line and imposed the update equations for field components according to (19) and (20), which significantly reduced the computer memory storage and simulation time.

In this study, we investigated two cases for validation purpose. One is for the food package to be exposed to microwave with frequency of 0.915GHz; the other is the same food package exposed to microwave with frequency of 2.45GHz. The modeled food had

the following dielectric parameters: $\varepsilon_f' = 4\varepsilon_0$, $\varepsilon_f'' = 0$. Therefore, for the case with

frequency of $f_0 = 0.915GHz$, the wavelength was $\lambda_f = \dfrac{c}{\sqrt{4}f_0} = \dfrac{c}{2f_0} = 0.16m$. Assuming

there were 80 discrete points per wavelength used in FDTD technique, the cell size was

then $\delta = \dfrac{\lambda_f}{80} = \dfrac{c}{160f_0} = 0.002m$, the time step was chosen according to equation

(15): $\delta t = \dfrac{\delta}{2c} = 3ps$. Thus, it required 320 time steps to complete the simulation for one

wave cycle. Since it usually needs four or five wave cycles to reach the steady-state, 1600

time steps were used in the simulation. The maximum absolute value of electrical field

$E_z(25, j)$ and $E_z(10, j)$ in the last half wave cycle were then recorded and compared

with the analytical results, computed using series expansion method (Jones, 1964). The

results are presented in Fig 3.3.
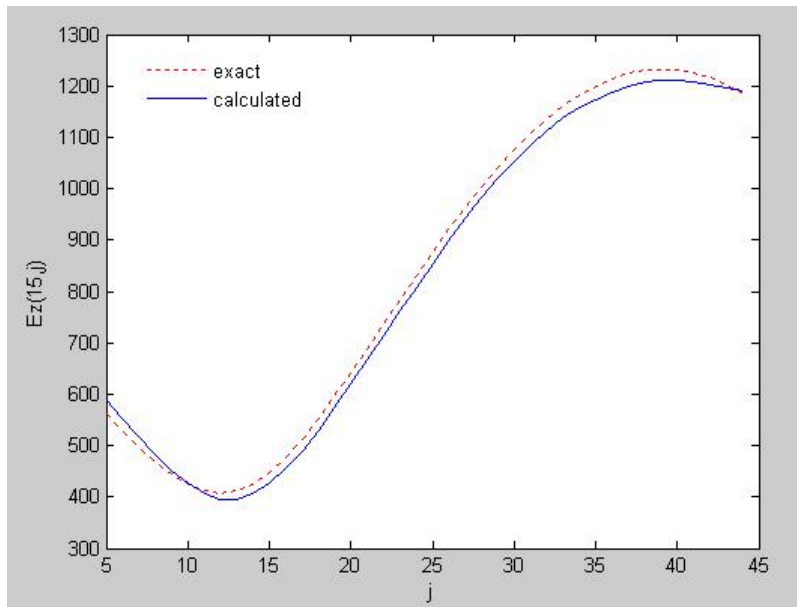
(a) Ez field at i = 15
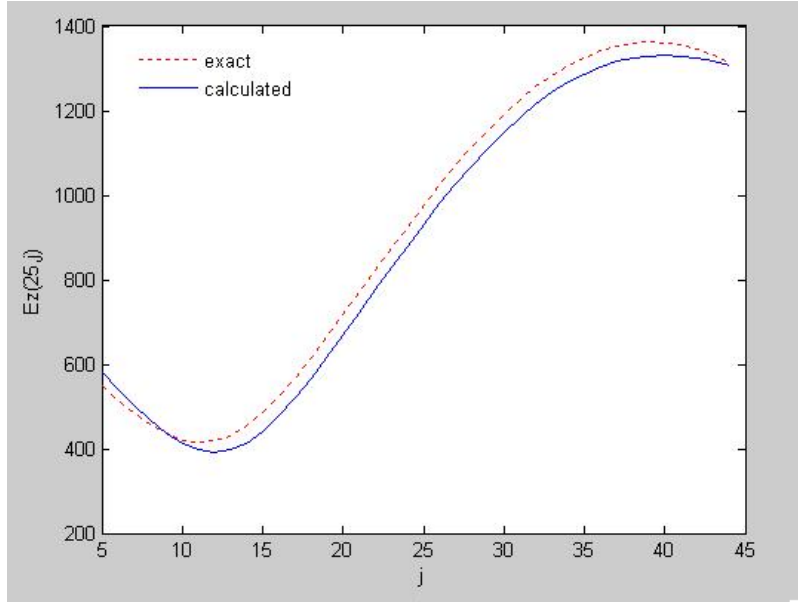
(b) Ez field at i = 25

Fig 3.3 comparison between numeric and analytical results for 915MHz microwave

irradiated cylindrical food package

Both results showed a good agreement. The numeric model correctly predicted

the location of peak and null of the envelope of the electrical field with a maximum error

of δ. It was also shown that the amplitude of the induced electrical field inside the

cylinder was approximated with only 5% error presented.

In the second case, the numeric results for the same cylindrical food under the

frequency of $f_0 = 2.45GHz$ were computed using exact same parameters as in the

literature (Taflove and Brodwin, 1975b) for validation and comparison purpose. At this

frequency, with the same deduction as the last example, we have $\lambda_f = \dfrac{c}{2f_0} = 0.06m$.

Since the wavelength is much smaller in this case, 20 discrete points per wavelength was

assumed to be enough for the simulation. Thus, the cell size used for this case

was $\delta = \dfrac{\lambda_f}{20} = 0.003m$, the time step was then $\delta t = \dfrac{\delta}{2c} = 5ps$. These selections required 80

time steps for simulating one complete wave cycle. As before, 5 wave cycles were used

to achieve the steady state. Results are shown in Fig 3.4.
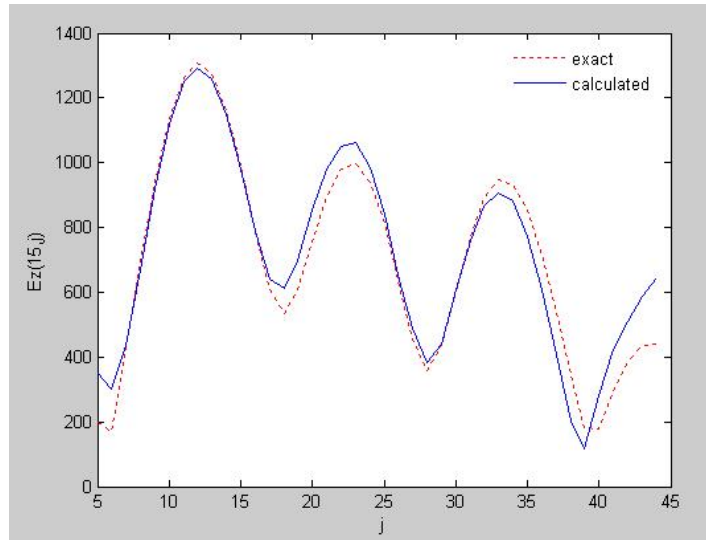
(a) Ez field at i = 15
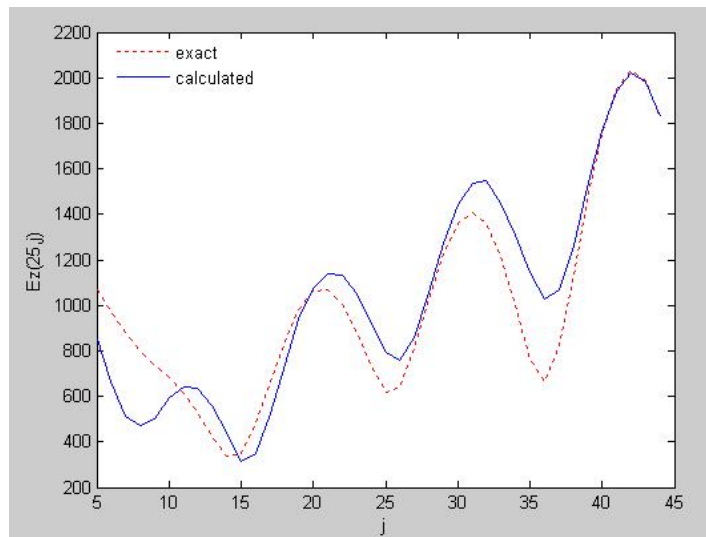
(b) Ez field at i = 25

Fig 3.4 comparison between numeric and analytical results for 2450MHz microwave

irradiated cylindrical food package

Again, similar results were achieved from simulated and analytical calculations. The maximum error of the amplitude of the electrical field is within 10% of the incident amplitude, while the expected location of field peaks deviated from analytical solution less than δ. Another observation was that there were only one nulls of the envelope of E_z in Fig 3.3 but four nulls in Fig 3.4. This was because the radius of cylinder was equal to wavelength in Fig 3.3 while equal to quart-wavelength in Fig 3.4. Therefore, single mode electromagnetic field was achieved with 915MHz while multi-mode was inevitable with 2450MHz. For food application, the multi-mode system brings up a critical problem that the cold spot can not be traced among different microwave heating processes. Since the temperature at cold spot needs to reach over 121°C to ensure the safety of the food (Guan, et al., 2004), it is desirable for a microwave heating system to keep the cold spot fixed which, however, is impossible for a multi-mode system. A novel technique which employs 915 MHz microwave heating process was fully described by Chen et al.(2007a; 2007b).

Numeric results

In the last section, we validated the numerical model. It correctly represented a microwave irradiated two-dimensional scattering object. By simply modifying the dielectric properties in each grid, this model can be used to generate field components for scatters with arbitrary constituent parameters. Since the temperature dependent dielectric properties is a unique feature involved in microwave related problem, it is worthwhile to investigate the effect of different dielectric properties on electrical field. The data we used in simulation is shown in Table 3.1.

Table 3.1 dielectric properties of whey protein gel

Temperature [^{o}C]	Dielectric constant $\varepsilon_r^{'} = \varepsilon^{'}/\varepsilon_0$	Dielectric loss $\varepsilon_r^{"} = \varepsilon^{"}/\varepsilon_0$
20	58.5	24.25
40	57.55	30.25
60	56.36	36.79
80	54.36	45.21
100	52.81	53.89
121	51.14	63.38

The dielectric properties were measured using an HP8491B network analyzer (Hewlett-Packard Company, CA, USA). The food used in these numeric experiments is whey protein gel, which was intensively used for research of MW sterilization at WSU.

First, the dielectric constant was changed according to the temperatures presented in Table. I, while the dielectric loss was maintained to zero.
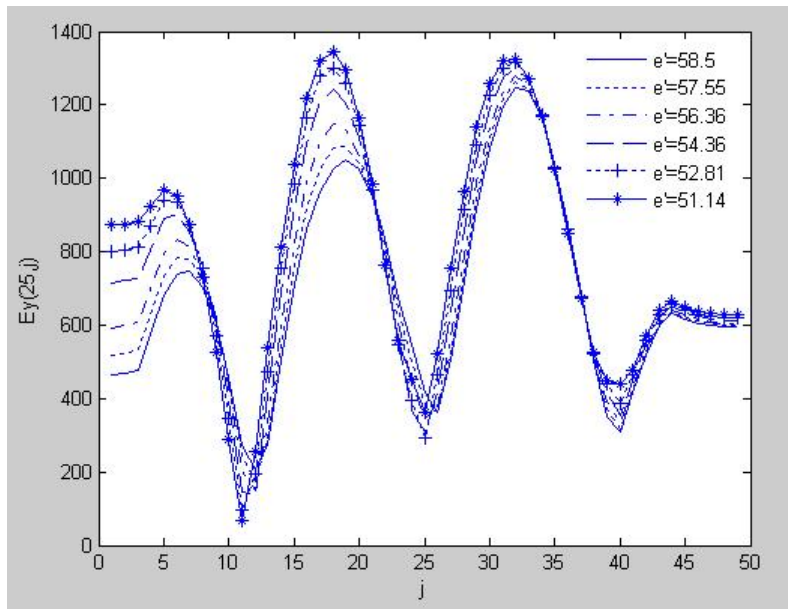
(a) Electrical field at i = 25 with different dielectric constant
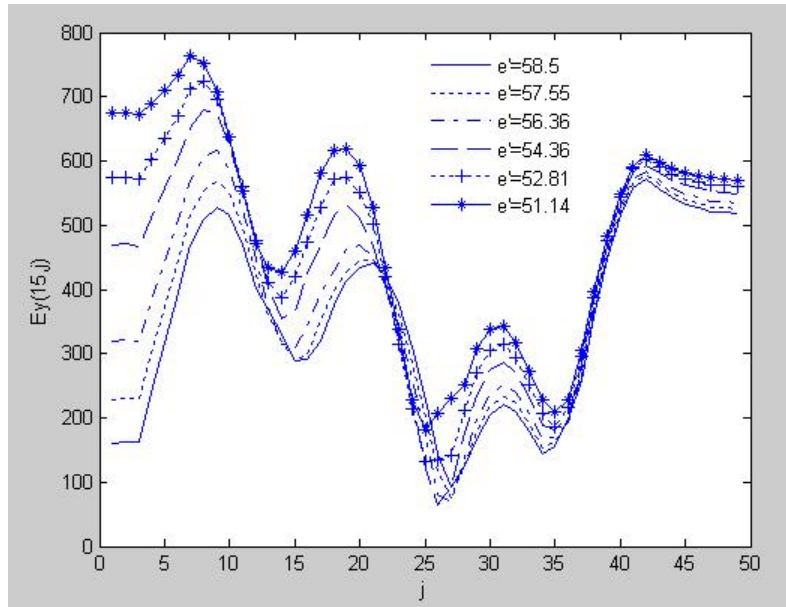
(b) Electrical field at i = 15 with different dielectric constant

Fig 3.5. Electrical field inside cylindrical whey protein gel with microwave frequency of 915MHz and different dielectric constant ($\varepsilon" = 0$)

Fig 3.5 plots the electrical fields along the wave propagation direction at two distinct locations. As before, the amplitude of incident electrical wave was assumed to be 1000. It is obvious that the electrical field inside the gel increased with decreasing dielectric constant. However, the location of peaks and nulls of electrical field remains the same with different dielectric constant.

In the following case, we applied different data of loss factor to the same gel used in case 1, but with the identical dielectric constant. Since temperature needs to reach over 121°C to ensure food safety (Guan, et al., 2004), the dielectric constant was assumed to be 51.14.
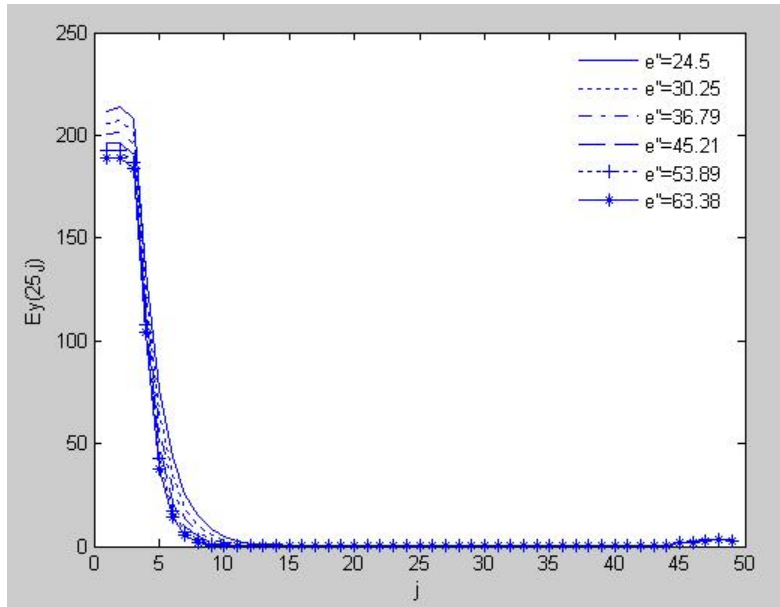
(a) Electrical field at i = 25 with different loss factor
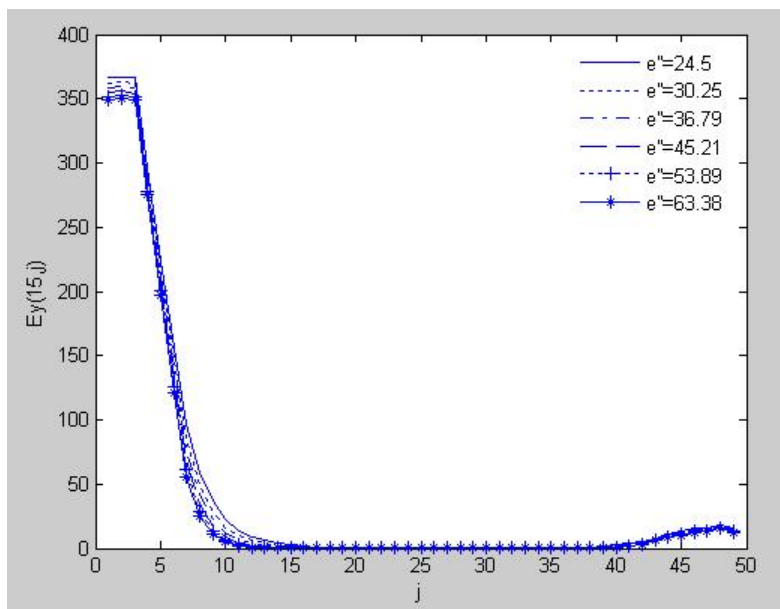
(b) Electrical field at i = 15 with different loss factor

Fig 3.6 Electrical field inside cylindrical whey protein gel with microwave frequency of

915MHz and different loss factor (ε' = 51.14)

It is obvious from Fig 3.6 that the higher the loss factor is, the lower the electrical field is. The electrical field drops abruptly from initial value to zero. Along wave propagation direction, the penetration depth decreases while increasing the loss factor.

We then generalize the application of previous cases to a more realistic case, where both dielectric constant and loss factor vary with temperatures. The numeric results are presented in Fig 3.7.
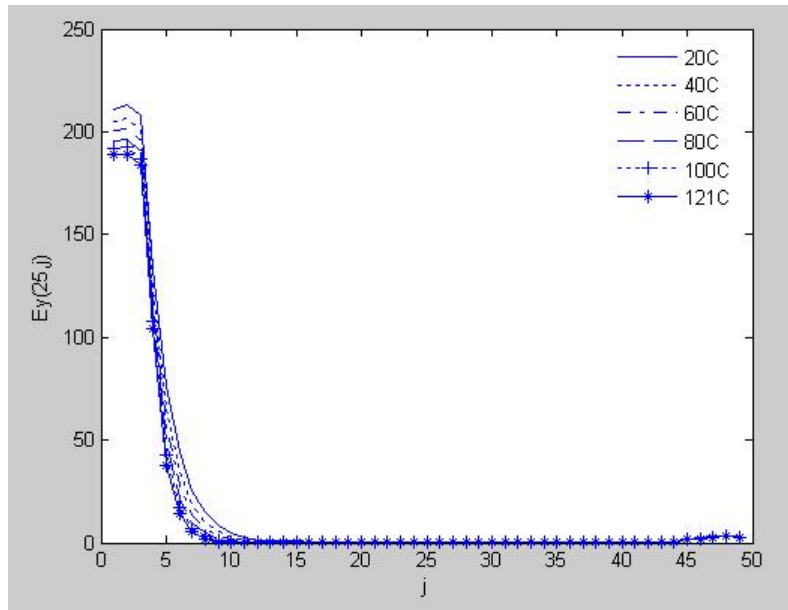
(a) Electrical field at i = 25 with different temperatures
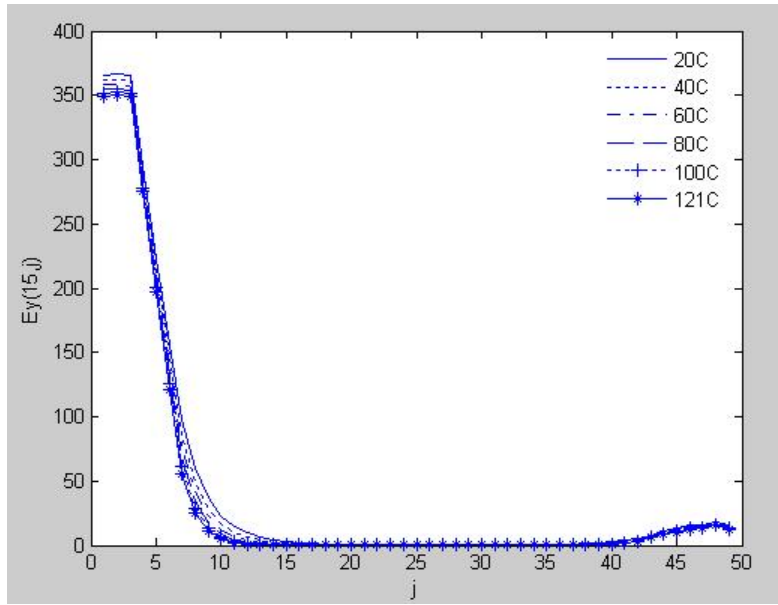
(b) Electrical field at i = 15 with different temperatures

Fig 3.7. Electrical field at different temperature levels

Fig 3.7 shows the electrical field inside the cylindrical gel at different temperatures. Compared with the results in Fig 3.5 and Fig 3.6, the results presented in Fig 3.6 are similar to those in Fig 3.6 instead of Fig 3.5. Therefore, inside the temperature range specified in Table 3.1, the effects of changing loss factor on electrical field are more significant than the effect of changing dielectric constant.

Conclusions

In this study, we have developed a numeric model to calculate the electrical or magnetic field inside a microwave irradiated food package. It employed a FDTD technique to solve the Maxwell's equations with appropriate boundary conditions. The FDTD method has several advantages over the other numerical methods. It approximates the Maxwell curl equations by explicitly using central differential equations so as to eliminate the matrice inversions and significantly reduce the simulation time. In addition,

66

it intrinsically keeps the field continuity along the media boundaries so that it is trivial to apply the same FDTD model to different food packages by assigning the proper dielectric properties in each computational grid. To truncate the lattice and still keep it invisible to the out-going waves, a second-order ABC was used in this paper. It simulated the wave propagation on the lattice boundaries with insignificant artifactitious wave reflections from all directions. When compared with analytical solutions, the numeric model presented an acceptable accuracy. However, the numeric errors are inevitable and mainly results from the fact of discretization in time and space (Taflove, 1998; Taflove and Brodwin, 1975b; Yee, 1966).

The proposed model was illustrated by a two-dimensional geometry. The calculated electrical fields were presented to show the effect with different dielectric properties. It provided an indication how the electromagnetic field responded to the variant of constitute parameters. For microwave heating applications, it is desirable to have a thermal model to explicitly calculate the temperature response to electrical field in each time step.

Acknowledgement

References

Ayoub, J., Berkowitz, D., Kenyon, E., & Wadsworth, C. (1974). Continuous microwave sterilization of meat in flexible pouches. *Journal of food science* 39, 303-313.

Balanis, C. A. (1982). *Antenna theory: analysis and design*, John Wiley & Sons, New York

Balanis, C. A. (1989). *Advanced engineering electromagnetics*, John Wiley & Sons, New York.

Barratt, L., & Simons, D. (1992). Experimental validation of a computer simulation of microwave heating. *in Proc. 27th Microwave Power Symp*, 118-122.

Bows, J., Patrick, M. L., Dibben, D. C., & Metaxas, A. C. (1997). Computer simulation and experimental validation of phase controlled microwave heating. *presented at the 6th Microwave and High Frequency Heating Conference*, Fermo, Italy.

Buffler, C. R. (1993). *Microwave cooking and processing*, Van Nostrand Reinhold, NY. USA.

Burfoot, D., Griffin, W., & James, S. (1988). Microwave pasteurization of prepared meals. *Journal of Food Engineering*, 8, 145-156.

Burfoot, D., Railton, C. J., Foster, A. M., & Reavell, R. (1996). Modelling the pasteurization of prepared meal with microwave at 896MHz. *Journal of Food Engineering*, 30, 117-133.

Campbell, G. S., Calissendorff, C., & Williams, J. H. (1991). Probe for Measuring Soil Specific-Heat Using a Heat-Pulse Method. *Soil Science Society of America Journal*, 55(1), 291-293.

Carson, J. R. (1929). Reciprocal theorems in radio communication. *Proc. IRE*, 17, 952-956.

Chen, H., Tang, J., & Liu, F. (2007a). Coupled simulation of an electromagnetic heating process using the Finite Difference Time Domain method *Journal. of Microwave Power and Electromagnetic Energy*, 41(3), 50-68.

Chen, H., Tang, J., & Liu, F. (2007b). Simulation model for moving food packages in microwave heating processes using conformal FDTD method. Accepted by *to Journal of Food Engineering*.

Clemens, J., & Saltiel, G. (1995). Numerical modeling of materials processing in microwave furnaces. *International Journal of Heat and Mass Transfer*, 39(8), 1665-1675.

Cook, H. F. (1952). A physical investigation of heat production in human tissues when exposed to microwaves. *Brit. J. Appl. Phys.*, 3, 1-6.

Curtis, J. M. (1999). Experimental verification for microwave processing of materials in a single mode rectangular resonant cavity., Virginia Polytechnic Institute and State University, Blacksburg, VA, USA.

DeCareau, R. (1985). *Microwaves in the food processing industry*, Academic press, Inc. NY. USA.

Desmarais, R., & Breuereis, J. (2001). How to select and use the right temperature sensor. *Sensor*, 18(1).

Dibben, D. C., & Metaxas, A. C. (1994a). Experimental verification of a finite element solution to heating problems in a multi-mode cavity. *in Proc. 2nd Int. Conf. Computation in Electromagnetics*, Nottingham, UK 135-137.

Dibben, D. C., & Metaxas, A. C. (1994b). Finite-Element Time-Domain Analysis of Multimode Applicators Using Edge Elements. *Journal of Microwave Power and Electromagnetic Energy*, 29(4), 242-251.

Eves, E. E., Kopyt, P., & Yakovlev, Y. Y. (2004). Determination of complex permittivity with neural networks and FDTD modeling. *Microwave and Optical Technology Letters*, 40(3), 183-188.

Giese, J. (1992). Advances in microwave food processing. *Food Technol.*, 46, 118-123.

Guan, D. (2003). Thermal processing of hermetically packaged low-acid foods using microwave-circulated water combination (MCWC) heating technology. Ph. D. Dissertation: Washington State University, Pullman, WA, USA.

Guan, D., Cheng, M., Wang, Y., & Tang, J. (2004). Dielectric properties of mashed potatoes relevant to microwave and radio-frequency pasteurization and sterilization processes. *Journal of Food Science*, 69(1), E30-E37.

Guan, D., Gray, P., Kang, D. H., Tang, J., Shafer, B., Ito, K., Younce, F., & Yang, C. S. (2003). Microbiological validation of microwave-circulated water combination heating technology by inoculated pack studies. *J. Food Sci.*, 68(4), 1428-1432.

Guan, D., Plotka, V., Clark, S., & Tang, J. (2002). Sensory evaluation of microwave treated macaroni and cheese. *Journal of Food Process. Preserv.*, 26, 307-322.

Guru, B. S., & Chen, K. M. (1976). A computer program for calculating the induced EM field inside an irradiated body. *Dept. of Electrical Engineering and System Science*, Michigan State Univ., East Lansing, MI 48824.

Guy, A. W., Lin, J. C., Kramar, P., & Emery, A. F. (1974). Measurement of absorbed power patterns in the head and eyes of rabbits exposed to typical microwave sources. *Proc. 1974 Conf. Precision Electromagnetic Measurements (London, England)*, 255-257.

Gwarek, W. K., Celuch-Marcysiak, M., Sypniewski, M., & Wieckowski, A. (1999). *QuickWave-3D Software Manual*, QWED, Warsaw, Porland.

Harlfinger, L. (1992). Microwave sterilization. *Food Technol.*, 46(12), 57-60.

Harms, P. H., Chen, Y., Mittra, R., & Shimony, Y. (1996). Numerical modeling of microwave heating systems. *Journal of Microwave Power and Electromagnetic Energy*, 31(2), 114-121.

Harms, P. H., Lee, J. F., & Mittra, R. (1992). A Study of the Nonorthogonal Fdtd Method Versus the Conventional FDTD Technique for Computing Resonant Frequencies of Cylindrical Cavities. *IEEE Transactions on Microwave Theory and Techniques*, 40(4), 741-746.

Harrington, R. F. (1959). On Scattering by large conducting bodies. *IRE Trans. Antennas Propagate*, AP-7(2), 150-153.

Harrington, R. F. (1961). *Time-Harmonic Electromagnetic Fields*, McGraw-Hill, New York.

Harrington, R. F. (1967). Matrix methods for field problems. *Proc. IEEE*, 55(2), 136-149.

Harrington, R. F. (1968). *Field Computation By Moment Methods* Macmillan, New York.

Harrington, R. F. (1992). *Origin and development of the method moments for field computation*, Computational electromagnetics, New York: IEEE Press.

Hayt, W. H., & Kimmerly, J. E. (1978). *Engineering Circuit Analysis*, 3rd ed., McGraw-Hill, New York,

Hilderbrand, F. B. (1962). *Advanced Calculus for Applications*, Prentice-Hall, Englewood Cliffs, N. J.

Holland, R. (1993). Pitfalls of Staircase Meshing. *Ieee Transactions on Electromagnetic Compatibility*, 35(4), 434-439.

Huygens, C. (1690). Traite de la lumiere. Translated into English by Thompson, S. P., London, 1919 and reprinted by the University of Chicago press, Chicago, IL.

Incropera, F. P., & DeWitt, D. P. (2001). *Introduction to heat transfer, 4th*, John Wiley & Sons, NY, USA.

Jones, D. S. (1964). *The theory of electromagnetism*, New York: Macmillan, pp. 450-452.

Jurgens, T. G., Taflove, A., Umashankar, K., & Moore, T. G. (1992). Finite-Difference Time-Domain Modeling of Curved Surfaces. *IEEE Transactions on Antennas and Propagation*, 40(4), 357-366.

Kalhori, S., Elander, N., Svennebrink, J., & Stone-Elander, S. (2003). A re-entrant cavity for microwave-enhanced chemistry. *J. Microwave Power & Electromagnetic Energy*, 38(2), 125-135.

Kastner, R., & Mittra, R. (1983). A new stacked two-dimensional spectral iterative technique (SIT) for analyzing microwave power deposition in biological media. *IEEE Trans Micro. Theo. Tech.*, MTT-31(1), 898-904.

Kim, H. J., & Taub, I. A. (1993). Intrinsic chemical markers for Aseptic processing of particulate foods. *Food Technol.*, 47(1), 91-97.

Kim, H. J., Taub, I. A., Choi, Y. M., & Prakash, A. (1996). Principles and applications of chemical markers of sterility in high-temperature-short-time processing of particular foods, Washington, D.C. 54-69.

Komarov, V. V., & Yakovlev, Y. Y. (2003). Modeling control over determination of dielectric properties by the perturbation technique. *Microwave and Optical Technology Letters*, 39(6), 443-446.

Kong, J. A. (1981). *Research Topics in Electromagnetic Theory*, New York: John Wiley, pp: 290-355.

Kopyt, P., & Celuch-Marcysiak, M. (2003). Coupled electromagnetic and thermal simulation of microwave heating process. *Proc. 2nd Intern. Workshop on Information Technologies and Computing Techniques for the Agro-Food Sector*, Barcelona, Spain, November-December, 2003, 51-54.

Kraus, J. D., & Carver, K. R. (1973). Electromagnetics. 464-467. McGraw-Hill, New York.

Kunz, K. S., & Lee, K. M. (1978). A Three-Dimensional Finite-Difference solution of the external response of an aircraft to a complex transient EM environment: part I – the method and its implementation. *IEEE Trans. Electromagnetic Compatibility*, EMC-20(2).

Lau, M. H. (2000). Microwave heating uniformity in model food systems. From *Microwave pasteurization and sterilization of food products*. Ph.D. Dissertation: Washington State University, Pullman, WA, USA.

Lau, M. H., Tang, J., Taub, I. A., Yang, T. C. S., Edwards, C. G., & Mao, R. (2003). Kinetics of chemical marker formation in whey protein gels for studying microwave sterilization. *Journal of Food Engineering*, 60(4), 397-405.

Lau, R. W. M., & Sheppard, R. J. (1986). The modelling of biological systems in three dimensions using the time domain finite-difference method: part I. The implementation of the model. *Phys. Med. Biol*, 31(11), 1247-1256.

Leo, R. D., Cerri, G., & Mariani, V. (1991). TLM techniques in microwave ovens analysis: Numerical and experimental results. *in Proc. 1st Int. Conf. Computation in Electromagnetics*, London, 361-364.

Livesay, D. E., & Chen, K. M. (1974). Electromagnetic fields induced inside arbitrary shaped biological bodies. *IEEE Trans Micro. Theo. Tech.*, MTT-22(12), 1273-1280.

Lorenson, C. (1990). The why's and how's of math modeling for microwave heating. *Microwave World*, 11(1), 14-23.

Ma, L. H., Paul, D. L., Pothecary, N., Railton, C., Bows, J., Barratt, L., Mullin, J., & Simons, D. (1995). Experimental Validation of a Combined Electromagnetic and Thermal Fdtd Model of a Microwave-Heating Process. *IEEE Transactions on Microwave Theory and Techniques*, 43(11), 2565-2572.

Madsen, N. K., & Ziolkowski, R. W. (1988). Numeric solution of maxwell's equations in the time domain using irregular nonorthogonal grids. *Wave Motion*, 10, 583-596.

McDonald, B. H., & Wexler, A. (1972). Finite-element solution of unbounded field problems. *IEEE Trans Micro. Theo. Tech.(1972 Symp, Issue)*, MTT-20, 841-847.

Mechenova, V. A., & Yakovlev, Y. Y. (2004). Efficiency optimization for systems and components in microwave power engineering. *J. Microwave Power & Electromagnetic Energy*, 39(1), 46-60.

Meredith, R. (1998). *Engineer's handbook of industrial microwave heating*, The institution of Electrical Engineers, London, UK.

Metaxas, A. C., & Meredith, R. J. (1993). *Industrial Microwave Heating*, London, UK.

Michaelson, S. M. (1969). Biological effects of microwave exposure. *Proc. Biological Effects and Health Implications of Microwave Radiation Symp*, Med. College Virginia (Richmond), Rep. BRH/DBE 70(2), 35-58.

Mittra(Ed.), R. (1973). *Computer Techniques for Electromagnetics*, Pergamon, New York.

Moore, J., & Pizer, R. (1984). *Moment Methods in Electromagnetics*, Wiley, New York.

Mudgett, R., & Schwartzberg, H. G. (1982). Microwave food processing: Pasteurization and sterilization: A review. *AIChe Symposium Series*, 78(218), 1-11.

O'Meara, J., Farkas, D., & Wadsworth, C. (1977). Flexible pouch sterilization using combined microwave-hot water hold simulator. *Contact No. (PN) DRXNM 77-120*, U.S. Army Natick Research & Development Laboratories, Natick, MA.

Ohlsson, T. (1987). Sterilization of foods by microwaves. *International Seminar on New Trends in Aseptic Processing and Packaging of Food stuffs*, 22 Oct. 1987;Munich. SLK Report nr 564. Goteborg, Sweden: The Swedish Institute for Food and Biotechnology.

Ohlsson, T. (1990). Controlling heating uniformity - The key to successful microwave products. *Euro. Food Drink Rev.*, 2, 7-11.

Ohlsson, T. (1991). Microwave heating uniformity. *AICHE Conference on Food Engineering*, Chicago. March 11-12.

Ohlsson, T. (1992). Development and evaluation of microwave sterilization process for plastic pouches. *Paper presented at the AICHE Conference on Food Engineering*, March 11-12, Chicago, IL

Okoniewski, M. (1993). Vector wave equation 2D-FDTD method for guided wave equation. *IEEE Micro. Guided Wave Lett.*, 3(9), 307-309.

Osepchuck, J. M. (1984). A history of microwave heating applications. *IEEE Trans. Microwave Theory Tech*, MTT-32, 1200-1224.

Palombizio, P., & Yakovlev, Y. Y. (1999). Parallel worlds of microwave modeling and industry: a time to cross? *Microwave World*, 20(2), 14-19.

Pandit, R. B., Tang, J., Liu, F., & Mikhaylenko, M. (2007a). A computer vision method to locate cold spots in foods in microwave sterilization processes. *Pattern Recognition*, 40, 3667-3676.

Pandit, R. B., Tang, J., Liu, F., & Pitts, M. (2007b). Development of a novel approach to determine heating pattern using computer vision and chemical marker (M-2) yield. *Journal of Food Engineering*, 78(2), 522-528.

Pandit, R. B., Tang, J., Mikhaylenko, G., & Liu, F. (2006). Kinetics of chemical marker M-2 formation in mashed potato - A tool to locate cold spots under microwave sterilization. *Journal of Food Engineering*, 76(3), 353-361.

Paoloni, F. (1989). Calculation of power deposition in a highly overmoded rectangular cavity with dielectric loss. *Journal of Microwave Power and Electromagn. Energy*, 24(1), 21-32.

Pathak, S., Liu, F., & Tang, J. (2003). Finite difference time domain(FDTD) characterization of a single mode applicator. *J. Microwave Power EE*, 38(1), 37-48.

Prakash, A., Kim, H. J., & Taub, I. A. (1997). Assessment of microwave sterilization of foods using intrinsic chemical markers. *Journal of Microwave Power and Electromagnetic Energy*, 32(1), 50-57.

Richmond, J. H. (1965). Digital computer solutions of the rigorous equations for scattering problems. *Proc. IEEE*, 53, 796-804.

Ruello, J. H. (1987). Seafood and microwaves: some preliminary observations. *Food Technol.in Australia.*, 39, 527-530.

Ryynanen, S., & Ohlsson, T. (1996). Microwave heating uniformity of ready meals as affected by placement, composition, and geometry. *Journal of Food Science*, 61(3), 620-624.

Sadiku, M. N. O. (2000). *Numerical Techniques in Electromagnetics*, 2 ed., CRC, NYC.

Sadiku, M. N. O. (2001). *Elements of Electromagnetics*, 3 ed., Oxford University Press, New York.

Schelkunoff, S. A. (1936). Some equivalence theorems of electromagnetics and their application to radiation problems. *Bell System Tech. J.*, 15, 92-112.

Schiffmann, R. (1990). Problems in standardizing microwave over performance. *Microwave World*, 11(3), 20-24.

Schwan, H. P. (1972). Microwave radiation: biophysical considerations and standards criteria. *IEEE Trans. Biomed. Eng.*, BME-19, 304-312.

Smyth, N. F. (1990). Microwave-Heating of Bodies with Temperature-Dependent Properties. *Wave Motion*, 12(2), 171-186.

Speigel, R. J. (1984). A review of numerical models for predicting the energy deposition and resultant thermal response of humans exposed to electromagnetic fields. *IEEE Trans. Microwave Theory and Techn.*, MTT-32, 730-746.

Spiegel, R. J. (1984). A review of numerical models for predicting the energy deposition and resultant thermal response of humans exposed to electromagnetic fields. *IEEE Trans. Microwave Theory and Techn.*, MTT-32, 730-746.

Stanford, M. (1990). Microwave oven characterization and implications for food safety in product development. *Microwave World*, 11(3), 7-9.

Stenstrom, L. (1972). Taming microwaves for solid food sterilization. *IMPI symposium*, Ottawa, Canada. May 24-26.

Taflove, A. (1980). Application of the finite-difference time-domain method to sinusoidal steady-state electromagnetic-penetration problems. *IEEE Trans. EM Comp.*, EMC-22(3), 191-202.

Taflove, A. (1998). Computational electrodynamics : the finite-difference time-domain method, Artech House, Boston, MA.

Taflove, A., & Brodwin, M. E. (1975a). Computation of the Electromagnetic Fields and Induced Temperatures Within a Model of the Microwave-Irradiated Human Eye. *IEEE Trans Micro. Theo. Tech.*, MTT-23(11), 888-896.

Taflove, A., & Brodwin, M. E. (1975b). Numerical solution of steady-state electromagnetic scattering problems using the time-dependent Maxwell's equations. *IEEE Micro. Theo. Tech.*, MTT-23(8), 623-630.

Taflove, A., & Umashankar, K. (1980). A hybrid moment method/finite-difference time-domain approach to electromagnetic coupling and aperture penetration into complex geometries. *IEEE Trans. Ant. Prop.*, AP-30(4), 617-627.

Taflove, A., & Umashankar, K. (1981). Solution of complex electromagnetic penetration and scattering problems in unbounded regions. *Computational methods for infinite domain media-structure interaction*, Washington, D.C: ASME, 46, 83-113.

Taflove, A., & Umashankar, K. (1990). The finite-difference time-domain method for numerical modeling of electromagnetic wave interactions. *Electromagnetics*, 10, 105-126.

Tang, J., Liu, F., Pathak, S., & Eves, G. (2006). Apparatus and method for heating objectives with microwaves. U.S. patent 7,119,313.

Thom, A., & Apelt, C. J. (1961). *Field Computations in Engineering and Physics*, D.Van Nostrand, London.

Torres, F., & Jecko, B. (1997). Complete FDTD analysis of microwave heating processes in frequency-dependent and temperature-dependent media. *IEEE Transactions on Microwave Theory and Techniques*, 45(1), 108-117.

Tsai, L. L. (1978). Moment methods in electromagnetics for undergraduates. *IEEE Trans. on Education*, E-21(1), 14-22.

Umashankar, K., & Taflove, A. (1982). A novel method to analyze electromagnetic scattering of complex objects. *IEEE Trans. EM Comp.*, EMC-24(4), 397-405.

Veronesi, P., Leonelli, C., De Marchi, G., & De Marchi, U. (2003a). Microwave assisted drying of water-based paints for wood. In: *Proc. 9th AMPERE Conf. on Microwave and High Frequency Heating, 169-172. Loughborough, U.K.*

Veronesi, P., Leonelli, C., Siligardi, C., & Sglavo, V. M. (2003b). Microwave assisted strengthening of soda-lime glasses. In: *Proc. 9th AMPERE Conf. on Microwave and High Frequency Heating, 67-70. Loughborough, U.K.*

Watanabe, W., & Ohkawa, S. (1978). Analysis of power density distribution in microwave ovens. *Journal of Microwave Power and Electromagnetic Energy*, 13(2), 173-182.

Webb, J. P., Maile, G. L., & Ferrari, R. L. (1983). Finite element solution of three dimensional electromagnetic problems. *IEEE Proceedings*, 130(2), 153-159.

Wu, T. K., & Tai, L. L. (1974). Numerical analysis of electromagnetic fields in biological tissues. *Proc. IEEE(Lett.)*, 62, 1167-1168.

Wylie, C. R. (1960). *Advanced Engineering Mathematics*, McGraw-Hill, New York.

Yakovlev, Y. Y. (2001). Improving quality of microwave heating by packaging - analytical approach. *The 2001 ASAE Annual Meeting, Sacramento, CA, Paper 01-6149*.

Yakovlev, Y. Y. (2004). Optimization of reflection and transmission characteristics of a waveguide window. In: *Proc. 4th World Congress on Microwave & Radio Frequency Applications, 172-174. Austin, TX*.

Yakovlev, Y. Y., & Murphy, E. K. (2004). FDTD-backed reconstruction of complex permittivity with neural networks. In: *Proc. 6th Seminar "Computer Modeling & Microwave Power Industry", 40-46. Austin, TX*.

Yee, K. S. (1966). Numerical solution of initial boundary-value problems involving Maxwell's equations in isotropic media. *IEEE Trans. Ant. Prop.*, AP-14, 302-307.

Z.Shou-Zheng, & C.Han-Kui (1988). Power distribution analysis in rectangular microwave heating applicator with stratified load. *Journal of Microwave Power and Electromagn. Energy*, 23(3), 139-143.

Zhang, H., & Datta, A. K. (2000). Coupled electromagnetic and termal modeling of microwave oven heating of foods. *Journal of Microwave Power and Electromagnetic Energy*, 35(2), 71-85.

Chapter 4 Coupled Simulation of an Electromagnetic Heating Process Using the Finite Difference Time Domain Method

Abstract

Due to the complexity of interactions between microwaves and food products, a reliable and efficient simulation model can be very useful tool to guide design of microwave heating systems and processes. This research developed a model to simulate coupled phenomena of electromagnetic heating and conventional heat transfer by combining commercial electromagnetic software with a customer built heat transfer model. Simulation results were presented and compared with experimental results for hot water and microwave heating in a single mode microwave system at 915 MHz. Good agreement was achieved, showing that this model was able to provide insight into industrial electromagnetic heating processes.

Index— FDTD, Temperature, Heat transfer, Electromagnetic heating

Introduction

Electromagnetic (EM) heating has attracted much attention for food application research because, unlike conventional heating, EM heating generates heat within food packages leading to higher heating rates and reduced heating processes (Osepchuck, 1984). Several studies with pilot-scale systems have demonstrated the possibilities for short time microwave sterilization processes to produce safe and high quality low-acid shelf-stable packaged foods (Guan, et al., 2003; Guan, et al., 2002). The main focuses of most recent research activities related to the development of novel thermal processing technologies based on microwave energy were to improve heating uniformity and develop processes with stable heating performance for industrial implementation. But EM fields inside a microwave cavity, governed by Maxwell's equations, are not uniform. Interactions between the cavity and load produce "hot spots" and "cold spots" within the heated object. If not given adequate time, these hot and cold spots cause severe temperature non-uniformity, adversely affecting product quality (Ma, et al., 1995). It is desirable to develop an effective numeric model to reliably simulate EM heating processes so that temperature distributions, especially the location of hot and cold spots, could be identified within commercial industrial heating systems as the first step in continuing efforts to improve heating uniformity. The numeric model should include solutions for two separate sets of partial differential equations that govern, respectively, propagation of EM waves and transfer of thermal energy generated by EM heating. These two sets of equations are in reality coupled with the heating progresses, because heat transfer due to the gradients generated by localized EM heating alters the dielectric properties of food, which in turn affect the EM field distribution.

Solving these coupled equations for a three-dimensional (3-D) transient EM heating process in an industrial system for foods with temperature-dependent dielectric properties is a challenging task that has not been addressed in the literature. Early researches used analytical models to describe EM fields inside domestic microwave ovens (Watanabe and Ohkawa, 1978; Z.Shou-Zheng and C.Han-Kui, 1988), but these were suitable only for oversimplified cases that did not represent real-world systems. Numeric models were developed for EM field distribution calculations in more complicated cases (Paoloni, 1989; Webb, et al., 1983). Coupled EM and heat transfer models were used for simple 1-D (Smyth, 1990) or 2-D cases (Barratt and Simons, 1992; Clemens and Saltiel, 1995). Detailed 3-D treatment of numeric models for coupled equations has not been explored until recently (Bows, et al., 1997; Burfoot, et al., 1996; Clemens and Saltiel, 1995; Dibben and Metaxas, 1994b; Harms, et al., 1996).

Several numerical techniques have been used to solve coupled Maxwell and heat transfer equations using the Finite Difference Time Domain (FDTD) method (Ma, et al., 1995; Torres and Jecko, 1997), Finite Element Method (Dibben and Metaxas, 1994a, 1994b; Webb, et al., 1983) and Transmission Line Method (Leo, et al., 1991). Spiegel(1984) reviewed numeric methods for medical applications and commented that the FDTD method is best suited for coupled EM and thermal processes because it does not require matrix computation, and thus saves computer memory and simulation time. However, a major limitation of the FDTD method is the use of rectangular meshes that are not applicable for irregular geometries such as curvature surfaces. The Finite Element Method (FEM) can handle more complex geometries. Zhang and Datta (2000) used two commercial software employing FEM together to simulate coupled EM and thermal

processes in a domestic oven. But FEM involves computation to inverse matrices that contain information for all elements of the discrete grids within the considered domain. This requires large computer memory and lengthy computation time, making it unsuitable for complicated systems.

A major development in FDTD applications with EM field simulation is the use of a conformal FDTD algorithm. This algorithm incorporates finite boundary grids that conform to geometry surfaces to accurately match detailed irregularities in a 3-D domain, while also including regular grids identical to those in the original FDTD algorithm for the other parts of the 3-D domain. Holland (1993) and Harms, et al. (1992) provide a detailed description of a conformal FDTD algorithm and its application to some simple cases. In brief, instead of Yee's original algorithm that uses differential forms of Maxwell's equations, the conformal FDTD algorithm uses integral forms of Maxwell's equations for the finite grids conformed to the edge or surface of the geometry, thus avoiding the need to approximate the curved and oblique surface using staircase grid. As a result, complex geometry can be modeled without sacrificing the speed of an FDTD algorithm. This method also saves computer memory and simulation time compared to the original FDTD algorithm when applied to complex geometries. The conformal FDTD algorithm can be used to model arbitrary shape structures and inhomogeneous, nonlinear, dispersive and loss mediums. Since the FDTD method does not require computation of inverse matrices which takes extensive computer memory for fine element grids, the conformal FDTD algorithm is much more efficient compared to the FEM. For example, for the model developed by Zhang and Datta (2000), it took six and half hours for an HP workstation to run a model consisting of 15,000 nodes for a single time step, while the

conformal FDTD used in the study reported here took only three hours to complete a coupled simulation that included 720 time steps for a complicated industrial system with 500,000 cells in a 3-D domain.

This paper presents a model that used conformal FDTD algorithms for EM field simulation and the regular FDTD method for heat transfer to simulate coupled processes in an EM heating system for industrial sterilization and pasteurization applications.

Experimental methods

Experimental set-up

Validation is a critical step in developing a new and reliable numeric model. In this study, this was achieved with a single-mode microwave sterilization system developed at Washington State University. The system consisted of a rectangular cavity with one horn-shaped applicator on the top and another identical applicator on the bottom (Fig 4.1 and Fig 4.2). Fig 4.1 shows a front view of the system with an exposed interior cut and vertical central plane, while Fig 4.2 shows the top view for the central section of the cavity. Microwave energy was provided by a 5 kW generator operating at 915 MHz through a standard waveguide that supported only TE_{10} mode (Fig 4.3). Fig 4.3 provides detailed information for the top and bottom rectangular waveguide sections having a length of 128mm and width of 124mm. After passing through a circulator, the microwave energy was equally divided at a T-junction and fed to the two horn applicators through two standard waveguides shown in Fig 4.3. The length of each leg of the waveguide after the T-junction could be adjusted to control the phase difference between the microwaves at the entry port of the two horn applicators, which meant the phase shift between the two waves interacting inside the cavity could be controlled to achieve the desired field

distribution. In this study, for simplification, a 0 phase shift was used between the entry ports of the top and bottom horn applicators. That was, microwaves coming to the top and the bottom entry ports of the horn applicators were in the same phase at any moment. The model, however, was able to simulate more complex cases with arbitrary phase differences.

The pilot scale system combined surface heating by circulating hot water and volumetric EM heating to improve heating uniformity and reduce heating time. Because microwave sterilization for low-acid foods (pH > 4.5) (Guan, et al., 2003) requires that food temperatures at cold spots be processed higher than 121˚C, the temperature of the circulation water in the cavity was set at 125˚C. The water was pressurized at 27 Pa by compressed air through a buffer tank in the water-circulating system (not shown) to prevent boiling. To maintain the steam inside the cavity, two windows made of microwave transparent material were secured at the mouth of both horn waveguides. During thermal processing, the packaged food was positioned at the central line of the cavity. Though it was possible to simulate a heating process with moving packages, only a simple stationary case was considered to better focus on the development and validation of the numeric model.

Temperature history and heating pattern determination

During the experiment, three fiber optic sensors (FOT-L, FISO, Québec, CANADA) were placed at three different points (within the cold and hot spots) to monitor the temperature changes with time. In addition to monitoring temperature changes at selected locations in the packaged foods, heating patterns were measured with the computer vision software IMAQ (National Instruments, TX, USA) using a chemical

marker method (Pandit, et al., 2007b). This method measures color changes as a result of the formation of a chemical compound commonly referred to as M-2, a product of a Millard reaction between protein amino acids and a reduced sugar (ribose). The color changes depend upon heat intensity at temperatures beyond 100°C and, therefore, served as an indicator of temperature distribution after heating. Detailed information about the kinetics of M-2 formation with temperature can be found elsewhere (Lau, et al., 2003; Pandit, et al., 2006). In brief, with increasing temperature during the heating process, the density of M-2 also increased following an Arrhenius relationship with temperature and first order kinetics with time. The density of M-2 was then transferred to pixel density, which was further mapped into red, green, and blue (RGB) values, where red indicates the hottest area and blues the coldest.

Experimental procedures

Whey protein gels (78% water, 20% protein, 1.7% salt, 0.3% D-ribose) were used as the model food because they have uniform properties and are easily formed. They also maintain stable shape during the process. Dielectric properties of the whey protein gels were measured with an open coaxial cable from a HP8491B dielectric probe kit connected to an HP8491B network analyzer (Hewlett-Packard, CA, USA; Table I). Thermal properties were measured with a KD2 device (Decagon, WA, USA) using the double needle method (Campbell, et al., 1991) (Table II). Table I shows dielectric property data at temperatures up to 121˚C to allow for sterilization (Guan, et al., 2004). Table II shows thermal property data only at temperatures up to 80˚C because of measurement difficulties beyond this temperature. For temperature over 80º C, thermal properties were assumed constant.

The whey protein gels were sealed in a 7 oz polymeric tray to maintain the food shape during EM heating. Prior to the experiment, six identical food trays containing whey gel slabs (95 mm x 140 mm x 16 mm) were removed from a refrigerator where they had been stored at 9°C overnight. Fiber optic sensors were inserted carefully to the locations shown in Fig 4.4 ith seals at the tray wall entry ports to prevent leakage of water. All six trays were secured in the center plane of the cavity with equal distance from the top and bottom windows of the cavity (Fig 4.1). Hot water at 125°C was filled at a speed of 40 lit/min into the cavity prior to microwave heating of the food. A uniform surrounding water temperature (125ºC) was assumed during the heating process. The thermal properties and dielectric properties were measured using the same methods as for whey protein gel.

In experiments and simulation, the gel samples were preheated with circulating pressurized water at 125°C. When the temperature at the cold spots (spot 1 or 2 measured in experiment in Fig 4.4 of the gel reached 60°C, microwave heating was started until the cold spot temperatures reached 121°C. Microwave power was then stopped, and cold tap water at 12ºC was pumped in to cool the gel packages. Temperature histories at the cold and hot spots were recorded via a data acquisition system, the heating pattern in the middle layer of the gel samples was determined using a chemical marker/computer imaging system to highlight the influence of the microwave fields. After each heating process, the gels were carefully sliced into upper and lower halves, and color images were taken of the middle layers. The intensity of the brown color was correlated with the heating intensity. The heating pattern was then obtained by mapping the pixel color intensity into an RGB value. Detailed procedures for capturing the color imaging are

provided in Pandit, et al.(2007a).
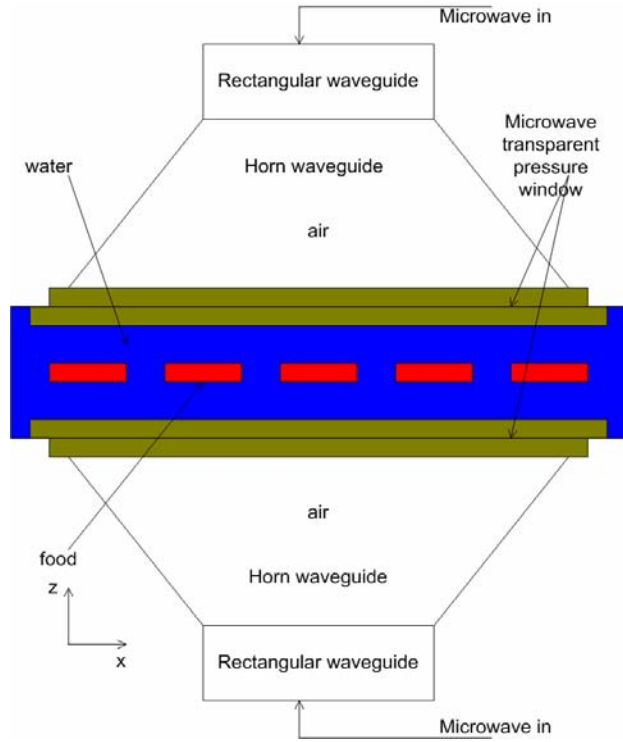
Fig 4.1 Pilot-scale EM heating system (front view).
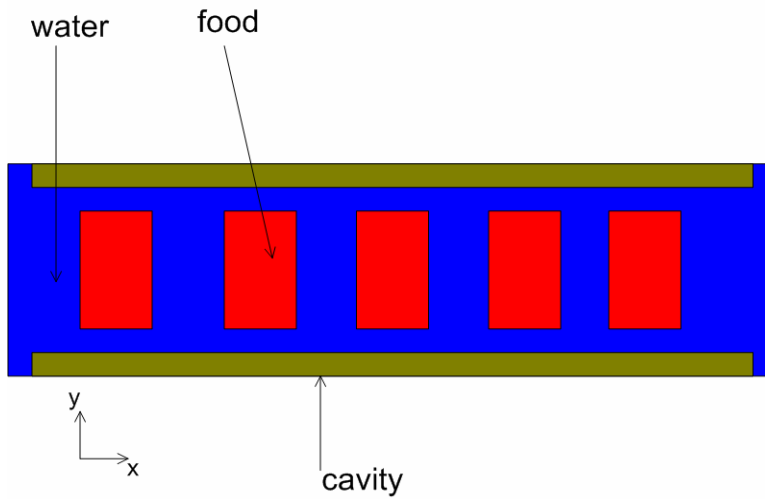
Fig 4.2. Pilot-scale microwave heating system (top view).
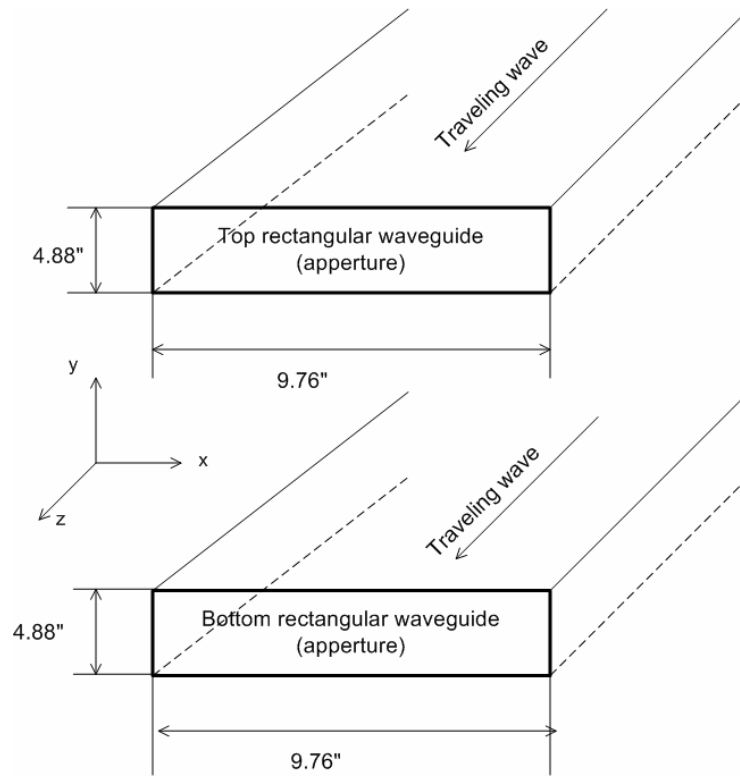
Fig 4.3 Rotate view of rectangular waveguide in Fig.1

Table 4.1 dielectric properties of whey protein gels

Temperature [°C]	Dielectric constant $\varepsilon_r' = \varepsilon'/\varepsilon_0$	Dielectric loss $\varepsilon_r'' = \varepsilon''/\varepsilon_0$
20	58.5	24.25
40	57.55	30.25
60	56.36	36.79
80	54.36	45.21
100	52.81	53.89
121	51.14	63.38

Table 4.2 Thermal properties of whey protein gels

Temperature [°C]	Volumetric specific heat $\rho c_p [MJ/m^3 K]$	Thermal conductivity $K[W/mK]$
0	3.839	0.513
20	3.973	0.537
35	3.901	0.550
50	3.814	0.561
65	3.883	0.578
80	3.766	0.588

Fig 4.4 Top view of the middle layer of a whey protein gel inside a 7 oz tray with three fiber optic sensors at hot (3) and cold spots (1 and 2).

Fundamentals for numeric modeling

Conformal FDTD method

The conformal FDTD algorithm used the time-domain integral form of Maxwell's equations for the EM field calculation:

$$\oint_C E \bullet dl = -\frac{\partial}{\partial t} \iint_S B \bullet ds \tag{1}$$

$$\oint_C H \bullet dl = \frac{\partial}{\partial t} \iint_S D \bullet ds + \iint_S (J_i + J_c) \bullet ds \tag{2}$$

$$\oiint_S D \bullet ds = Q^e \tag{3}$$

$$\oiint_S B \bullet ds = 0 \tag{4}$$

where E is the electric field, H is the magnetic field, D=εE is the electric flux density, B=μH is the magnetic flux density, Q^e is the electric charge surrounded by surface S, and μ and ε are permeability and permittivity, respectively. Permeability μ is assumed equal to the $μ_0$ constant in free space. The dielectric permittivity $ε = ε_0ε_r = ε_0(ε'_r-j\ ε''_r)$. C is a contour path surrounding the surface S, while J_i and J_c are source current density and conduction current density, respectively.

In this study, a commercial EM solver Quick-Wave 3D (QW3D) was used to solve the set of Maxwell's equations in (1)-(4). First, the computational domain was specified and the Maxwell's equations were discretized to setup the conformal FDTD algorithm. Then, the required conformal mesh with its appropriate boundary condition was constructed by a built-in mesh generator of QW3D. At last, the EM field components on each mesh grid were calculated until the steady state was established.

In the development of the model, the conformal FDTD algorithm was chosen to handle more complex geometry compared with classic Yee algorithm. The conformal FDTD method keeps all the traits introduced by standard FDTD approach, including mathematical manipulation, short simulation time and small memory usage. It also simulate curvature surface accurately by deforming the cells intersected by surface instead of using staircase grids in standard FDTD approach. Since the deformation only happens on the surfaces while the grid layer inside the simulated geometry is still same as that in standard FDTD approach, it does not introduce too much computational overhead compared with the standard one. In Fig 4.5 and Fig 4.6, a remarkable improvement was observed on 3-D and 2-D modeling of a sphere (Gwarek, et al., 1999).
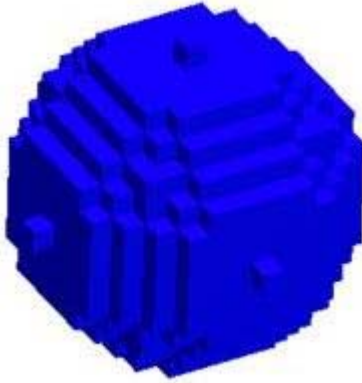
(a)
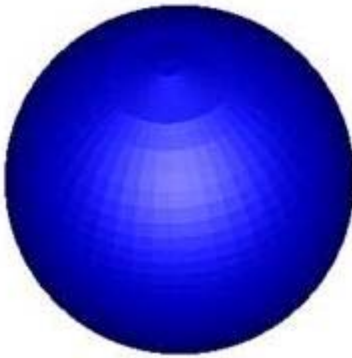
(b)

Fig 4.5 Sphere modeled by FDTD approach.(Gwarek, et al., 1999):

(a) classic method; (b) conformal method
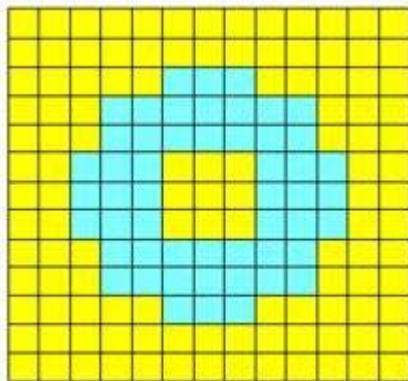
(a)
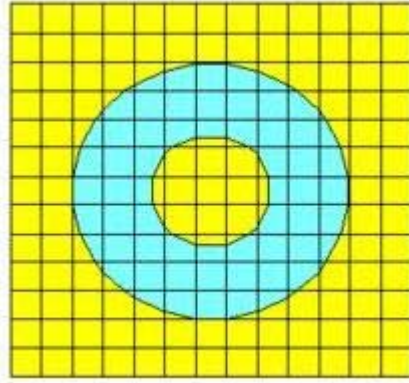
Fig 4.6 Circular modeled by FDTD approach.(Gwarek, et al., 1999):

(a) classic method; (b) conformal method

Finite difference equations for EM fields

Discretization of Maxwell's equations in the integral form was obtained by computing the field components (E, H) at discrete nodes (Taflove, 1998):

$$H_z^{n+\frac{1}{2}}(i+\frac{1}{2},j+\frac{1}{2},k)=H_z^{n-\frac{1}{2}}(i+\frac{1}{2},j+\frac{1}{2},k)-\frac{\Delta t}{\mu}\begin{bmatrix}\frac{1}{\Delta y_j}\left(E_x^n(i+\frac{1}{2},j+1,k)-E_x^n(i+\frac{1}{2},j,k)\right)\\-\frac{1}{\Delta x_i}\left(E_y^n(i+1,j+\frac{1}{2},k)-E_y^n(i,j+\frac{1}{2},k)\right)\end{bmatrix} \qquad (5)$$

$$E_z^{n+1}(i,j,k+\frac{1}{2})=E_z^n(i,j,k+\frac{1}{2})+\frac{\Delta t}{\varepsilon}\begin{bmatrix}\frac{1}{h_{y_j}}\left(H_x^{n+\frac{1}{2}}(i,j+\frac{1}{2},k+\frac{1}{2})-H_x^{n+\frac{1}{2}}(i,j-\frac{1}{2},k+\frac{1}{2})\right)\\-\frac{1}{h_{x_i}}\left(H_y^{n+\frac{1}{2}}(i+\frac{1}{2},j,k+\frac{1}{2})-H_y^{n-\frac{1}{2}}(i-\frac{1}{2},j,k+\frac{1}{2})-J_{iz}^{n+\frac{1}{2}}(i,j,k+\frac{1}{2})\right)\end{bmatrix} \qquad (6)$$

where Δx_i and Δy_j denote the cell size in x and y directions and *i, j,* and *k* denote the index numbers for numeric computation in x, y, and z directions, respectively. Δt denotes the time step in simulation. The ½ appeared in the equations because of the leapfrog structure for the FDTD mesh. The $J_{iz}^{n+\frac{1}{2}}(i,j,k+\frac{1}{2})$ in (6) was the z component of source current J_i at node (i, j, k+½), which is only involved in the computation where the

input source was specified. Equations (5) and (6) only gave part of Maxwell's equations in their integral forms. The updated equations for other field components could be obtained similarly by shifting i, j, and k clockwise in (5) and (6) to get the components in x, y, and z directions, respectively (Taflove, 1998).

The presentation of Δx_i, Δy_j, and Δz_k (in difference equations for other field components not presented here) provides the possibility for using non-uniform mesh so that the grids can conform to the curvature surface. For the leapfrog arrangement, the h_{x_i}, h_{y_j} and h_{z_k} were defined as in (Taflove, 1998):

$$h_{x_i} = (\Delta x_i + \Delta x_{i-1})/2, \quad h_{y_j} = (\Delta y_j + \Delta y_{j-1})/2, \quad h_{z_k} = (\Delta z_k + \Delta z_{k-1})/2 \qquad (7)$$

By numerically solving the above equations, the E and H fields were obtained so that the dissipated power per unit volume $\dot{q}(r,T)$ inside the food could be easily determined. Here r denotes that the dissipated power per unit volume is a spatial dependent variable. In fact, $\dot{q}(r,T)$ was determined from the root mean square value of the electrical field E_{rms}:

$$E_{rms}^2 = \frac{\int_V (\vec{E}^* * \vec{E})dV}{2V} \qquad (8)$$

$$\dot{q}(r,T) = 2\pi\varepsilon_0 f E_{rms}^2 \varepsilon_r''(r,T) \qquad (9)$$

Finite difference equations for thermal fields

One important unique feature in EM heating is that the dielectric properties change with temperature. Therefore, after calculating E and H by solving the integral

form of Maxwell's equations numerically, temperature responses to the EM fields must be calculated by solving the heat transfer equation.

Heat conduction took place inside food package while on the boundary a convective boundary condition was applied to take into account the effect of circulating water in the system. QW3D contains a built-in Basic Heating Module (BHM) that can be used to calculate temperature response of heat conduction. But it only allows adiabatic boundary condition on the surface between two different mediums, which, apparently, does not satisfy our needs. Therefore, a thermal model was developed to consider convective heat transfer boundary conditions.

The heat transfer equation and its boundary condition are presented in the following equations (Incropera and DeWitt, 2001):

$$\rho(T)c_p(T)\frac{\partial T}{\partial t} = \nabla \cdot (K(T)\nabla T) + \dot{q}(r,T) \tag{10}$$

$$q = hA(T_s - T) \tag{11}$$

where $K(T)$ is thermal conductivity at temperature T, $\rho(T)$ is mass density at temperature T, $c_p(T)$ is specific heat at temperature T, q is thermal energy exchanged between food and water on the boundary, h is the heat transfer coefficient of $220\text{Wm}^{-2}\text{k}^{-1}$, A is the boundary surface area, and T_s is surrounding temperature. Here we assume that $K(T)$ is isotropic so that its subscript for spatial variable was dropped in (10).

To use the same mesh generated for the EM field calculation, the heat transfer equation was also solved numerically with the FDTD method. Away from the surface, since only heat conduction took place, its finite difference form is:

$$T^{n+1}(i,j,k) = (1-12F_0)*T^n(i,j,k) + F_0[T^n(i-1,j,k) + T^n(i+1,j,k)$$

$$+ T^n(i,j-1,k) + T^n(i,j+1,k) + 4T^n(i,j,k-1) + 4T^n(i,j,k+1)] + \frac{\dot{q}(i,j,k)\Delta t}{\rho c_p} \quad (12)$$

where $F_0 = \frac{\alpha \Delta t}{\Delta x^2}$ and $i, j,$ and k have the same meaning as the finite difference form of the

EM field. For simplification, $\Delta x = \Delta y = 2\Delta z$ was used for all the finite difference equations

for illustration purpose.

At the food surface, both heat conduction between interior nodes and convection

between food and water happened at the same time, hence the finite difference form of

the heat transfer equation was slightly modified on the surface nodes by replacing the

conduct terms in (12) with the corresponding convective terms. For example, for the

nodes on the surface plane vertical to the z-plane, the boundary condition from (11) can

be written:

$$q = h*\Delta x*\Delta y*[T_s - T(i,j,k,n)] \quad (13)$$

The conduction term $[T(i,j,k+1,n) - T(i,j,k,n)]*K*\Delta x$ was replaced by (13) for the

corresponding surface nodes.

Numeric model

An EM solver QW3D was used to compute the field components using finite

difference equations such as those in equations (5) and (6). Before computer simulation

was conducted, the desired microwave propagation mode was set up, which included

specifying the excitation type, input power and boundary condition that represented the

simulated physical system. Since gel movement was not considered, the whole industrial

EM heating system was treated as a metal box with a Perfect Electrical Conductor

boundary condition on the surface. Because it worked at 915 MHz, the only propagation

wave in TE_{10} mode propagated through a rectangular waveguide on the top and bottom via an electrical field with E_y as its only component (Balanis, 1989). A 915 MHz sine wave was used as an excitation, with its amplitude determined from the input power. Front and top views of the numeric model are shown in Fig 4.7.
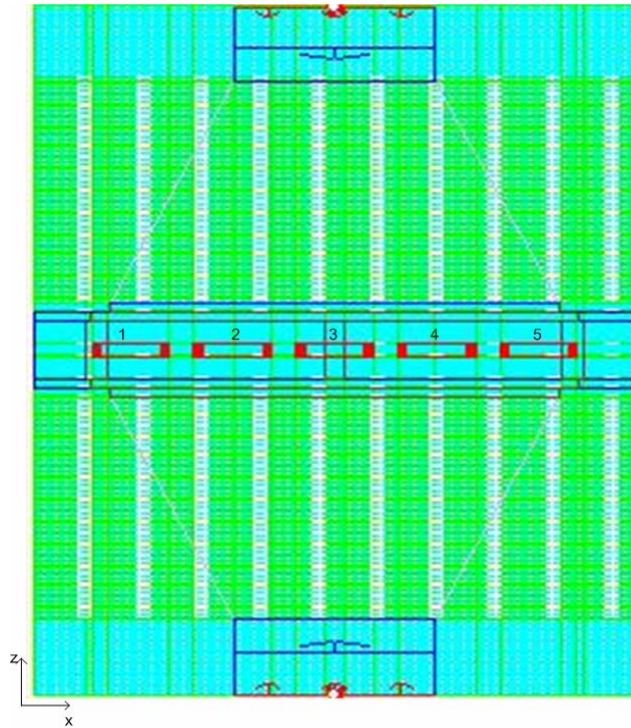
Fig 4.7. Geometry of the EM heating system with five identical trays (front view, middle layer)
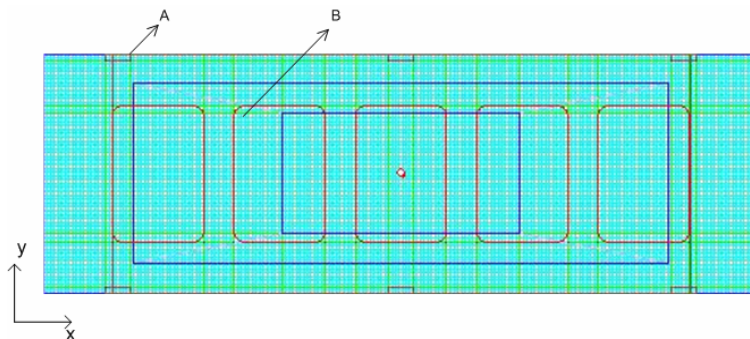
Fig 4.8 Geometry of the EM heating system with five identical trays (top view)

In QW3D, it was possible to define physical geometry in a user defined object as a parameterized macro. The macro defined the physical geometry and settings for the EM field discussed in the last paragraph and formed the basis of the EM model. A heat transfer model using explicit finite difference equations such as (12) and (13) was also required to calculate the temperature response to the EM field. The mesh for EM field calculation in QW3D was kept in an external file for use in the heat transfer model, which saved computer memory and computation time because the numeric model did not need extra adaptation to the computational grids for temperature calculation. The EM model was then coupled with a customized thermal model by defining a script to communicate QW3D with an external heat transfer program and exchange data between them. The dissipated power per unit volume was thus calculated by QW3D and then used in the heat transfer model to calculate the temperature information.

The electromagnetic field intensity was calculated in the order of nanoseconds while the thermal response in the order of seconds. At a specific heat transfer time step, EM field was obtained by QW3D, the corresponding dissipated power was then used as the heating source for heat transfer calculation. Between each heat transfer time step, the dissipated power in each cell was assumed to be constant. Because of the temperature-dependent dielectric properties of food, after every heat transfer time step, new dielectric properties were calculated from Table 4.1 and then fed back to QW3D for the EM calculation of the next heat transfer time step. This coupled calculation loop did not end until the required heating time was reached. Fig 4.9 summarizes the above simulation schema for the coupled model. The node transformation process shown in Fig 4.9 was

used to exchange the data between computational nodes for power and computational nodes for temperature, which will be discussed in detail in the next section.
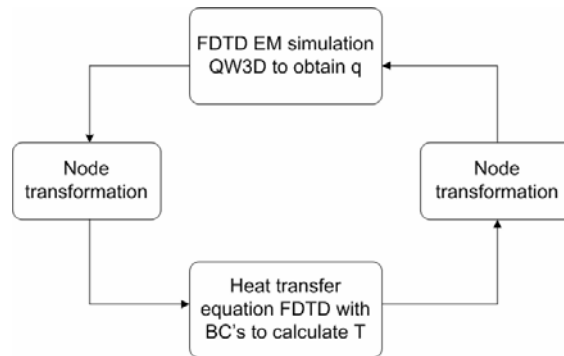
Fig 4.9 Numeric schema for coupled simulation of the EM heating process

Communication algorithm

QW3D allowed the whole computed domain to be discarded and the dissipated power extracted at the place occupied by the gel. This dramatically decreased the size of the data set handled by the heat transfer model and therefore greatly reduced the simulation time. After obtaining the temperature distribution during the period when the EM power dissipated inside the gel, new dielectric properties were calculated with a linear interpolation technique in QW3D. To facilitate the coupling function, the heat transfer model not only acted as a tool to calculate the temperature response to EM heating, but also served as an interface to communicate with QW3D. Special care was taken during this communication, for each single cell containing dissipated power dumped from QW3D, the power nodes were assumed to be placed in the cell centre. To avoid numeric instability, the temperature nodes needed to be placed on the corners of each cell. Because nodes for EM calculation (cells in QW3D) were different from those for heat transfer calculation, it was necessary to calculate the dissipated power associated with the temperature nodes using the following formula:

$$q_T(i,j,k) = [q(i,j,k)\Delta x_i \Delta y_j \Delta z_k + q(i-1,j,k)\Delta x_{i-1}\Delta y_j \Delta z_k$$
$$+ q(i,j-1,k)\Delta x_i \Delta y_{j-1}\Delta z_k + q(i-1,j-1,k)\Delta x_{i-1}\Delta y_{j-1}\Delta z_{k-1}$$
$$+ q(i,j,k-1)\Delta x_i \Delta y_j \Delta z_{k-1} + q(i-1,j,k-1)\Delta x_{i-1}\Delta y_j \Delta z_{k-1}$$
$$+ q(i,j-1,k-1)\Delta x_i \Delta y_{j-1}\Delta z_{k-1} + q(i-1,j-1,k-1)\Delta x_{i-1}\Delta y_{j-1}\Delta z_{k-1}]/(8h_{x_i}h_{y_j}h_{z_k})$$

(14)

where $q_T(i,j,k)$ is the dissipated power associated with the temperature node $T(i,j,k)$.

Equation (14) was only used to calculate the power associated with the inner temperature node. For the temperature nodes on the boundary, some of the power terms on the right hand side of (14) were replace by zero if any of their index numbers ($i, j,$ or k) exceeded the specified computation domain.

After heat transfer calculation, the temperature data were transformed back to the dissipated power nodes so that they could be used in QW3D for updating the EM field. This was done in (15):

$$T_q(i,j,k) = [T(i,j,k) + T(i-1,j,k) + T(i,j-1,k) + T(i-1,j-1,k)$$
$$T(i,j,k-1) + T(i-1,j,k-1) + T(i,j-1,k-1) + T(i-1,j-1,k-1)]/8$$

(15)

where $T_q(i, j, k)$ is the temperature at the cells ($i, j,$ and k) associated with the dissipated power nodes. The algorithm is shown in the following:

1. Obtain dissipated power from QW3D.

2. Initialize temperature for computation in the next time step based on previous temperature distribution.

3. Loop through the whole computational grids:

    (a).   for inner nodes, calculate dissipated power based on (14),

    (b).   for boundary nodes, set the corresponding power terms in (14) to zero,

    (c).   conduct heat transfer calculation.

4. Find the temperature distribution based on Equation (15) and feed back to QW3D.

Boundary treatment

Although only stationary case was considered in this study, the actual physical system had a left and right end open to allow food trays to move in and out of the cavity. Therefore, in the numeric model, the left and right ends of the cavity needed to be terminated with proper boundary conditions to represent the real system as close as possible. A perfect matched layer was used as the absorbing boundary condition to terminate the finite grid. With the perfect matched layer method, the electrical or magnetic field components on the boundary were split into two components, which allowed for assigning different losses at different grids (Taflove, 1998). After choosing the proper loss at each sub-layer, the numeric reflection gradually decreased with the layers further away from the boundary, and eventually disappeared as if the wave propagated into a far region. It therefore acted like an open boundary without physical wave reflection. To set up the PML layer, 8 sub-layers parallel to y-z plane were assigned to terminate the numeric grids. The Exponential Time-Stepping algorithm was used to assign the conductivity at each sub-layer as: A*exp(B*x), where A = 0.02, B = 4, and x = distance from perfect matched layer divided by the layer thickness. The perfect matched layer method accurately modelled the boundary in the presented system, though it also introduced more computational complexity and increased simulation time. However, since the system was single mode and EM waves were concentrated on the central portion of the microwave section, the field intensity was very small near the absorbing boundary. For this reason, the perfect matched layer might be replaced by a simpler

perfect electric conductor boundary condition without introducing too much inaccuracy. The maximum difference observed on the left and right ends of the cavity was only 5%, while the minimum difference (< 2%) was observed in the centre of the cavity.

Numeric convergence

Numeric error always occurs when modelling a process by a finite grid. Since large errors significantly affect final results, a study is necessary to make sure that the model converges to a final value. Because the models used in this study included both EM and heat transfer, these were examined separately. From Table 4.1 and Equation (9), the dielectric properties did not have significant change with the temperature and the dielectric properties did not cause much change in dissipated power at 915 MHz. Therefore, it was assumed that convergence for the coupled model could be achieved once convergences for the EM and heat transfer models were guaranteed separately.

Convergence Study for the EM Model

For an FDTD model to satisfy numeric stability, the maximum time step has to be selected as the following:

$$\Delta t \leq \sqrt{\frac{\mu\varepsilon}{1/(\Delta x)_{min}^2 + 1/(\Delta y)_{min}^2 + 1/(\Delta z)_{min}^2}} \tag{16}$$

where $(\Delta x)_{min}$, $(\Delta y)_{min}$, $(\Delta z)_{min}$ represent the minimum cell size of non-uniform mesh in each direction, respectively.

In addition, the standard FDTD rule of thumb indicates that at least ten cells need to be used per wavelength (Pathak, et al., 2003):

$$\Delta cell \leq \frac{1}{10 f \sqrt{\mu\varepsilon}} \tag{17}$$

One result of using a conformal FDTD algorithm is that the mesh in the computational domain is not necessarily uniform. Therefore, only the maximum cell size was specified in each direction with QW3D. The actual cell size was generated automatically by QW3D. According to Equation (17), the maximum cell size was 10 mm in free space, while 4 mm in water and gel. Therefore, cell size was chosen to be 4mm in x and y directions. We selected 2 mm in the z direction since the food tray dimension in z direction was much smaller than that in x and y directions. Though the cell size was chosen to be as small as possible to avoid numeric instability, it was still able to affect the propagation velocity of the numeric wave in the finite-difference-grid approximation of the wave equation (Taflove, 1998). The numeric convergence study for a simple 1-D system was analyzed using an eigenvalue method and the concept of numeric dispersion. However, in a very complicated 3-D case such as an industrial EM heating system, there is no closed-form solution for wave equations. In practice, one way to check the convergence of a numeric model is to track the numeric results at different cell sizes and time steps. If the numeric results remain stable as cell sizes are reduced and simulation time increased, the model could be considered to converge. In the model discussed here, the cell size on a vertical plane was chosen to be half the cell size in the horizontal plane, and the change of cell size in the horizontal plane automatically changed the cell size in the vertical plane. Therefore, for this special grid arrangement, model convergence in the horizontal plane led to the convergence of the overall 3-D domain. Fig 4.10(a) and (b) (horizontal plane) show the convergence in terms of discretization of space.
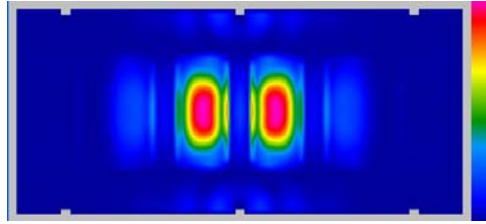
(a) $\Delta x = \Delta y = 10$, $\Delta z = 5$
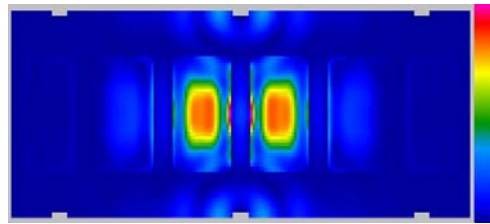
(b) $\Delta x = \Delta y = 4$, $\Delta z = 2$

Fig 4.10 Convergence check for EM fields at different cell sizes

Usually it is highly possible for singularity to occur at the interface between two different mediums as well as the sharp edge of the geometry. Therefore, model stability was checked on the corners of both the food and Ultem material (A, B in Fig 4.8) inside the microwave cavity. Fig 4.11 shows the electrical field converges to a final value as the simulation time proceeded.
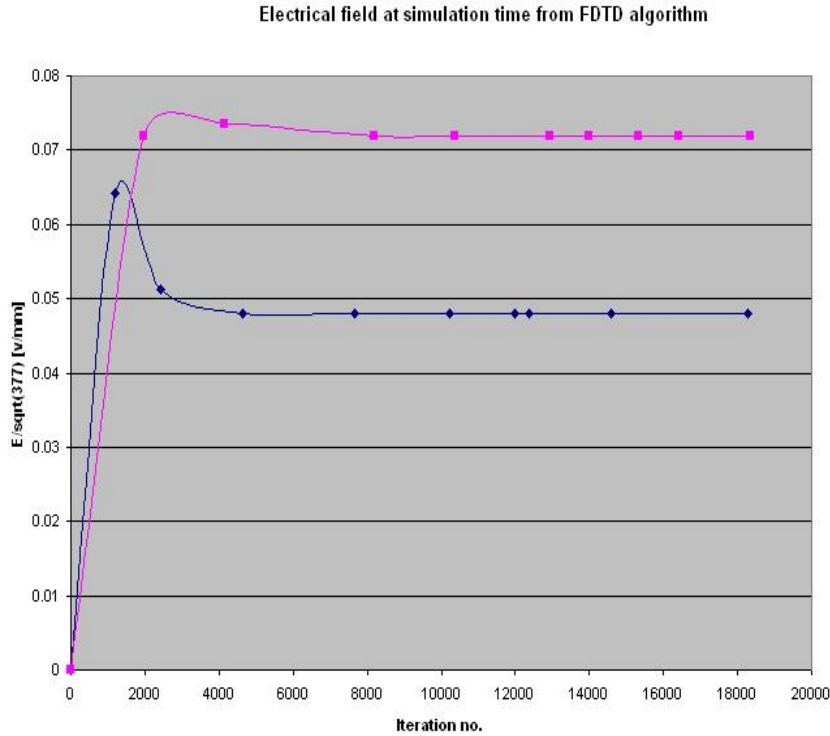
Fig 4.11 EM model convergence with simulation time

Convergence study for the heat transfer model

In addition to the numeric convergence of the EM model, accuracy of the heat transfer model was considered. Fig 4.12 presents a result from the heat transfer model used in coupled simulation in comparison with those from the FEM model and experimental measurement. The FEM thermal model was also developed in our group to validate the FDTD heat transfer model. The experiment measurement was conducted in a water bath where the gel placed in a 7 oz polymetric tray was heated and the temperature profile at its centre point was monitored using a fiber optic sensor (± 0.5°C). The solid red line is the simulation result calculated using FDTD method; the dashed blue line is the simulation result calculated using the FEM model and the yellow solid-dash line presents the measured temperature profile from experiment. Good agreement was

106

achieved. The difference between the calculated temperature and actual measurement was less than 1°C. It is worth noting that with different heat transfer coefficient the simulated heating curve varies. In this study, the heat transfer coefficient 220Wm^{-2}k^{-1} was chosen based on agreement between simulation and experiment results for hot water heating.
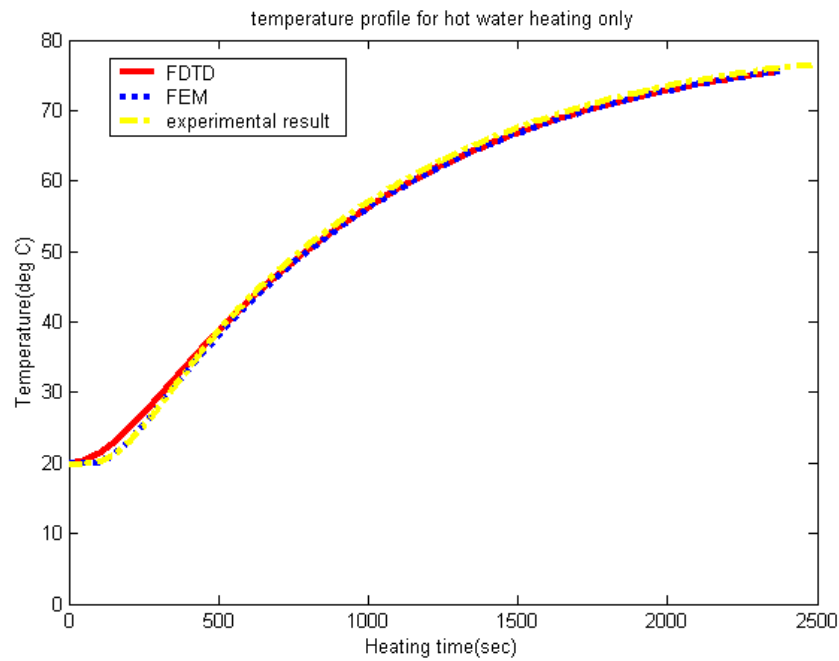
Fig 4.12 Validation of the heat transfer model

Validation of the coupled model

This section describes validation of the coupled model by comparing the simulated temperature distribution and temperature profile with experimental results. Excitation in the model was a sinusoidal source at 915 MHz and amplitude was the square root of the required input microwave power. Fig 4.13(a) and (b) show the temperature profiles in two separate runs with the simulated results, respectively. The temperature profile at point 1 (Fig 4.4) is represented by a solid line, the temperature profile at point 2 by a dashed line, the temperature profile at point 3 by a solid-dash line,

each indicating the measured and simulated results. It was clear from both experimental and simulated results that the heating rate increased significantly when microwave power was on. The heating rate calculated from the simulation was similar to the experimental measurement. The difference between the simulated final temperature and measured final temperature was less than 5ºC, which is generally considered adequate considering the complex nature of the heating process.

Experimentally obtained heating pattern as reflected by color changes in the middle layer on the horizontal plane of the gel, and temperature distribution from simulation after a 5.5min heating process are presented in Fig 4.14(a) and (b), respectively. In the experimental heating pattern, deep blue color corresponds to low heating intensity while light yellow indicates high heating intensity. For the simulated temperature distribution, red color corresponds to high temperature while blue indicates low temperature. From Fig 4.14, the experimental heating pattern correlates well with simulated temperature distribution, especially the locations of cold and hot spots. The good agreement between these results showed that the model correctly represented the real system in consideration. However, there were some mismatches between the simulation and experimental results; for example, the simulated temperature distribution was more symmetric than the heating pattern obtained from experiment. It was very difficult to place the fiber optic sensors at the exact locations as those used in the simulation and to maintain the exact geometry of food trays during the thermal processes. Another source of error was introduced by the heat transfer model because the surrounding temperature was assumed to be uniform (125ºC), but in reality it might have changed with time and space.
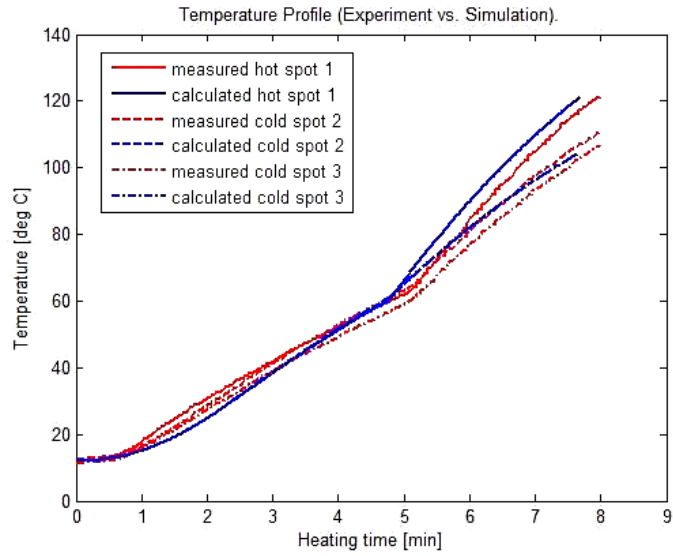
(a) run-1
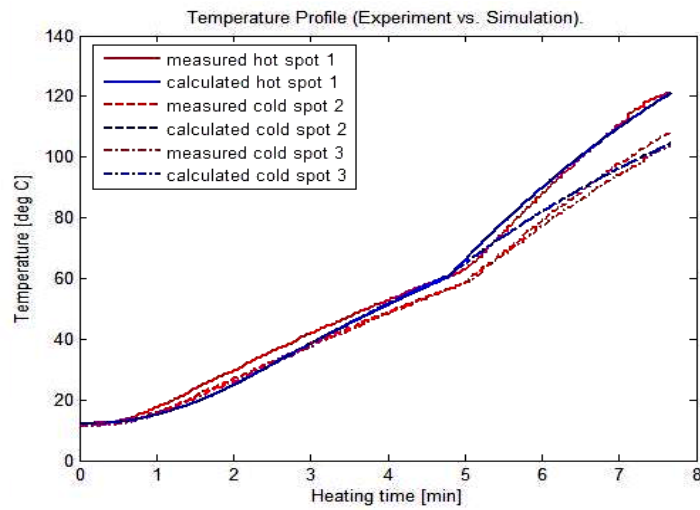
(b) run-2

Fig 4.13 Comparison of simulation results for temperature evolution at hot and cold spots

with experiment results from two identical experimental runs
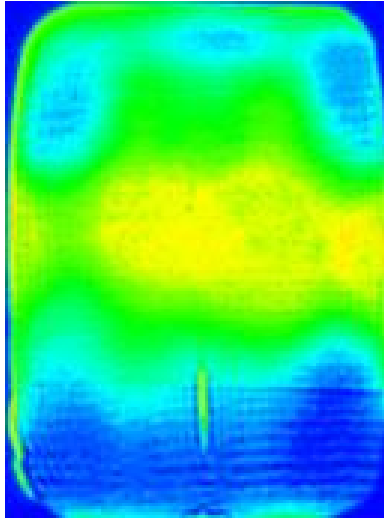
(a) Colour image from chemical marker
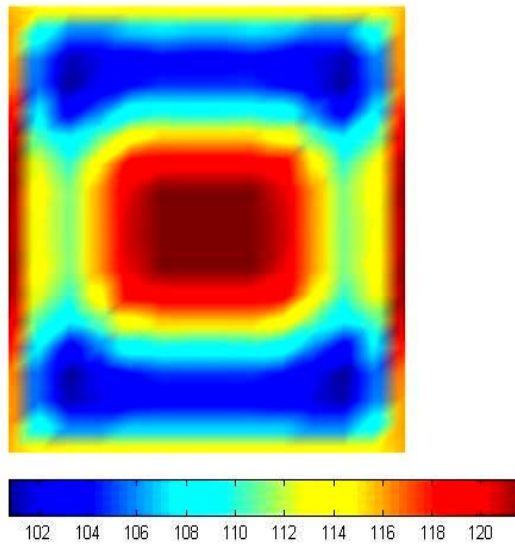
(b) Simulated temperature profile

Fig 4.14 heating pattern on the middle layer of the food

Conclusions

A model was developed that enables computer simulation for a 915 MHz pilot-scale microwave sterilization system in which conventional hot water heating and MW heating took place at the same time. Because the hot water heated the product from the outside while the microwave heated it from the inside, the combination of these two

heating mechanisms improved heating uniformity and shortened heating time. The model presented in this paper used a commercial EM solver combined with a user-defined heat transfer program to simulate the MW heating process. The combination of using commercial software with a thermal solver in this model was unique compared with other methods reported in the literature. It employed a conformal FDTD algorithm so that the details of the physical geometry could be modeled accurately without requiring significant computer memory or simulation time. The EM portion was modified automatically as a macro with an external script to quickly construct different geometries for EM field calculation, and then coupled with the customized heat transfer model to simulate a MW heating process at different system configurations. In addition, the external user-defined heat transfer model provided extra flexibility to control the heating process in different ways, which was a big advantage for system optimization of industrial microwave sterilization.

Acknowledgment

References

Balanis, C. A. (1989). *Advanced engineering electromagnetics*, John Wiley & Sons,

Barratt, L., & Simons, D. (1992). Experimental validation of a computer simulation of microwave heating. *in Proc. 27th Microwave Power Symp*, 118-122.

Bows, J., Patrick, M. L., Dibben, D. C., & Metaxas, A. C. (1997). Computer simulation and experimental validation of phase controlled microwave heating. *presented at the 6th Microwave and High Frequency Heating Conference*, Fermo, Italy.

Burfoot, D., Railton, C. J., Foster, A. M., & Reavell, R. (1996). Modelling the pasteurization of prepared meal with microwave at 896MHz. *Journal of Food Engineering*, 30, 117-133.

Campbell, G. S., Calissendorff, C., & Williams, J. H. (1991). Probe for Measuring Soil Specific-Heat Using a Heat-Pulse Method. *Soil Science Society of America Journal*, 55(1), 291-293.

Clemens, J., & Saltiel, G. (1995). Numerical modeling of materials processing in microwave furnaces. *International Journal of Heat and Mass Transfer*, 39(8), 1665-1675.

Dibben, D. C., & Metaxas, A. C. (1994a). Experimental verification of a finite element solution to heating problems in a multi-mode cavity. *in Proc. 2nd Int. Conf. Computation in Electromagnetics*, Nottingham, 135-137.

Dibben, D. C., & Metaxas, A. C. (1994b). Finite-Element Time-Domain Analysis of Multimode Applicators Using Edge Elements. *Journal of Microwave Power and Electromagnetic Energy*, 29(4), 242-251.

Guan, D., Cheng, M., Wang, Y., & Tang, J. (2004). Dielectric properties of mashed potatoes relevant to microwave and radio-frequency pasteurization and sterilization processes. *Journal of Food Science*, 69(1), E30-E37.

Guan, D., Gray, P., Kang, D. H., Tang, J., Shafer, B., Ito, K., Younce, F., & Yang, C. S. (2003). Microbiological validation of microwave-circulated water combination heating technology by inoculated pack studies. *J. Food Sci.*, 68(4), 1428-1432.

Guan, D., Plotka, V., Clark, S., & Tang, J. (2002). Sensory evaluation of microwave treated macaroni and cheese. *Journal of Food Process. Preserv.*, 26, 307-322.

Gwarek, W. K., Celuch-Marcysiak, M., Sypniewski, M., & Wieckowski, A. (1999). *QuickWave-3D Software Manual*, QWED, Porland.

Harms, P. H., Chen, Y., Mittra, R., & Shimony, Y. (1996). Numerical modeling of microwave heating systems. *Journal of Microwave Power and Electromagnetic Energy*, 31(2), 114-121.

Harms, P. H., Lee, J. F., & Mittra, R. (1992). A Study of the Nonorthogonal Fdtd Method Versus the Conventional Fdtd Technique for Computing Resonant Frequencies of Cylindrical Cavities. *Ieee Transactions on Microwave Theory and Techniques*, 40(4), 741-746.

Holland, R. (1993). Pitfalls of Staircase Meshing. *Ieee Transactions on Electromagnetic Compatibility*, 35(4), 434-439.

Incropera, F. P., & DeWitt, D. P. (2001). *Introduction to heat transfer, 4th*, John Wiley & Sons,

Jurgens, T. G., Taflove, A., Umashankar, K., & Moore, T. G. (1992). Finite-Difference Time-Domain Modeling of Curved Surfaces. *IEEE Transactions on Antennas and Propagation*, 40(4), 357-366.

Lau, M. H., Tang, J., Taub, I. A., Yang, T. C. S., Edwards, C. G., & Mao, R. (2003). Kinetics of chemical marker formation in whey protein gels for studying microwave sterilization. *Journal of Food Engineering*, 60(4), 397-405.

Leo, R. D., Cerri, G., & Mariani, V. (1991). TLM techniques in microwave ovens analysis: Numerical and experimental results. *in Proc. 1st Int. Conf. Computation in Electromagnetics*, London, 361-364.

Ma, L. H., Paul, D. L., Pothecary, N., Railton, C., Bows, J., Barratt, L., Mullin, J., & Simons, D. (1995). Experimental Validation of a Combined Electromagnetic and Thermal Fdtd Model of a Microwave-Heating Process. *Ieee Transactions on Microwave Theory and Techniques*, 43(11), 2565-2572.

Osepchuck, J. M. (1984). A history of microwave heating applications. *IEEE Trans. Microwave Theory Tech*, MTT-32, 1200-1224.

Pandit, R. B., Tang, J., Liu, F., & Mikhaylenko, M. (2007a). A computer vision method to locate cold spots in foods in microwave sterilization processes. *Pattern Recognition*, 40, 3667-3676.

Pandit, R. B., Tang, J., Liu, F., & Pitts, M. (2007b). Development of a novel approach to determine heating pattern using computer vision and chemical marker (M-2) yield. *Journal of Food Engineering*, 78(2), 522-528.

Pandit, R. B., Tang, J., Mikhaylenko, G., & Liu, F. (2006). Kinetics of chemical marker M-2 formation in mashed potato - A tool to locate cold spots under microwave sterilization. *Journal of Food Engineering*, 76(3), 353-361.

Paoloni, F. (1989). Calculation of power deposition in a highly overmoded rectangular cavity with dielectric loss. *Journal of Microwave Power and Electromagn. Energy*, 24(1), 21-32.

Pathak, S., Liu, F., & Tang, J. (2003). Finite difference time domain(FDTD) characterization of a single mode applicator. *J. Microwave Power EE*, 38(1), 37-48.

Smyth, N. F. (1990). Microwave-Heating of Bodies with Temperature-Dependent Properties. *Wave Motion*, 12(2), 171-186.

Spiegel, R. J. (1984). A review of numerical models for predicting the energy deposition and resultant thermal response of humans exposed to electromagnetic fields. *IEEE Trans. Microwave Theory and Techn*, MTT-32, 730-746.

Taflove, A. (1998). Computational electrodynamics : the finite-difference time-domain method, Artech House, Boston.

Torres, F., & Jecko, B. (1997). Complete FDTD analysis of microwave heating processes in frequency-dependent and temperature-dependent media. *IEEE Transactions on Microwave Theory and Techniques*, 45(1), 108-117.

Watanabe, W., & Ohkawa, S. (1978). Analysis of power density distribution in microwave ovens. *Journal of Microwave Power and Electromagn. Engergy*, 13(2), 173-182.

Webb, J. P., Maile, G. L., & Ferrari, R. L. (1983). Finite element solution of three dimensional electromagnetic problems. *IEE Proceedings*, 130(2), 153-159.

Z.Shou-Zheng, & C.Han-Kui (1988). Power distribution analysis in rectangular microwave heating applicator with stratified load. *Journal of Microwave Power and Electromagn. Energy*, 23(3), 139-143.

Zhang, H., & Datta, A. K. (2000). Coupled electromagnetic and termal modeling of microwave oven heating of foods. *Journal of Microwave Power and Electromagnetic Energy*, 35(2), 71-85.

Chapter 5 Simulation Model for Moving Food Packages in Microwave Heating Processes Using Conformal FDTD Method

Abstract

A numeric model was developed to couple electromagnetic (EM) and thermal field calculations in packaged foods moving in pressurized 915MHz microwave (MW) cavities with circulating water at above 120°C. This model employed a commercial EM package with a customized heat transfer sub-model to solve the coupled EM field and thermal field equations. Both methods applied finite-difference-time-domain (FDTD) method to solve the partial differential equations. An interface was built to facilitate the communication between electromagnetic and thermal models to incorporate the coupling feature which is unique to microwave heating process. Special numerical strategies were implemented to simulate the movement of food packages. The simulation model was validated with a pilot-scale microwave system using direct temperature measurement data and indirect color patterns in whey protein gels via formation of the thermally induced chemical marker M-2. Good agreements were observed, suggesting that the developed model could correctly simulate MW sterilization processes for moving food packages. Four cases were also studied using to investigate the influence of power input and package gaps on heating uniformity. These applications demonstrated the flexibility of the model to allow its usage for system and process optimization.

Introduction

Electromagnetic (EM) energy at Microwave (MW) frequencies is increasingly being used in industrial applications to increase heating rates and reduce process times as alternatives to conventional heating methods (Ohlsson, 1987, 1992). One of the major challenges in developing novel thermal processing technologies based on MW energy is non-uniform electromagnetic field distribution (Ohlsson, 1990; Ryynanen and Ohlsson, 1996). Inside a microwave cavity where microwave heating takes place, localized hot and cold spots occur due to uneven electrical field distributions. Since the process time is short, these hot and cold spots may cause severe non-uniform heating that adversely influences product quality (Ma, et al., 1995; Osepchuck, 1984).

Computer simulation based on fundamental electromagnetic wave and heat transfer equations can assist with the design of microwave applicators and selection of appropriate process parameters to alleviate non-uniform heating. The electric permittivity of food materials typically changes with temperature (Guan, et al., 2004) at microwave frequencies, in particular at 915 MHz, a frequency allocated by FCC for high power microwave heating systems. As a result, food temperature influences microwave field distribution. Microwave heating also influences heat transfer, not only because of the generated thermal energy but also the temperature dependency of thermal properties (Zhang and Datta, 2000). That is, electromagnetic wave patterns are significantly influenced by temperature of foods, and vise versa. It is therefore critical to solve coupled electromagnetic field and heat transfer equations for a 3-dimensional transient MW heating process in a practical industrial system, especially when packaged food moves.

The literature contains numerous reports on analytical models to describe

118

electromagnetic fields inside domestic microwave ovens (Paoloni, 1989; Watanabe and Ohkawa, 1978; Webb, et al., 1983; Z.Shou-Zheng and C.Han-Kui, 1988). But only electromagnetic field distributions were considered in these studies. While Smyth (1990), Baratt and Simons (1992) considered one- and two-dimensional temperature dependent microwave heating processes, detailed treatment of three dimensional coupled electromagnetic field and heat transfer equations has not been explored until recently. However, even these studies are limited to domestic ovens (Smyth, 1990; Zhang and Datta, 2000) or stationary cases were studied (Bows, et al., 1997; Burfoot, et al., 1996; Clemens and Saltiel, 1995; Harms, et al., 1996; Zhang and Datta, 2000).

Many numeric techniques can be used to solve coupled Maxwell and heat transfer equations. Those techniques include the Finite Difference Time Domain (FDTD) method (Ma, et al., 1995; Torres and Jecko, 1997), Finite Element Method (FEM) (Dibben and Metaxas, 1994b; Webb, et al., 1983) and Transmission Line Method (TLM) (Leo, et al., 1991). Of these, the FDTD method is the most popular for the coupled electromagnetic and thermal processes because it uses less computer memory and simulation time. However, for complex geometry, the FEM is often preferred; though it involves lengthy computation to inverse matrixes the size of which increases sharply with the number of elements needed to ensure accuracy (Speigel, 1984; Zhang and Datta, 2000).

The traditional FDTD method that uses staircase grids can not handle complex geometries and boundaries. The newly developed conformal FDTD algorithm overcomes this drawback by solving the integral form of Maxwell's equations. This algorithm creates finite boundary grids that conform to geometric surfaces to accurately match detailed irregularities, while retaining the simplicity of the regular grids used in the

conventional FDTD algorithm for the other parts of the three-dimensional domain. A detailed description of the conformal FDTD algorithm is provided in numerous literatures (Harms, et al., 1992; Holland, 1993; Madsen and Ziolkowski, 1988). Holland (1993) discussed the disadvantages of the classic staircase FDTD algorithm that significantly hindered its practical applications. Harms et al. (1992), Madsen and Ziolkowski (1988) used the conformal algorithm to accurately model the irregularities without excessive memory overhead.

In industrial microwave heating operations, food packages are transported on conveyor belts to achieve desired throughputs and improve heating uniformity along the moving direction. However, no numeric model has been reported in the literature to deal with load movement for industrial microwave applications. The current study extends the coupled model described by Chen et al.(2007a) that used conformal FDTD algorithms for electromagnetic field simulation and conventional FDTD method for thermal field to simulate microwave heating of moving food packages in continuous industrial microwave sterilization and pasteurization processes.

Problem statement

The industrial system we attempted to model in this study was a single-mode 915 MHz MW sterilization system developed at Washington State University (Tang, et al., 2006). A simplified version of this system is described in details by Chen, et al. (2007a). In brief, the system consisted of four sections: two MW heating sections in the center, and a loading section and a holding section on each end (Fig 5.1). MW energy was provided by two 5 kW generators operating at 915MHz, each connected by standard waveguides WR975 (Fig 5.2) that supported only TE_{10} mode to a T-split (not shown

120

inFig 1). Fig 5.3(a) and (b) show a close-up front and top view, respectively, of the MW heating section, which consisted of a rectangular cavity with one horn shaped applicator on the top and an identical applicator on the bottom. The loading and holding sections were also rectangular cavities. Microwaves of equal intensity after the split were directed to the entry ports of the top and bottom horn applicators of each cavity. The length of the waveguides could be adjusted to regulate phase difference between the two waves entering the top and bottom applicators, which affected the EM field distribution inside the MW cavity and the food being heated. It was therefore possible to improve the heating uniformity by properly adjusting the phase shift between the two waves to achieve the desired field distribution in each cavity (Balanis, 1989; Jurgens, et al., 1992). For simplicity, the model described here was limited to zero phase shift between the entry ports of the top and bottom horn applicators for both cavities, though the model could be extended to general case with arbitrary phase differences. To achieve zero phase shifts, two pieces of waveguides with quarter wavelength each were added to one path after the T-split so that the interacting waves had the same phase in the central plane of the cavity.

The pilot system included both circulating hot water to provide heating from outside food packages and MW sources for volumetric heating, which significantly improved heating uniformity and reduced processing time. The temperature of the circulation water in the cavity was set at 125˚C, and the food temperature at cold spots reached over 121ºC to ensure that low-acid foods (pH>4.5) were properly processed as shelf-stable products. The depth of the water was the same as the depth of microwave cavity. An overpressure of 276 KPa was provided through a buffer tank to prevent water from boiling at 125ºC and prevent packages from bursting due to internal vapor pressure.

At the base of the top and bottom horn shaped waveguides, two MW-transparent windows were secured to keep pressurized hot water from entering waveguides. During continuous thermal processing, packaged food was moved from the loading section through the two MW heating sections to the holding section.

Fundamentals for numerical modeling

Governing equations for EM field.

The EM fields were calculated using the conformal FDTD algorithm based on the integral form of Maxwell's equations (Balanis, 1989; Jurgens, et al., 1992):

$$\oint_C \vec{E} \bullet d\vec{l} = -\frac{\partial}{\partial t} \iint_S \vec{B} \bullet d\vec{s} \tag{1}$$

$$\oint_C \vec{H} \bullet d\vec{l} = \frac{\partial}{\partial t} \iint_S \vec{D} \bullet d\vec{s} + \iint_S (\vec{J}_i + \vec{J}_c) \bullet d\vec{s} \tag{2}$$

$$\oiint_S \vec{D} \bullet d\vec{s} = Q^e \tag{3}$$

$$\oiint_S \vec{B} \bullet d\vec{s} = 0 \tag{4}$$

where, $\vec{E}$ is the electric field, $\vec{H}$ is the magnetic field, $\vec{D} = \varepsilon\vec{E}$ is the electric flux density, $\vec{B} = \mu\vec{H}$ is the magnetic flux density. Q^e is the electric charge surrounded by surface S. μ and ε are the permeability and permittivity, respectively. The permeability μ is assumed equal to free space value μ_0. The dielectric permittivity $\varepsilon = \varepsilon_0\varepsilon_r = \varepsilon_0(\varepsilon'_r\text{-j }\varepsilon''_r)$. C is a contour path surrounding the surface S. J_i and J_c are source current density and conduction current density, respectively.

The Maxwell's equations in the integral form were solved by a commercial electromagnetic solver QuickWave-3D (QW3D, Warsaw, Poland) using the conformal

FDTD algorithm (Gwarek, et al., 1999; Taflove, 1998). The advantage of the conformal FDTD algorithm over conventional FDTD has been discussed in detail by Taflove (1998).

Governing equations for heat transfer.

Since the MW heating process considered in this study included heating from MW energy and circulating hot water, the EM fields were coupled with heat transfer equations to take into consideration the temperature dependent dielectric properties.

For the thermal field calculations, heat conduction was assumed to take place inside the food package while convective boundary conditions were applied to the food surface to take into account the effect of the circulating water in the system. The heat transfer equation and its boundary condition are as followings (Incropera and DeWitt, 2001):

$$\frac{\partial T}{\partial t} = \frac{1}{\rho_v(T)} \nabla(K(T) \bullet \nabla T) + \frac{\dot{q}}{\rho_v(T)} \tag{5}$$

$$q = hA(T_s - T) \tag{b}$$

where $K(T)$ is thermal conductivity, $\rho_v(T) = \rho(T)c_p(T)$ is volumetric specific heat, $\rho(T)$ is mass density, $c_p(T)$ is specific heat, q is thermal energy provided by circulating water on the boundary, h is heat transfer coefficient of $220 Wm^{-2}K^{-1}$, A is the boundary surface area and T_s is circulating water temperature. $\dot{q}$ is derived from the root mean square value of electrical field:

$$\dot{q}(r,T) = 2\pi\varepsilon_0 f \varepsilon_r''(T) \left[\frac{\int_V (\vec{E}*\vec{E})dV}{2V} \right] \tag{7}$$

123

To be consistent with the EM model and in order to simplify the mathematical computation, the heat transfer equation was solved numerically using the FDTD method. We only considered semi-solid or solid foods in which heat conduction was the dominant heat transfer mode. The heat conduction equation 5 was differentiated as:

$$T^{n+1}(i,j,k) = (1 - \alpha_t(\frac{2}{\Delta x_{i-1}\Delta x_i} + \frac{2}{\Delta y_{j-1}\Delta y_j} + \frac{2}{\Delta z_{k-1}\Delta z_k}))T^n(i,j,k) + \alpha_t(\frac{T^n(i+1,j,k)}{h_{x_i}\Delta x_i} + \frac{T^n(i-1,j,k)}{h_{x_i}\Delta x_{i-1}} + \frac{T^n(i,j+1,k)}{h_{y_j}\Delta y_j}$$
$$+ \frac{T^n(i,j-1,k)}{h_{y_j}\Delta y_{j-1}} + \frac{T^n(i,j,k+1)}{h_{z_k}\Delta z_k} + \frac{T^n(i,j,k-1)}{h_{z_k}\Delta z_{k-1}}) + \frac{\dot{q}\Delta t}{\rho_v} \tag{8}$$

where $\Delta x_i, \Delta y_j, \Delta z_k$ are cell sizes in x-, y-, z- direction, respectively. $\rho_v = \rho c_p \quad \alpha_t = \frac{K\Delta t}{\rho_v}$.

Here ρ_v and α_t are functions of $T^n(i,j,k)$. We drop subscription for better presentation. h_x, h_y, h_z are defined as the mean value of adjacent cell sizes in x-direction, y-direction and z-direction respectively:

$$h_{x_i} = (\Delta x_i + \Delta x_{i-1})/2, \quad h_{y_j} = (\Delta y_j + \Delta y_{j-1})/2, \quad h_{z_k} = (\Delta z_k + \Delta z_{k-1})/2 \tag{9}$$

The temperature responses at food surface nodes served as the interface between conduction heat (interior nodes) and convection heat (circulation water). Therefore, the finite difference form for the heat transfer equation was slightly modified on the surface nodes by replacing the conduction term in Eq 8 with corresponding convective term. For example, for the nodes on the top surface of food package (parallel with x-y plane), the difference form in Eq. 8 for the boundary condition was modified by using $q=h*\Delta x_i*\Delta y_j*[T_s-T^n(i,j,k)]$ to replace the conduction term $[T^n(i,j,k+1)-T^n(i,j,k)]*K(T)*\Delta z_k$.

Numerical mode for simulating moving package

In MW heating processes with moving packages, food packages enter the heating chamber in sequence. However, conducting computer simulation for all moving food packages in the microwave cavities would involve dynamically allocating and de-

124

allocating a large amount of memory several times during each simulation process and transferring computation information back and forth between internal memory and external disk storage. In addition, since the focus of this study was on the heat distribution inside a representative moving food package, the simulation model solved the coupled equations at the grids inside the selected food package, while only EM field patterns were calculated for domains outside of this food package boundary.

The EM field patterns were assumed not to influence the temperature distribution of circulating water because of the large flow rate (~130 L/min). The simulation model traced the temperature profile of the single food package at equally spaced positions as it travelled through the heating cavities. The temperature distribution calculated for the package at one position served as the initial condition for its next position.

The simulation considered two different stages: 1) food package heated by circulating water in the loading section; and 2) simultaneous MW and surface water heating when food packages moved through the two MW heating sections. At the first stage, only heat transfer equations were used to caluclate the termperature distribution, as a result of surface hot water heating, this temperature distribution was then used as the initial condition for the second stage to calculate the temperature response from the combined hot water and MW heating.

The MW power density in the packages at a particular position was calculated from Maxwell's equations using temperature-dependent dielectric properties. Since the EM process is much faster than the thermal process, its steady state was established before the thermal reaction took place and the field intensity within the food package was assumed constant until the package was moved to its subsequent position. Temperature

response was then calculated by the heat transfer submodel with constant power density at each node for each time increment between the two positions. At the next position, the temperature-dependent dielectric properties and thermal properties were recalculated based on the temperature of each element in the food package in consideration. When the food package traveled from one MW chamber to the other, the geometry and mesh layout generated in QW3D for the EM computation were modified automatically to adapt to the different system configuration. During simulation, the generated mesh information used for EM calculation was kept in an external file readily accessible by the thermal model, so that the mesh grids used for numeric solutions of the Maxwell's equations and thermal equations were consistent, thus dramatically reducing the complexity of mathematical manipulations. Temperature dependent dielectric and thermal properties of the food used in the experiment were updated in the simulation package by using interpolation techniques from the properties measured at distinct temperatures. This coupled calculation loop continued until the required heating time was reached. Fig 5.4(a) presents the simulation scheme for the coupled model. The node transformation procedure in Fig 5.4(b) was used to exchange the data between the computational nodes for thermal energy generation due to MW heating and computational nodes for EM field updates due to thermal effects.

Node transformation

The simulation model consisted of two node transformation blocks necessary to facilitate the communication between the QW3D and customized heat transfer model (Kopyt and Celuch-Marcysiak, 2003). The temperature nodes were defined on grid lines while the nodes for EM energy generation from microwaves (used in QW3D to calculate

the power distribution) were located in the center of each cell. This layout avoided the numerical instability of the heat transfer model, which might occur otherwise. The node transformation included two steps in sequence. The first step was to re-distribute the EM energy from the center node to each temperature node. For each temperature node, only its neighboring cells were assumed to contribute to the EM energy that caused temperature change. The second step, after the heat transfer model had been employed to obtain the temperature at each temperature node, was to calculate the temperature associated with the EM nodes used in QW3D for the next EM field computation. For each single cell, only temperature nodes at the corners were assumed to contribute to the dielectric change. The following two equations show the mathematic manipulations for the first and second steps, respectively.

$$
\begin{aligned}
q_T(i,j,k) = [&q(i,j,k)\Delta x_i \Delta y_j \Delta z_k + q(i-1,j,k)\Delta x_{i-1}\Delta y_j \Delta z_k \\
&+ q(i,j-1,k)\Delta x_i \Delta y_{j-1}\Delta z_k + q(i-1,j-1,k)\Delta x_{i-1}\Delta y_{j-1}\Delta z_{k-1} \\
&+ q(i,j,k-1)\Delta x_i \Delta y_j \Delta z_{k-1} + q(i-1,j,k-1)\Delta x_{i-1}\Delta y_j \Delta z_{k-1} \\
&+ q(i,j-1,k-1)\Delta x_i \Delta y_{j-1}\Delta z_{k-1} + q(i-1,j-1,k-1)\Delta x_{i-1}\Delta y_{j-1}\Delta z_{k-1}]/(8h_{x_i}h_{y_j}h_{z_k})
\end{aligned}
\tag{22}
$$

$$
\begin{aligned}
T_q(i,j,k) = [&T(i,j,k) + T(i-1,j,k) + T(i,j-1,k) + T(i-1,j-1,k) \\
&T(i,j,k-1) + T(i-1,j,k-1) + T(i,j-1,k-1) + T(i-1,j-1,k-1)]/8
\end{aligned}
\tag{23}
$$

where $q_T(i,j,k)$ is the dissipated power associated with the temperature node $T(i,j,k)$. Equation 10 was used for the first step and could be applied to nodes on the boundary or inside food package. For the terms where the index number (i,j,k) exceeded the specified computation domain, they were simply replaced by zero. Equation 11 was used for the second step, where $T_q(i,j,k)$ is the temperature at cell (i,j,k) associated with dissipated power node. The complete algorithm is presented in the following diagram Fig 4(b).

Experimental methods

Temperature history and heating pattern determination

The Pilot-scale MW system shown in Fig 5.1 was used to validate the model. During the experiment, one optic sensor that traveled with the food packages was placed at the cold spots which were predetermined by a chemical marker method (Pandit, et al., 2007a; Pandit, et al., 2007b). This method measured color changes in response to formation of a chemical compound (M-2) due to a Millard reaction between the amino acids of proteins and a reducing sugar, ribose. The color response depended on the heat intensity at temperatures beyond $100^{o}C$ and, therefore, served as an indicator of temperature distribution after MW heating. Detailed information about the kinetics of M-2 formation with temperature can be found elsewhere (Lau, et al., 2003; Pandit, et al., 2006). After MW processing, the heating patterns inside the whey protein gels were obtained with computer vision software IMAQ (National instrument, TX, USA) using a computer vision method described in Pandit, et al.(2007b).

Processing of model food

To minimize the experimental error, it was desirable to use a model food that could be made with consistent dielectric and thermal properties. Its shape also needed to be easily maintained during the heating process so that the fiber optic sensor could be secured to a fixed position in the food . For these reasons, pre-formed whey protein gels (78% water, 20% protein, 1.7% salt, 0.3% D-ribose) sealed in a 7oz polymeric tray (140mm x 95mm x 16mm) were selected as a model food in our experiment. The gels were made by mixing 78% water, 20% protein, 1.7% salt, and 0.3% D-ribose; the mixtures were heated in a container in a water bath at 80 ˚C for about 30 minutes until solidification; the gels were then stored in refrigerator at 4 ˚C over night. The dielectric

properties of the whey protein gels at the different temperatures shown in Table 5.1 were measured by an HP8491B network analyzer (Hewlett-Packard Company, CA, USA) using an open coaxial cable. The double needle method (Campbell, et al., 1991) was used to measure the thermal properties (Table 5.2) with a KD2 device (Decagon, WA, USA). Since the hot water was pumped into the cavity at 40 liters per minute, its temperature was assumed uniform at the temperature of 121°C during the whole process. The dielectric properties of the hot water were measured also using an HP8491B network analyzer. For the sterilization purpose, food temperature needs to reach 121°C (Guan, et al., 2004).

Prior to the experiment, the packaged whey gel slab (95mmx140mmx16mm) was stored in a refrigerator at 9°C overnight. Fig 5.5 shows the location of the cold spot where the fiber optic sensor was inserted carefully with proper seals at the tray wall entry ports to prevent water leakage.

For MW processing, the tray with the probe placed in the middle of five other trays without probes was loaded to a conveyor belt in the loading section. The pressure door was closed, and hot water at 125°C at 276 KPa gauge pressure was introduced in the opposite direction to that of the tray movement (from the holding section to the loading section). When the temperature at the cold spot in the trays reached 60°C, they started moving in the preheating section and through two microwave heating sections at a pre-determined belt speed (0.3inch/sec) so that the temperature at the cold spot could reach a minimum of 121°C. When the last of the six trays moved outside of the two MW heating section, microwave power was turned off, and 12°C tap water was pumped into the cavities to replace the hot water and cool the food packages.

The temperature profile at the cold spot in the food was recorded using a pre-calibrated fiber optic sensor (FOT-L, FISO, Québec, CANADA). To focus more on the effect of microwave energy on the heating performance, the middle layer of the gel sample was selected to reveal the heating pattern using chemical marker with computer imaging system because the middle layer was heated the least by circulation hot water as compared to other parts in the tray. The color image at the middle layer of the whey protein gel was taken with its intensity correlated with heating intensity. The heating pattern was then obtained by using IMAQ.

Model verification and discussion

Computer model implementation

In simulating a MW heating process for moving packages, only one food tray was chosen to model coupled EM and heat transfer to reduce computer memory usage. In the simulated system, six trays shown in Fig 5.3 were considered to represent six different snapshots at different time steps for one tray. For each different step, the dissipated power distribution inside the food package was put into the heat transfer model to calculate the heat distribution. The time step was determined from the tray moving speed and spatial distance between adjacent snapshots, i.e. the distance between the centres of two neighbouring trays.

A sine wave at frequency of 915MHz was used as the excitation and its amplitude was the square root of input power (2.7KW in this study). The rectangular waveguide shown in Fig 5.2 was configured to support the propagating wave with TE_{10} mode. The MW sections had open ends on right and left sides, which then required the

numeric model to terminate with proper absorbing boundary conditions (ABC). However, Chen et al. (2007a) concluded that both perfect electrical conductor (PEC) and ABC leaded to similar simulation results with the maximum error less than 5%. It was argued that the PEC boundary condition was more suitable for simulating this system because it involved less mathematical manipulation. Therefore, instead of ABC, two PEC metals were imposed on the left and right ends of MW cavity to reduce the complexity of system modification for moving food package.

Validation results

A detailed convergence study for simulating a MW sterilization system with stationary packages was reported as well as the validation of a heat transfer model by Chen et al. (2007a). To verify that the model correctly simulates a MW heating process involving moving packages, the simulated heating pattern and temperature profile were compared with experimental results. The temperature profiles measured with a fiber optical sensor in two identical experiments are presented in Fig 5.6, along with the simulated result. Both experiment and simulated results show the temperature change with time along the moving direction. In the preheating section where no microwave energy existed, food package with initial temperature of 9°C was heated by hot water at 125°C. Because of the large gradient of temperature between food package and hot water, product temperature increases rapidly. The temperature difference between product and surrounding water, however, decreases as the temperature of food package goes up, resulting in lower heating rate especially at the cold spot. The heating rate at the cold spot becomes infinite small when the temperature approaches to 121°C. The microwave heating was used in our system to sustain continued temperature increase beyond the

initial heating after the driving potential due to conventional heat transfer becomes small. The heating rate decreased when food moves out from the microwave heating cavity (1) and increases again after food enters into the microwave heating cavity (2). Fig 5.7(a) and (b) compare the temperature distributions from the experiment and simulation, respectively. Fig 5.7(a) shows the temperature distribution calculated from the simulation, while Fig 5.7(b) shows the color of the measured heating pattern reflected by chemical marker using the computer vision method, which indicated the heat intensity inside food packages after microwave heating process. The two are similar, indicating the locations of hot and cold spot were accurately predicted by the numeric model.

Discussion

The simulated temperature profile in Fig 5.6 clearly shows that the food package was traveling from the preheating zone at product of 9°C to the unloading zone at product of 121°C during the heating process. It generally agrees with the measurements from two duplicated experiments. The measurements were not perfectly matched because it is impossible to conduct two experiments that are exactly same. In addition, the fiber optical sensor could not be placed at the exact location as specified in the simulation. For example, if the fiber optical sensor happened to be placed closer to the hot area, the measured temperature profile would be like the higher curve compared to that of the simulated one in Fig 5.6. Similarly if location of fiber optical sensor was closer to the physical cold spot than that specified in the simulation, the measured temperature profile should correspond to the lower curve presented in Fig 5.6.

Usually, for MW sterilization and pasteurization applications, the final temperature of foods after a heating process at a cold spot is more important than the

intermediate temperatures during the process. The final temperatures from three curves in Fig 5.6 have discrepancies less than 1ºC. Fig 5.7 shows the temperature distribution from simulation and the heating patterns obtained from the experiment are similar; especially the locations of hot and cold spots were correctly predicted by the numerical model. The main reason for the disagreement between simulated and measured patterns was that the obtained simulation image was a final snapshot of temperature distribution for the moving package while the measured heating pattern was an accumulated result reflected by a color image from a chemical marker. Another reason was that the water floatation made it impossible in reality to control the middle layer of the gel during heating process, especially when package was moving. Instead, during simulation, the gel was assumed to stay in the middle of the cavity in the z direction all the time. In addition, because of the complexity of the problem, the developed numeric model was more employed to be an indicator of the heating pattern after process that roughly located the critical points to minimize the experiment efforts.

Model applications

One important criterion for heating performance after MW sterilization process is heating uniformity, which, in this study, was defined as the difference between the hot spot and cold spots, i.e. $\Delta T_2 = (T_{max} - T_{min})_2$. The subscript 2 means the heating uniformity is calculated with respect to a two-dimensional plane since the focus was on the heat distribution at the middle layer of food packages. Obviously, a smaller ΔT_2 indicates better heating uniformity.

Four different cases summarized in Table 5.3 were used to illustrate the effectiveness of the validated simulation model in assisting the design of operation

parameters to improve heating uniformity. P_1 and P_2 are input powers for the first and second MW sections, respectively. L is the distance between neighboring packages. In those cases, the input powers for the two cavities and the distance between the two neighboring food trays were deliberately changed to explore their effects on heating uniformity.

Fig 5.8 shows the top view of two MW sections for the simulated moving food packages. The preheating and holding sections are presented in Fig 5.1. Temperature profiles and distributions for each case were obtained using the FDTD model developed in this paper. These results are presented in Fig 5.9(a)-(d). The heating uniformity for each case was calculated based on the temperature difference between the hot and cold spots at the middle layer (xy plane), as shown in Fig 5.10.

The distance between the neighboring packages was kept the same in both Case 1 and 2, while the input power was changed for both MW cavities. In particular, the input power of the first microwave cavity was increased by 2.3 KW, and the input power of the second MW cavity was reduced by 0.7 KW. The heating uniformity was found to worsen by 30% from Case 1 to Case 2. The distance between the neighboring packages in Cases 3 and 4 was doubled from that used in Cases 1 and 2, and the effect of two different sets of input powers was investigated. From Fig 10, the heating uniformities obtained in Case 3 and Case 4 were significantly improved as compared to those from Case 1 and Case 2. For example, when doubling the distance between two adjacent packages from Case 2 to Case 3, the temperature difference was changed from 13.6°C to 7.7°C, leading heating uniformity improved by 43.4%. In addition, it was concluded that the closer the neighboring packages, the more sensitive the heating uniformity to the input power

specified on cavities.

Conclusions

A model was developed to simulate MW sterilization processes for moving food packages in a 915MHz pilot scale system by coupling EM and thermal phenomena. This model relied on the conformal FDTD technique to solve the EM equations and a user-defined FDTD model for thermal field. By explicitly solving the coupled partial differential equations, the FDTD models intrinsically maintained the field continuity along the boundary between different media, and used a leap frog strategy to simulate MW heating in a representative moving package, which significantly reduced the computational complexity and simulation time. Direct temperature measurements and color patterns of color changes based on chemical marker M-2 formation in the whey protein gel were used to validate the simulation model. The validated model was used for four different cases to demonstrate its applications to improve heating uniformity by properly setting appropriate operational parameters such as input powers or gaps between moving packages.

Though only homogeneous food packages were considered in validating the model, the model can be easily extended for inhomogeneous food packages due to the explicit nature of FDTD method. In addition, the simulation results for homogeneous packages provided useful reference for studying the heating patterns for inhomogeneous food because of the single-mode system. For instance, the calculated temperature distributions showed which area had significant microwave energy focused and which area did not. Based on this information, inside an inhomogeneous food package, the dielectric properties could be deliberately altered so as to redirect surplus microwave to

the area with less initial energy, which resulted in more uniform heating.

Acknowledgment

NOMENCLATURE

A   Boundary surface area

B   Magnetic flux density

C   Contour path

D   Electrical flux density

E   Electrical field intensity (volt/meter)

H   Magnetic field intensity (amperes/meter)

J_i Source current density (amperes/square meter)

J_c Conduction current density (amperes/square meter)

$K(T)$ Thermal conductivity at temperature T (W/m.K)

Q^e Electrical charge surrounded by a surface S

S   Surface for computation domain

T   Temperature (˚C)

T_s Circulating water temperature (˚C)

μ   Dielectric permeability

ε   Dielectric permittivity

$c_p(T)$ Specific heat at temperature T (J/kg.K)

$\rho(T)$ Mass density at temperature T (kg/m^3)

$\rho_v(T)$ Volumetric specific heat at temperature T (J/m^3.K)

h   Heat transfer coefficient (W/m^2.K)

q   Thermal energy provided by circulating water on the boundary (W)

$\dot{q}$ Dissipated power density provided by heating source (W/m^3)

Δx_i Cell size in x-direction (meter)

Δy_j Cell size in y-direction (meter)

Δz_k Cell size in z-direction (meter)

References

Balanis, C. A. (1989). *Advanced engineering electromagnetics*, John Wiley & Sons,

Barratt, L., & Simons, D. (1992). Experimental validation of a computer simulation of microwave heating. *in Proc. 27th Microwave Power Symp*, 118-122.

Bows, J., Patrick, M. L., Dibben, D. C., & Metaxas, A. C. (1997). Computer simulation and experimental validation of phase controlled microwave heating. *presented at the 6th Microwave and High Frequency Heating Conference*, Fermo, Italy.

Burfoot, D., Railton, C. J., Foster, A. M., & Reavell, R. (1996). Modelling the pasteurization of prepared meal with microwave at 896MHz. *Journal of Food Engineering*, 30, 117-133.

Chen, H., Tang, J., & Liu, F. (2007). Coupled simulation of an electromagnetic heating process using the Finite Difference Time Domain method *Journal. of Microwave Power and Electromagnetic Energy*, 41(3), 50-68.

Clemens, J., & Saltiel, G. (1995). Numerical modeling of materials processing in microwave furnaces. *International Journal of Heat and Mass Transfer*, 39(8), 1665-1675.

Dibben, D. C., & Metaxas, A. C. (1994). Finite-Element Time-Domain Analysis of Multimode Applicators Using Edge Elements. *Journal of Microwave Power and Electromagnetic Energy*, 29(4), 242-251.

Guan, D., Cheng, M., Wang, Y., & Tang, J. (2004). Dielectric properties of mashed potatoes relevant to microwave and radio-frequency pasteurization and sterilization processes. *Journal of Food Science*, 69(1), E30-E37.

Gwarek, W. K., Celuch-Marcysiak, M., Sypniewski, M., & Wieckowski, A. (1999). *QuickWave-3D Software Manual*, QWED, Warsaw, Porland.

Harms, P. H., Chen, Y., Mittra, R., & Shimony, Y. (1996). Numerical modeling of microwave heating systems. *Journal of Microwave Power and Electromagnetic Energy*, 31(2), 114-121.

Harms, P. H., Lee, J. F., & Mittra, R. (1992). A Study of the Nonorthogonal Fdtd Method Versus the Conventional Fdtd Technique for Computing Resonant Frequencies of Cylindrical Cavities. *IEEE Transactions on Microwave Theory and Techniques*, 40(4), 741-746.

Holland, R. (1993). Pitfalls of Staircase Meshing. *Ieee Transactions on Electromagnetic Compatibility*, 35(4), 434-439.

Incropera, F. P., & DeWitt, D. P. (2001). *Introduction to heat transfer, 4th*, John Wiley & Sons, New York.

Jurgens, T. G., Taflove, A., Umashankar, K., & Moore, T. G. (1992). Finite-Difference Time-Domain Modeling of Curved Surfaces. *IEEE Transactions on Antennas and Propagation*, 40(4), 357-366.

Kopyt, P., & Celuch-Marcysiak, M. (2003). Coupled electromagnetic and thermal simulation of microwave heating process. *Proc. 2nd Intern. Workshop on Information Technologies and Computing Techniques for the Agro-Food Sector*, Barcelona, Spain, November-December, 2003, 51-54.

Lau, M. H., Tang, J., Taub, I. A., Yang, T. C. S., Edwards, C. G., & Mao, R. (2003). Kinetics of chemical marker formation in whey protein gels for studying microwave sterilization. *Journal of Food Engineering*, 60(4), 397-405.

Leo, R. D., Cerri, G., & Mariani, V. (1991). TLM techniques in microwave ovens analysis: Numerical and experimental results. *in Proc. 1st Int. Conf. Computation in Electromagnetics*, London, 361-364.

Ma, L. H., Paul, D. L., Pothecary, N., Railton, C., Bows, J., Barratt, L., Mullin, J., & Simons, D. (1995). Experimental Validation of a Combined Electromagnetic and Thermal Fdtd Model of a Microwave-Heating Process. *IEEE Transactions on Microwave Theory and Techniques*, 43(11), 2565-2572.

Madsen, N. K., & Ziolkowski, R. W. (1988). Numeric solution of maxwell's equations in the time domain using irregular nonorthogonal grids. *Wave Motion*, 10, 583-596.

Ohlsson, T. (1987). Sterilization of foods by microwaves. *International Seminar on New Trends in Aseptic Processing and Packaging of Food stuffs*, 22 Oct. 1987; Munich. SLK Report nr 564. Goteborg, Sweden: The Swedish Institute for Food and Biotechnology.

Ohlsson, T. (1990). Controlling heating uniformity - The key to successful microwave products. *Euro. Food Drink Rev.*, 2, 7-11.

Ohlsson, T. (1992). Development and evaluation of microwave sterilization process for plastic pouches. *Paper presented at the AICHE Conference on Food Engineering*, March 11-12, Chicago, IL.

Osepchuck, J. M. (1984). A history of microwave heating applications. *IEEE Trans. Microwave Theory Tech*, MTT-32, 1200-1224.

Pandit, R. B., Tang, J., Liu, F., & Mikhaylenko, M. (2007a). A computer vision method to locate cold spots in foods in microwave sterilization processes. *Pattern Recognition*, 40, 3667-3676.

Pandit, R. B., Tang, J., Liu, F., & Pitts, M. (2007b). Development of a novel approach to determine heating pattern using computer vision and chemical marker (M-2) yield. *Journal of Food Engineering*, 78(2), 522-528.

Pandit, R. B., Tang, J., Mikhaylenko, G., & Liu, F. (2006). Kinetics of chemical marker M-2 formation in mashed potato - A tool to locate cold spots under microwave sterilization. *Journal of Food Engineering*, 76(3), 353-361.

Paoloni, F. (1989). Calculation of power deposition in a highly overmoded rectangular cavity with dielectric loss. *Journal of Microwave Power and Electromagnetic Energy*, 24(1), 21-32.

Ryynanen, S., & Ohlsson, T. (1996). Microwave heating uniformity of ready meals as affected by placement, composition, and geometry. *Journal of Food Science*, 61(3), 620-624.

Smyth, N. F. (1990). Microwave-Heating of Bodies with Temperature-Dependent Properties. *Wave Motion*, 12(2), 171-186.

Speigel, R. J. (1984). A review of numerical models for predicting the energy deposition and resultant thermal response of humans exposed to electromagnetic fields. *IEEE Trans. Microwave Theory and Techn*, MTT-32, 730-746.

Taflove, A. (1998). Computational electrodynamics : the finite-difference time-domain method, Artech House, Boston, MA.

Tang, J., Liu, F., Pathak, S., & Eves, G. (2006). Apparatus and method for heating objectives with microwaves. U.S. patent 7,119,313.

Torres, F., & Jecko, B. (1997). Complete FDTD analysis of microwave heating processes in frequency-dependent and temperature-dependent media. *IEEE Transactions on Microwave Theory and Techniques*, 45(1), 108-117.

Watanabe, W., & Ohkawa, S. (1978). Analysis of power density distribution in microwave ovens. *Journal of Microwave Power and Electromagnetic Energy*, 13(2), 173-182.

Webb, J. P., Maile, G. L., & Ferrari, R. L. (1983). Finite element solution of three dimensional electromagnetic problems. *IEEE Proceedings*, 130(2), 153-159 .

Z.Shou-Zheng, & C.Han-Kui (1988). Power distribution analysis in rectangular microwave heating applicator with stratified load. *Journal of Microwave Power and Electromagnetic Energy*, 23(3), 139-143.

Zhang, H., & Datta, A. K. (2000). Coupled electromagnetic and termal modeling of microwave oven heating of foods. *Journal of Microwave Power and Electromagnetic Energy*, 35(2), 71-85.
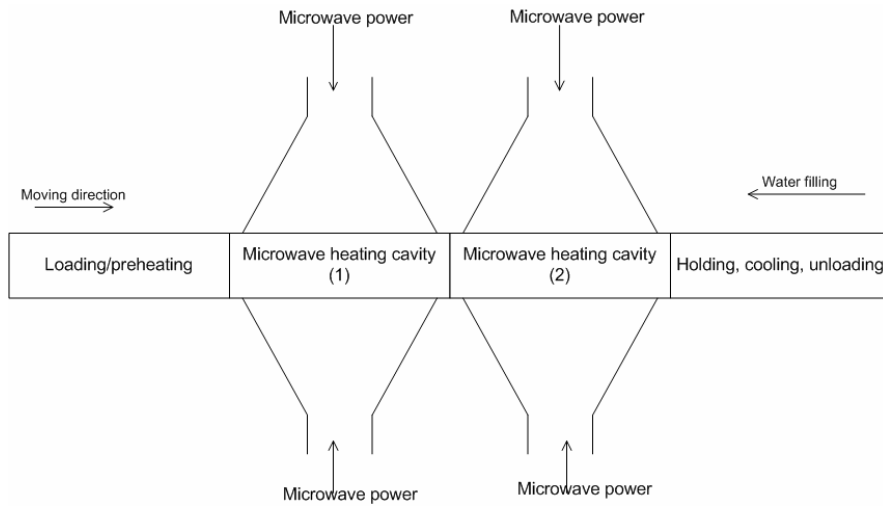
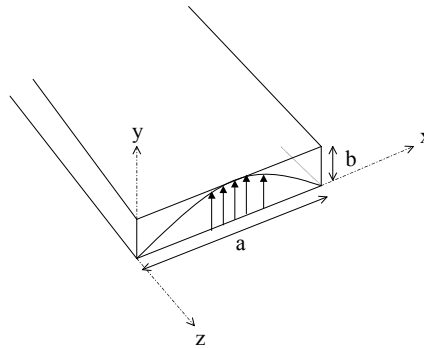Fig 5.1 Continuous microwave heating system (front view)

Fig 5.2 Geometrical configuration of single mode waveguide with dominant mode TE10
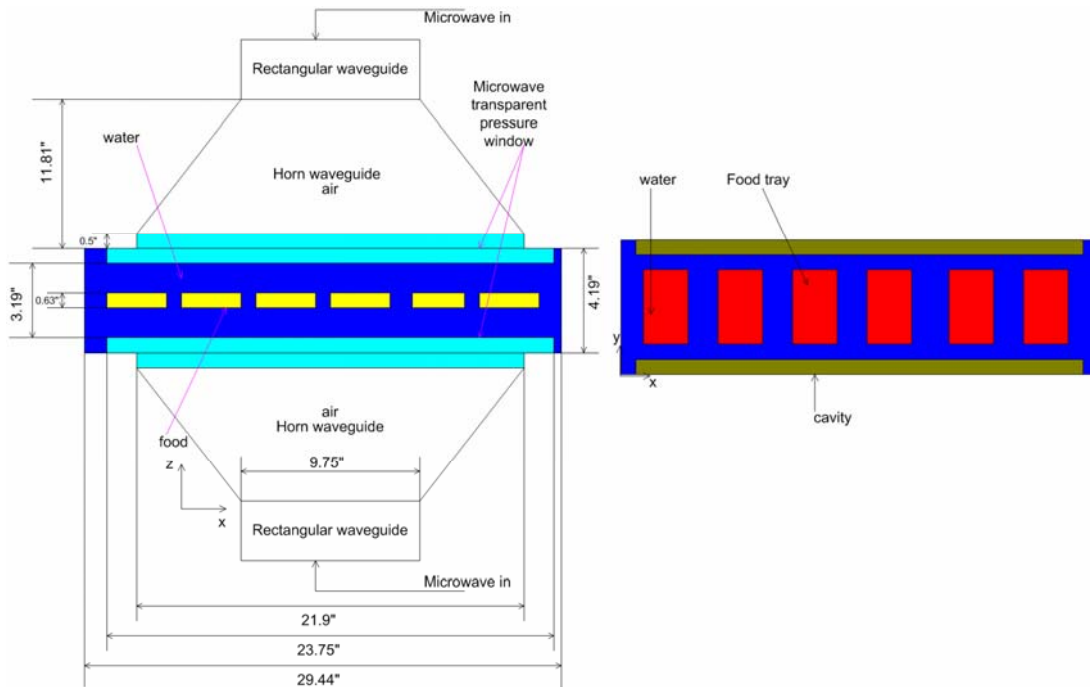
144

Fig 5.3 Schematic view of one microwave section: front view (left), top view (right)
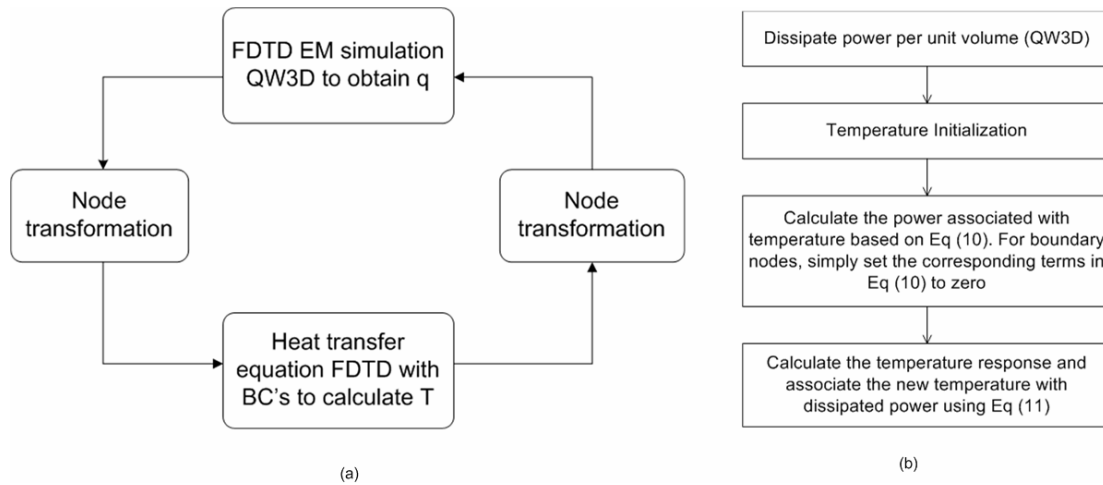

Fig 5.4 Coupled model for microwave heating: (a) numeric schema, (b) communication
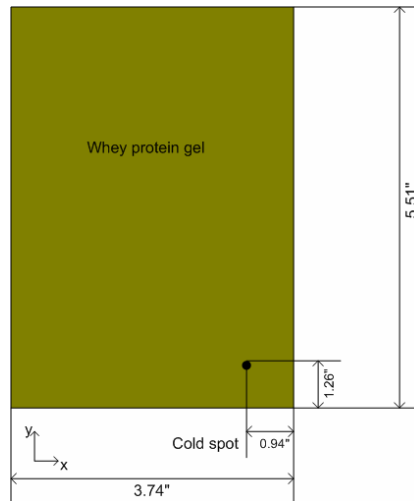
flowchart

Fig 5.5 Top view of middle layer of whey protein gel inside a 7oz tray with fiber optic
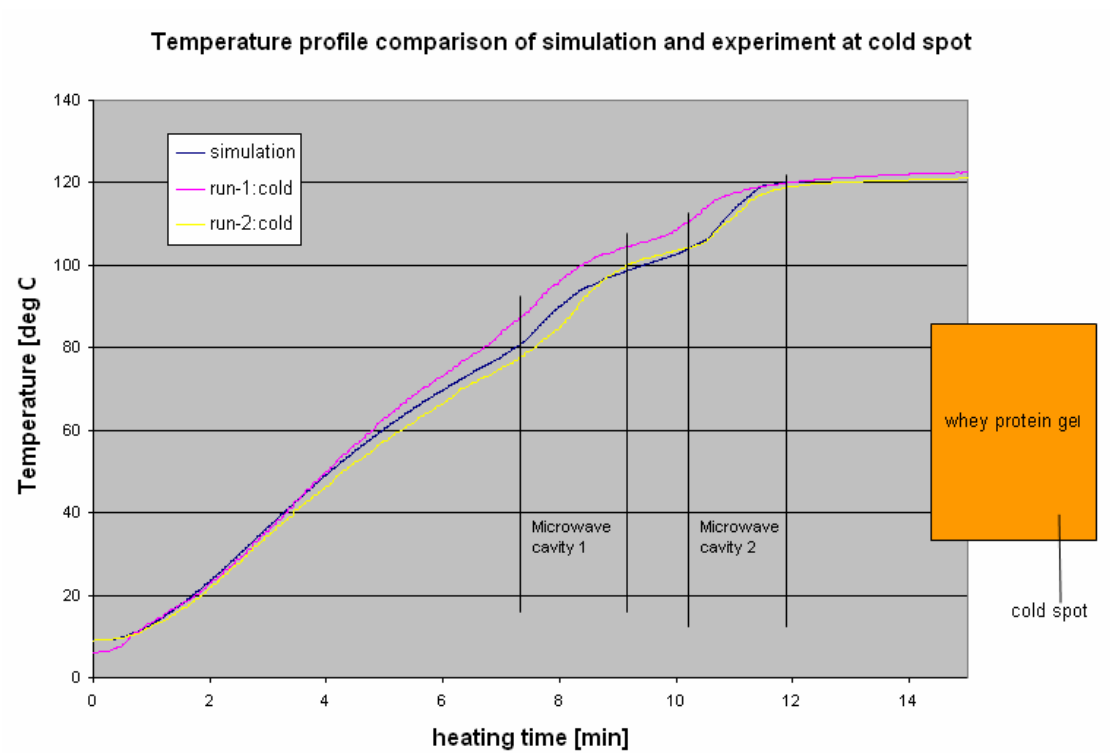
sensor at cold spot

Fig 5.6 Comparison of simulation results for temperature evolution at cold spot with

experiment results from two identical experimental runs
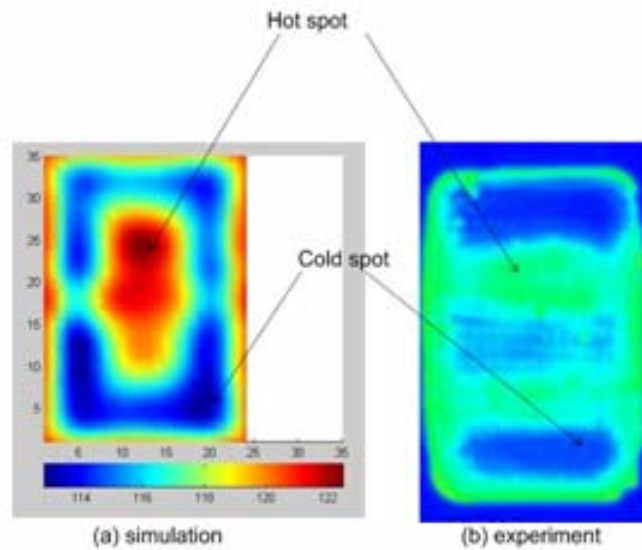
Fig 5.7 Final snapshot of temperature distribution (°C) from simulation (a) and accumulated heating pattern reflected by color image from chemical marker (b) at the middle layer of whey protein gel (top view) after 3.2min MW heating time.

Fig 5.8 Arrangement of simulation for moving packages at several cases
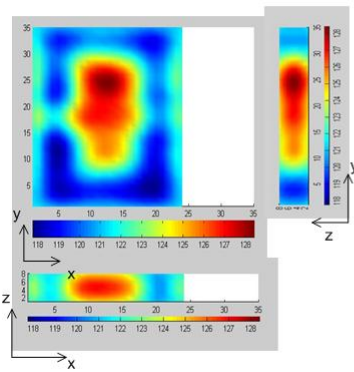
(a) Case 1
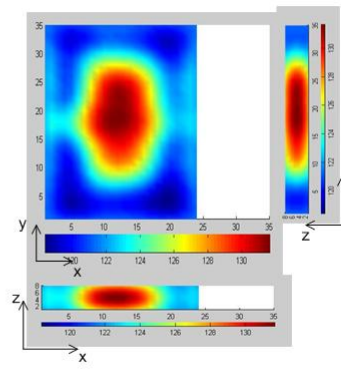
(b) Case 2
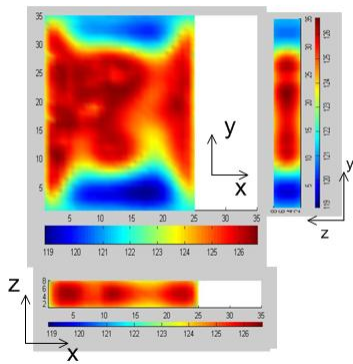
(c) Case 3
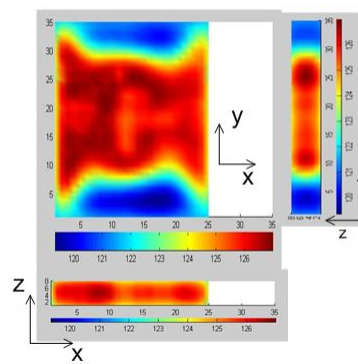
(d) Case 4

Fig 5.9 Temperature distribution (°C) at the middle layer from top, front and side view

for different cases

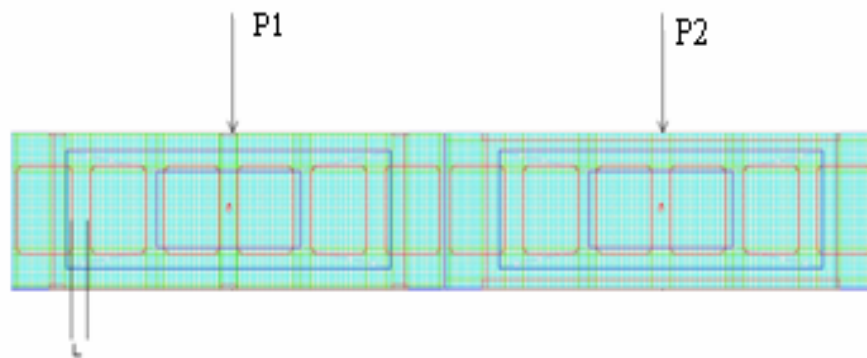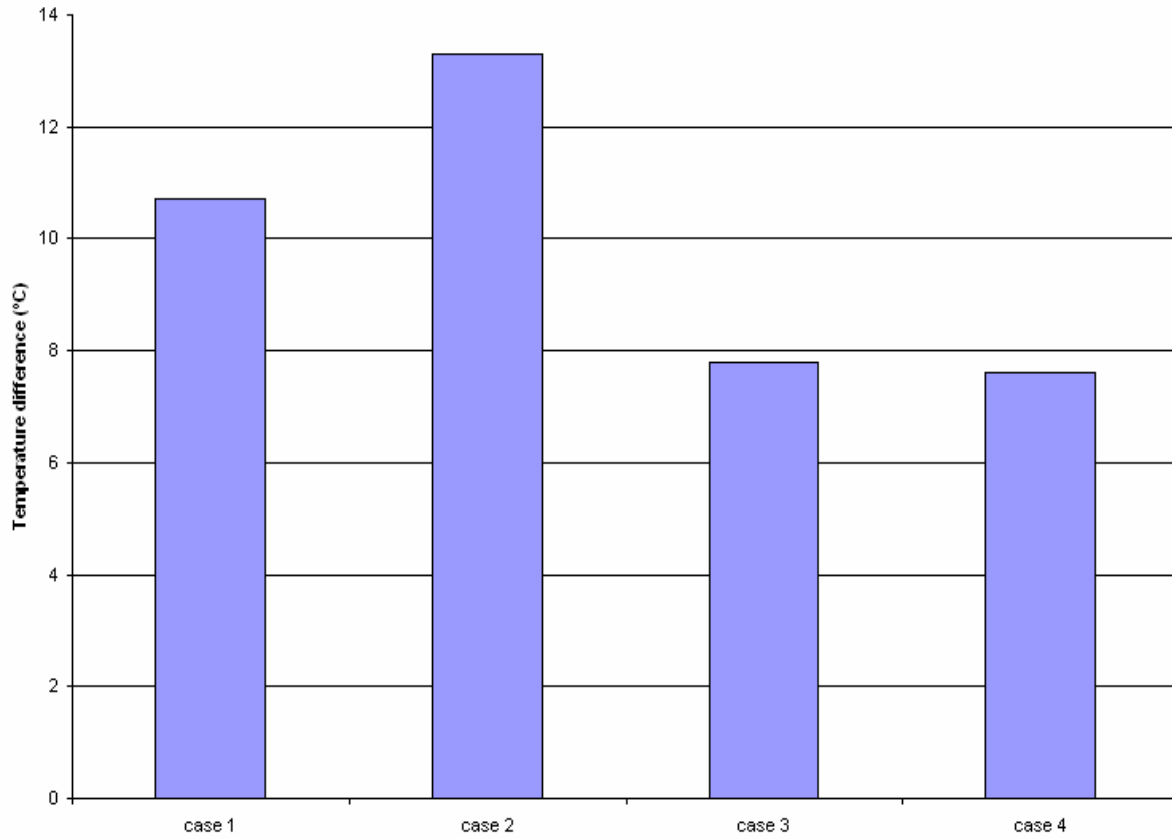Fig 5.10 Heating uniformity at the middle layer of whey protein gel

Table 5.1 Dielectric properties of whey protein gel

Temperature [^oC]	Dielectric constant $\varepsilon_r^{'} = \varepsilon^{'}/\varepsilon_0$	Dielectric loss $\varepsilon_r^{"} = \varepsilon^{"}/\varepsilon_0$
20	58.5	24.25
40	57.55	30.25
60	56.36	36.79
80	54.36	45.21
100	52.81	53.89
121	51.14	63.38

Table 5.2 Thermal properties of whey protein gel

Temperature [°C]	Volumetric specific heat $\rho c_p [MJ/m^3 K]$	Thermal conductivity $K[W/mK]$
0	3.839	0.513
20	3.973	0.537
35	3.901	0.550
50	3.814	0.561
65	3.883	0.578
80	3.766	0.588

Table 5.3 Case study of heating uniformity

	$P_1(KW)$	$P_2(KW)$	$L(inch)$
Case 1	2.7	2.7	1.25
Case 2	5.0	2.0	1.25
Case 3	2.7	2.7	2.5
Case 4	5.0	2.0	2.5

Chapter 6 Model Application

Abstract

Computer Aided Design (CAD) has been significantly used in predicting system performance, retrieving information and proposing process optimization. CAD has numerous advantages over the traditional experimental methods. It provides insight into complicated physical phenomenon without using closed-form analytical solutions. In this study, several applications were explored by a coupled model to simulate industrial microwave industrialization processes. These applications included EM field distribution examination and system performance optimization in terms of heating uniformity as well as the effect of dielectric properties on EM field patterns. In addition, an algorithm was developed to achieve the desired temperature required for food sterilization applications. Results showed that the computer model can be an efficient tool for system design and process optimization.

Introduction

Unlike communication, network, and signal processing industries, the manufacture in food industry is slow to use CAD to predict the system performance and provide the optimization proposal due to high cost computers and its rather stable use of traditional processing methods. However, until recently, since the development of advanced computational techniques and sharply reduced hardware cost, increasing investment in CAD has been applied for equipment design and process optimization in food industry.

Numerical modeling gained increasing usage for food applications, including microwave heating, since the end of 1980s (Lorenson, 1990; Palombizio and Yakovlev, 1999). Yakovlev (2001) provided a numeric approach to improve MW heating quality by using advanced three dimensional simulation. He developed a computer simulation model to analyze the problem of control and optimization of electrical field by focusing on the material specification for food packages. Veronesi, et al.(2003) discussed a MW assisted drying application that used a combination of hot air and MW energy to achieve much shorter drying time compared with conventional drying methods. Another application was for chemistry enhanced by MW using a re-entrant cavity (Kalhori, et al., 2003). In this application, numeric techniques such as Finite Difference Time Domain (FDTD) and Finite Element Method (FEM) were employed to design a re-entrant cavity that provided high MW power absorption rate in a small liquid or solid chemical sample. Komarov, et. al. (2003) utilized EM modelling to determine the temperature dependent dielectric properties by using perturbation technique and the complex permittivity was obtained by applying FDTD modelling with the principle of neural network (Eves, et al., 2004). In detail, the dielectric properties were reconstructed by matching the computed reflection coefficients with the measured counterpart. It provided a high accurate and cavity-independent method to obtain the dielectric properties (Yakovlev and Murphy, 2004). Mechenova, et. al (2004) optimized the MW thermal processing by examining the coupled energy in terms of the numeric characteristics of system efficiency. Basically, it provided a scheme suitable for programming to find the minimum zenith of reflection coefficient based on Maxwell's equations and output the material properties associated

with it. Another optimization algorithm was also provided by Yakovlev (2004), which proposed a design of waveguide window by minimizing the reflection characteristics.

Though numerous researches were conducted to employ CAD for MW applications, there are few endeavors carried out to use CAD for MW sterilization processes. In this chapter, a numeric model was applied to explore several cases in different sterilization scenarios. Then based on the simulation results, an algorithm was developed to optimize the process in order to achieve the desired temperature at cold and hot spot required for sterilization purpose.

Microwave sterilization process

Physical system

The considered microwave sterilization system was a pilot-scale system developed at Washington State University (WSU, Pullman, WA, USA). The system consisted of a rectangular cavity with one horn-shaped applicator on the top and another identical applicator on the bottom (Fig.1 and Fig.2 in Chapter 4). Fig.1 shows a front view of the system with an exposed interior cut and vertical central plane, while Fig.2 shows the top view for the central section of the cavity. Microwave energy was provided by a 5 kW generator operating at 915 MHz through a standard waveguide that supported only TE_{10} mode (Fig.3). Fig.3 provides detailed information for the top and bottom rectangular waveguide sections having a length of 128mm and width of 124mm. After passing through a circulator, the microwave energy was equally divided at a T-junction and fed to the two horn applicators through two standard waveguides shown in Fig.3 (in Chapter 4). The length of each leg of the waveguide after the T-junction could be adjusted to control the phase difference between the microwaves at the entry port of the

two horn applicators, which meant the phase shift between the two waves interacting inside the cavity could be controlled to achieve the desired field distribution. More details about the system could be found in Chapter 4.

Numerical modeling for microwave sterilization process

A reliable computer model can be an efficient tool to investigate the microwave sterilization process. It significantly reduces the design cycle by using advanced technologies and the state-of-art computational techniques. It also has additional advantage over conventional experimental methods because it can be used to investigate some abnormal cases which are not doable with physical measurement otherwise. By predicting microwave heating results during sterilization processes, the model provides hardware and design engineers deep insights into system performance, thus facilitating the corresponding optimization.

Several challenges are present for numerically simulating microwave sterilization technique due to the complex natures of solving Maxwell's equations and thermal equations simultaneously. That is, during a microwave sterilization process, microwave energy is dissipated into dielectric foods, which are heated from inside because of the dissipated energy. The dielectric properties of food are then changed with temperature increased by microwave heating. In the meantime, the changed dielectric properties have significant effects on the electromagnetic field. Therefore, the electrical and magnetic fields need to be updated at each step when the dielectric properties are changed. The coupling feature was discussed in detailed in previous chapters, along with several state-of-art computational techniques such as Finite Difference Time Domain (FDTD) method, Finite Element Method (FEM), Transmission Line Method (TLM), and Moment of

Method (MoM). Among all these methods, FDTD is most popular because it explicitly solves Maxwell's equations without computing the inversion of matrix and it also preserves the high accuracy of modelling the irregularities of geometry without introducing mathematic overhead.

A computer model for simulating microwave sterilization process containing stationary and moving food packages was successfully developed in the last two chapters (Chen, et al., 2007a, 2007b). The model accurately simulated the temperature profile at the cold spot of a food package. The overall simulated temperature patterns agreed with the accumulated experimental heating patterns. Preliminary studies were conducted to apply the developed model to investigate the sterilization process under different conditions. In this chapter, more applications will be explored.

EM patterns for different cavity configurations

The considered MW sterilization process combined the MW heating and hot water heating. MW was responsible for heating the inner of food packages, while hot water responsible for surface heating. Compared with conventional hot water heating, this combination sharply reduced the heating time so as to significantly preserve the food quality. However, as mentioned in previous chapters, one major concern about MW heating is the non-uniform heating caused by non-uniform EM distributions. Since a short process time is used for MW heating during which the role of heat conduction to alleviate non uniform heating is minimum, the final temperature distribution is largely dependent on the EM distribution inside food packages. For this reason, the heating uniformity can be improved only if better uniformity of EM distribution is obtained. In this section, several MW cavities with different configurations were investigated.
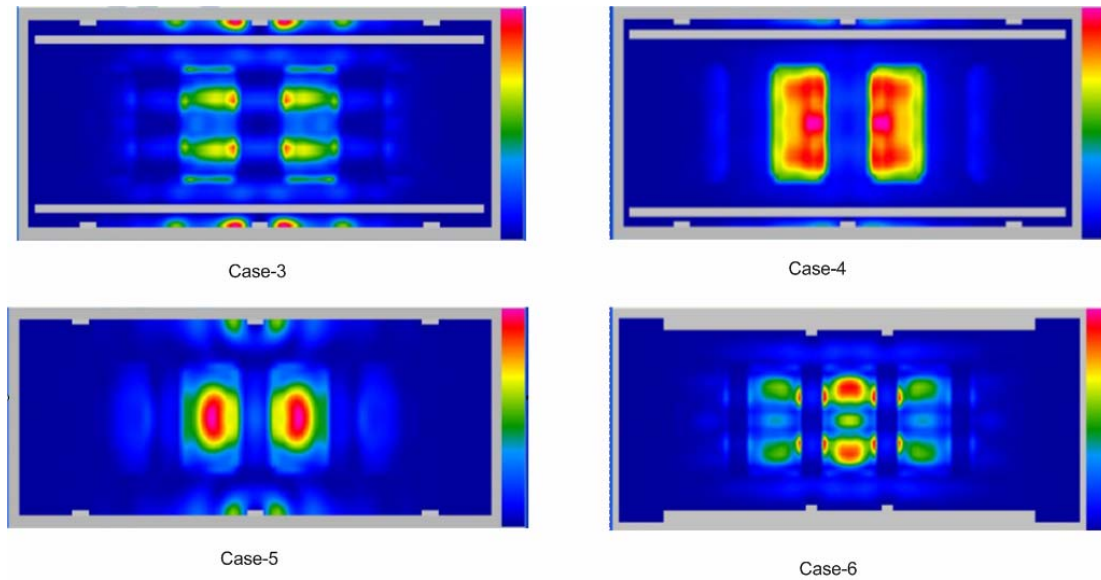
Fig 6.1 EM field distribution at middle layer inside different cavities

Fig 6.1 showed the EM distributions inside cavities with different physical configurations. The heated objects are whey protein gels at 121˚C (ε'=51.14, ε''=63.38). The details about microwave system were described in Chapters 4 and 5. Therefore, only distinction between four different cavity configurations will be discussed here. In Case-3, there were two rectangular plates (610mm x 25.4 x 81mm) made of ultem material in the front and back of the cavity, respectively. These two ultem plates were kept 5.75 inch away from each other. In Case-4, the two ultem bars were moved away from cavity center by 0.4 inch. In Case-5, the two ultem bars were removed from the cavity, while in Case-6, two ultem plates were placed against the front and back wall of cavity.

Significant difference in EM field patterns can be observed from Fig 6.1, indicating that the physical configuration could be deliberately altered to achieve distinct EM distributions. This created possibilities that the EM distributions inside different cavities in a system could be accumulated together along the moving direction of food

package to achieve better heating uniformity. In Chapter 5, the MW sterilization process is to move the food package from the loading section to the unloading section through two different MW sections in the middle. The two MW sections were configured as Case-5 and Case-6, respectively. Usually, there should be numerous MW sections incorporated into the sterilization process for industrial application. Therefore we can deliberately add new MW cavities into existing ones to improve the final accumulated field distribution.

Optimization algorithm

For sterilization purpose, the temperature at the cold spot in a package needs to reach over 121˚C, with the temperature at hot spot below 130˚C to prevent package burst (Guan, et al., 2004). However, the temperatures at the cold and hot spots after a microwave sterilization process in our study were initially unknown so that it was difficult to choose proper parameters such as the moving speed for the food packages. For this reason, an algorithm was developed to facilitate the selection of right parameters by adaptively updating the parameters based on the latest simulated results. The flowchart for the algorithm is presented as the following:
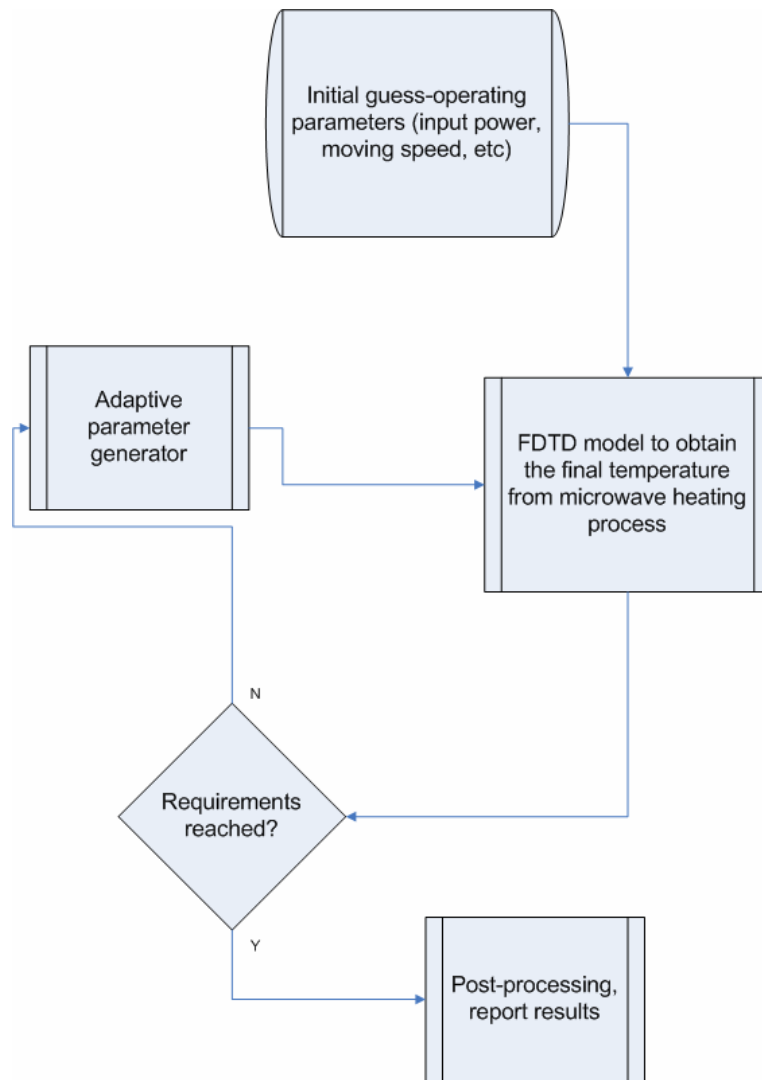
Fig 6.2 optimization scheme for process parameters specification

In the optimization algorithm, the initial value of parameters such as input power and moving speed were provided based on previous experience, and then the coupled simulation model was launched to calculate the final temperature distribution. Once the temperatures at the cold and hot spots were obtained and if they are within the range of $(121^{\circ}C, 130^{\circ}C)$, the final results were reported. Otherwise, the predetermined parameters such as input power and moving speed would be adjusted accordingly. This process

158

continued until the final temperature fell into the desired temperature range as shown in Fig 6.2.

The adaptive parameter generator automatically produces process parameters according to the latest simulation results.

$$\frac{L}{v(i,j)} \Leftarrow \frac{L}{v(i,j)} * \alpha\left(\left|T_c - T_{cs} + T_{c,thresh}\right|, \left|T_h - T_{hs} - T_{h,thresh}\right|\right) \tag{1}$$

$$\alpha\left(\left|T_c - T_{cs} + T_{c,thresh}\right|, \left|T_h - T_{hs} - T_{h,thresh}\right|\right) = \begin{cases} 1 - \dfrac{T_c - T_{cs} + T_{c,thresh}}{T_h - T_c} & T_c < T_{cs} - T_{c,thresh} \\ 1 - \dfrac{T_h - T_{hs} - T_{h,thresh}}{T_h - T_c} & T_h > T_{hs} + T_{h,thresh} \end{cases} \tag{2}$$

Equations (1) and (2) show how the adaptive generator works for optimization purpose. L in equation (1) is the distance between neighbouring snapshots defined in Chapter 5, $v(i, j)$ is the ith snapshot in the jth cavity for simulating the MW heating of moving packages. T_c and T_h are temperatures at the cold and hot spots, respectively, determined from numeric model for each iteration of optimization loop. $T_{cs} = 120°C$ and $T_{hs} = 130°C$ are the temperatures at the cold and hot spots necessary to satisfy sterilization purpose. Since in reality, it is difficult to obtain the exact same temperature as the desired one, we set thresh holds for cold and hot spots, i.e. $T_{c, thresh} = 1°C$, $T_{h, thresh} = 5°C$. The parameter generator altered the heating time for each snapshot according to the latest temperature value. When the simulated temperature value was less than $T_{cs} - T_{c, thresh}$, the moving speed was reduced to increase the heating time, and if the simulated temperature value was larger than $T_{hs} + T_{h,thresh}$, the moving speed was increased to shorten the heating time. By following these procedures, we can determine the appropriate moving speed to achieve the desired temperature range.

As an example, we simulated four microwave cavities along the moving direction for a MW sterilization process, those four cavities were combined to improve the heating uniformity. To estimate the appropriate moving speed, we applied the numeric model with optimization algorithm on a process with four cavities involved. That is, four different cavities shown in Fig 6.3 were connected in sequence, and the overall heating pattern in a food package was the result of the sum of four electromagnetic fields after it travelled through the four cavities. The required final temperatures at cold and hot spot were ensured by the optimization loop.
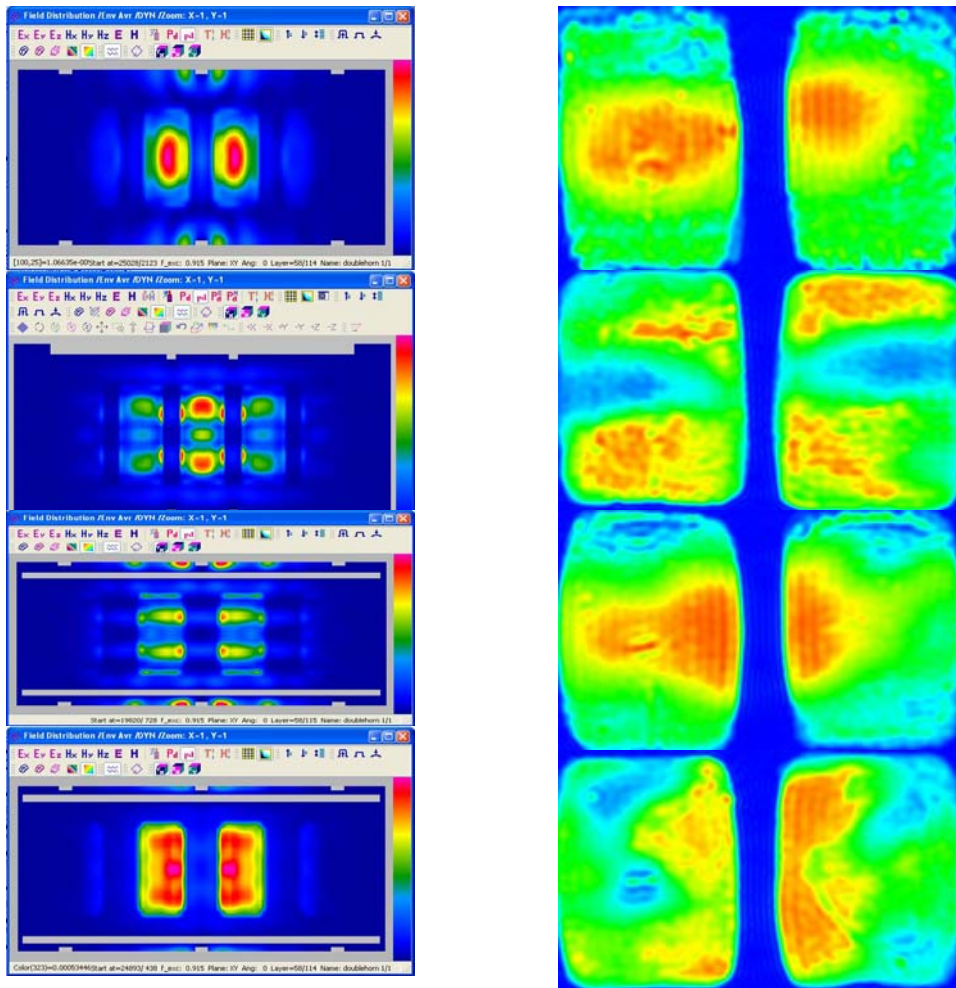
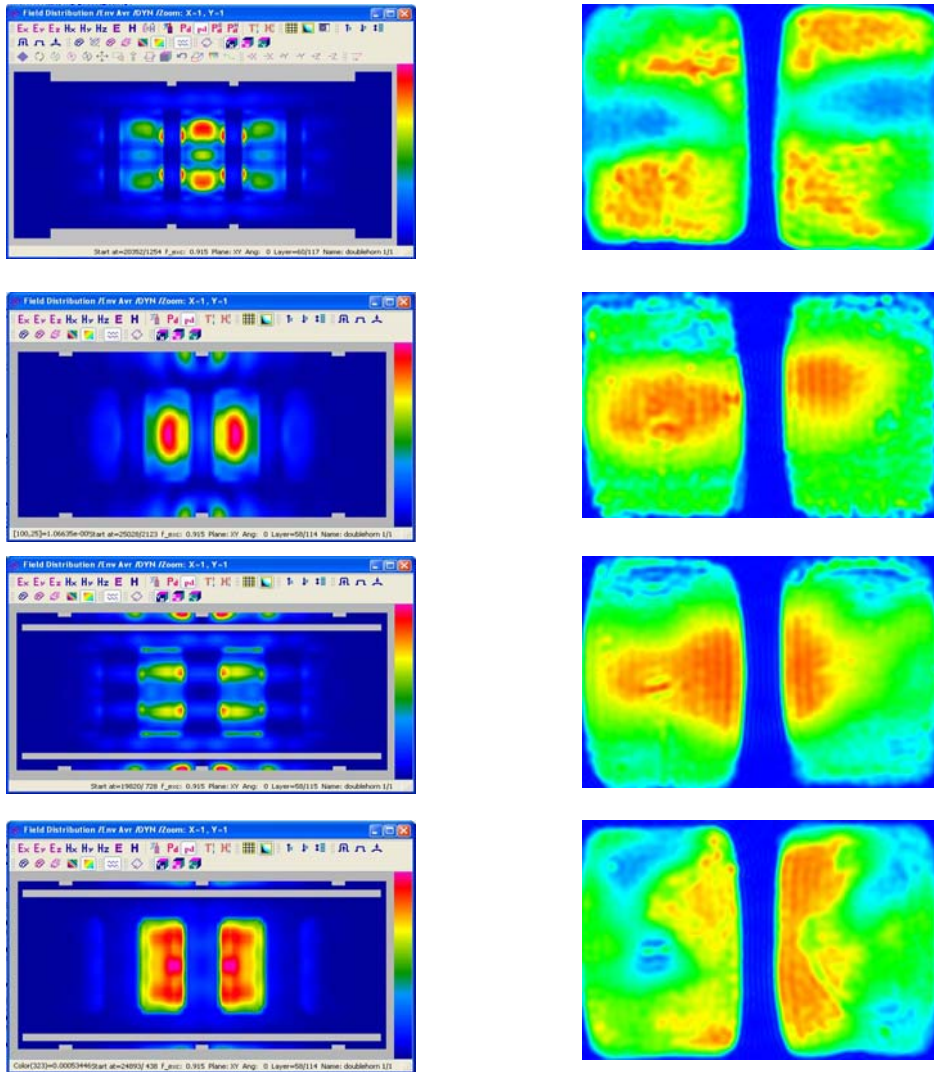(a) Case combination: simulation (left); experiment (right)
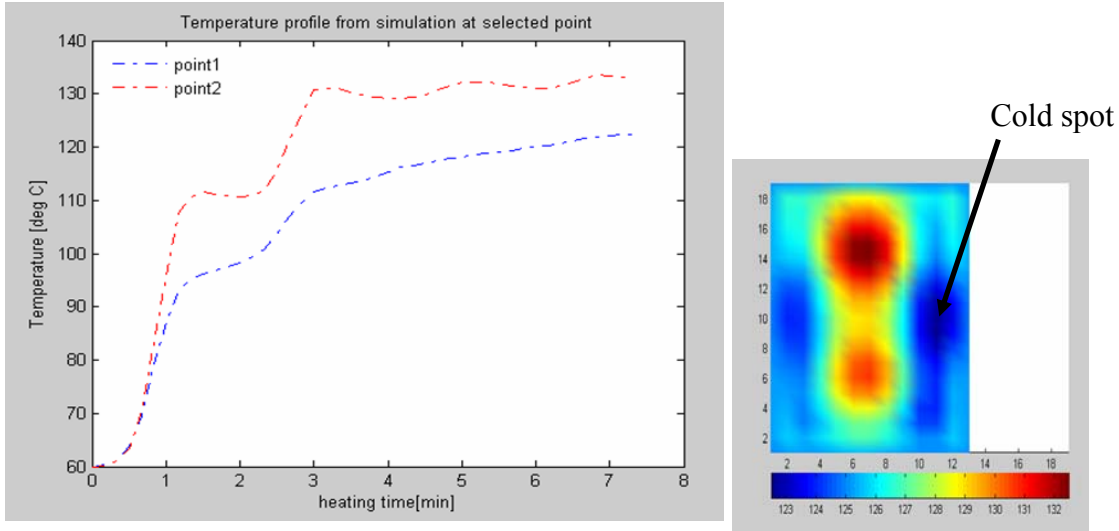
(b) Simulated temperature profile and heating pattern (No. of cells in x- and y- directions)
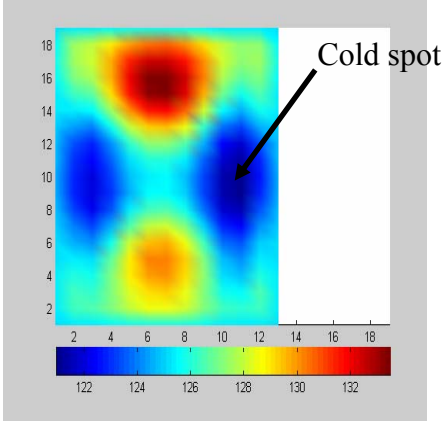
at middle layer of food package

Fig 6.3 Simulation results for MW sterilization process with four cavities

(case5-case6-case3-case4)

Fig 6.3 shows the heating pattern in the food package after a MW sterilization process with four MW sections. Different cavities were combined in a particular order: case-5, case-6, case-3, and case-4 as shown for left to right. To verify the correctness of the numeric model, experimentally determined patterns for each cavity were shown in Fig 3 for comparison. The measured patterns were the accumulated heating pattern of the middle layer of the food package. They were determined using a chemical marker/computer imaging system to highlight the influence of the microwave fields. The detailed measurement procedures were described in Chapter 4. The simulated temperature profile and heating pattern were shown in Fig 6.3(b). The temperatures at cold and hot spot were set into desired range due to optimization algorithm. The process time was found to be 7.5min.

To demonstrate the flexibility of the model with the proposed optimization algorithm, three more processes with different case combinations were obtained in Fig 6.4-Fig 6.6.

(a) Case combination: simulation (left); experiment (right)

Cold spot

(b) Simulated temperature profile and heating pattern (No. of cells in x- and y- directions)
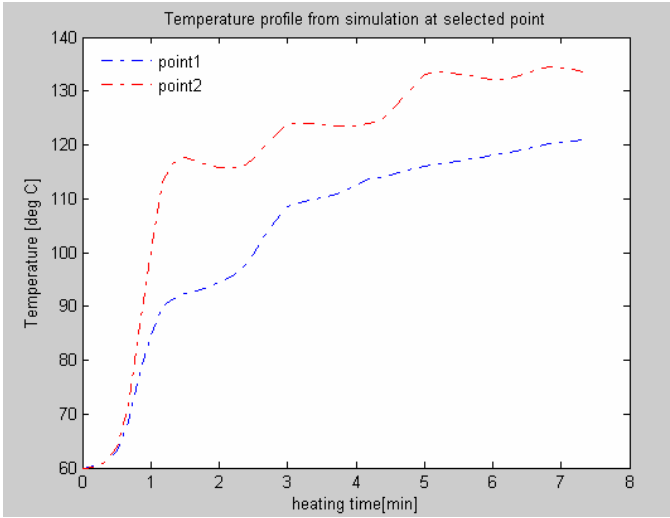
at middle layer of food package

Fig 6.4 Simulation results for MW sterilization process with four cavities

(case6-case5-case3-case4)

(a) Case combination: simulation (top); experiment (bottom)

(b) Simulated temperature profile and heating pattern (No. of cells in x- and y- directions)

at middle layer of food package

Fig 6.5 Simulation results for MW sterilization process with four cavities
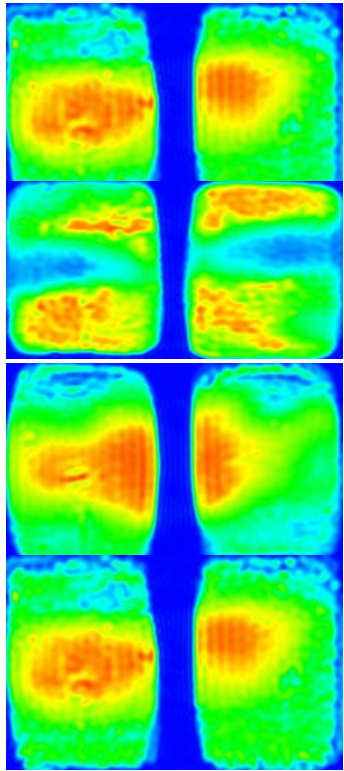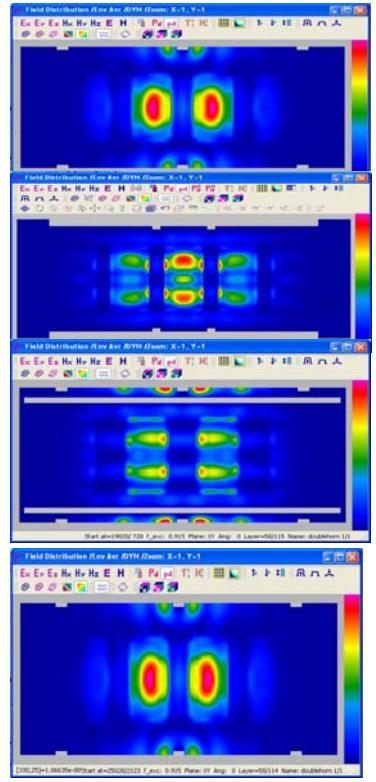
(case5-case6-case3-case5)

(a) Case combination: simulation (left); experiment (right)
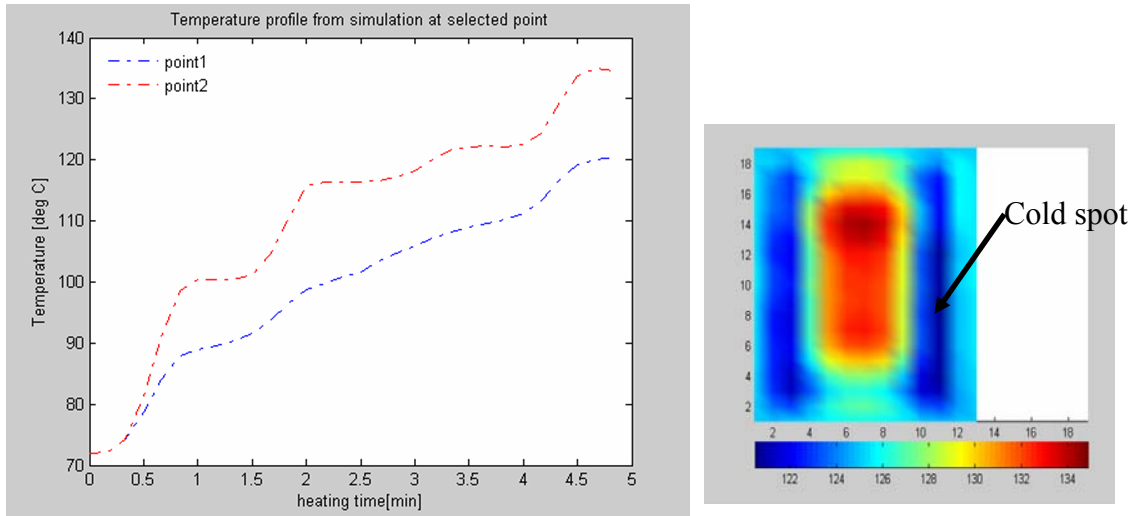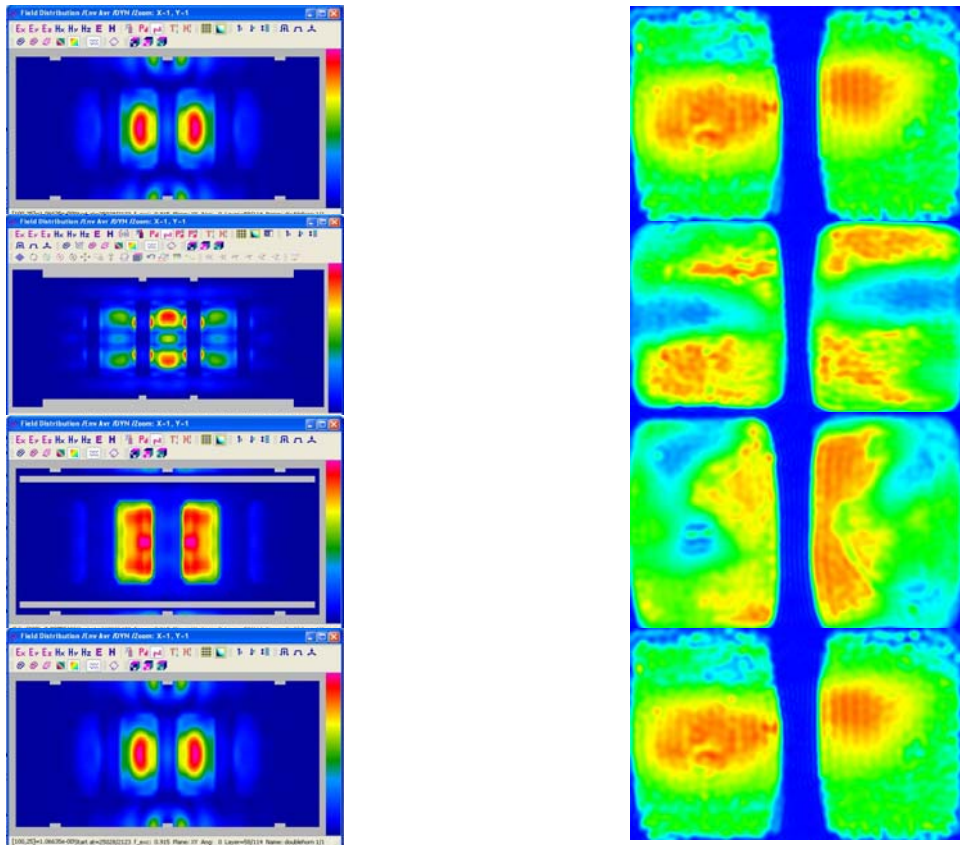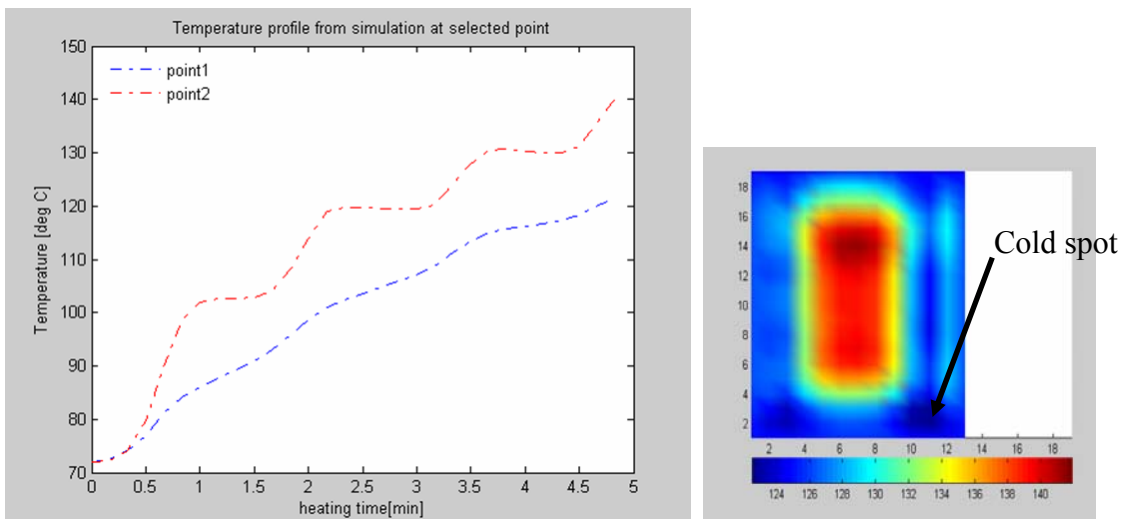

(b) Simulated temperature profile and heating pattern (No. of cells in x- and y- directions)

at middle layer of food package

Fig 6.6 Simulation results for MW sterilization process with four cavities (case5-case6-case4-case5).

In Fig 6.4-Fig 6.6, we present the simulation results for an industrial sterilization process with four MW cavities, each having different physical configurations and input powers. Along the moving direction of food package, the four MW cavities are combined together in different sequences so that they will provide distinct final heating patterns. The details of combination were shown in the top part of each picture along with simulated and measured field patterns. The temperature profiles at cold and hot spot were observed in the lower part of each picture along with the heating pattern at the middle layer of food package. Therefore, the developed numeric model can be applied to simulate processes with different case combinations. In addition, with the aid of optimization algorithm, the final temperature of food package fell into the range required for sterilization purpose.

Sensitivity of heating pattern

The numeric model has been employed to investigate the EM patterns at different cavities and the heating patterns for distinct sterilization processes. Another important consideration was the variation of heating patterns due to changing dielectric properties since it is a unique feature for food processing. In our novel MW sterilization technology, MW energy has much more significant effects on heating pattern than surrounding hot water because of the much shorter heating time. For this reason, the heating patterns could be mirrored by EM field patterns with equally distributed heating and sharply reduced simulation time. In this section, three different levels of salt content in meshed

potato shown in Table 6.1 were explored in cavities of case-5 and case-6, respectively.

For the sake of illustration, the meshes for case 5 and case 6 are presented in Fig 6.7.

Table 6.1 Dielectric properties of meshed potato at different salt levels
(Guan, et al., 2004)

Salt content	Dielectric constant (ε')	Loss factor (ε'')
0%	54.5	38.1
0.5%	52.3	68.5
1.0%	48.7	95.2

Fig 6.7 mesh for modelled geometry

Fig 6.8 EM field patterns at the middle layer inside the cavities with meshed potato at different salt contents (Guan, et al., 2004).

In Fig 6.8, the indicated salt level corresponding to the salt concentration of food in consideration, while the e' and e'' are the corresponding dielectric constant and loss factor, respectively. It was observed that the EM distribution does not vary with salt contents, though the intensity does. This favourable feature indicates that the sterilization system has the capability of providing stable heating patterns for the same food packages even if the average temperature is not the same. Fig 6.8 only shows the top view of heating pattern in the middle layer. However, in practice, our interest is focused on the food package in three dimensions (top view, front view, and side view).
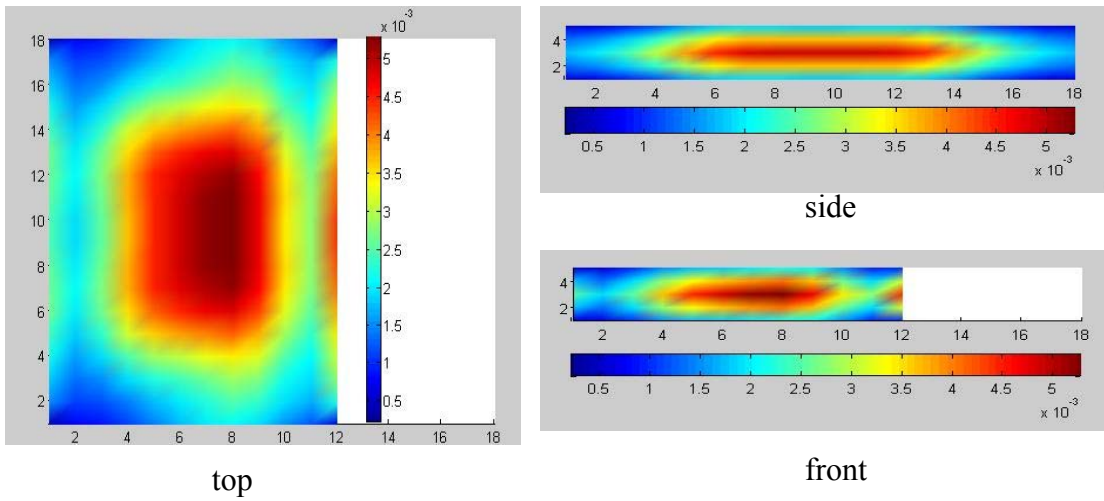
(a) EM distribution (W/m^3) inside a food package in case-5 with 0% salt content.
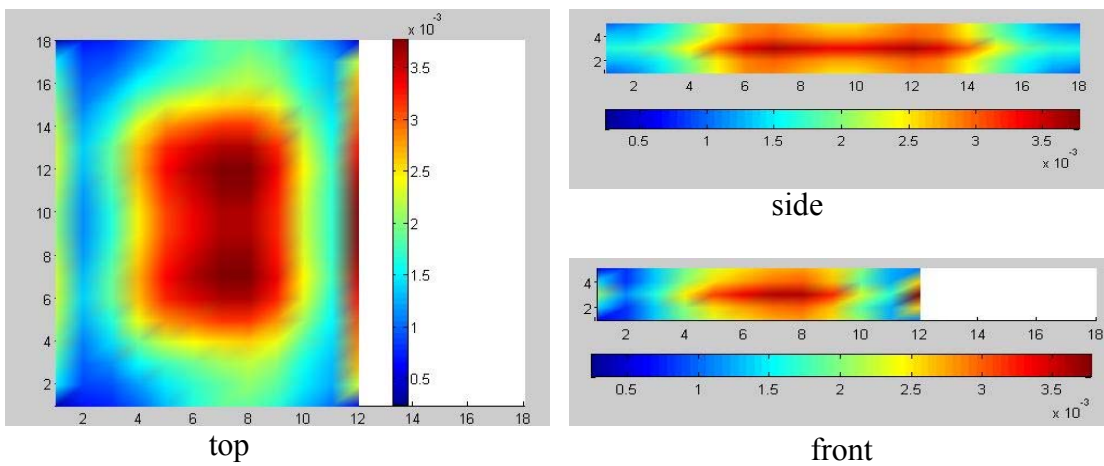
(b) EM distribution (W/m^3) inside a meshed potato in case-5 with 0.5% salt content.
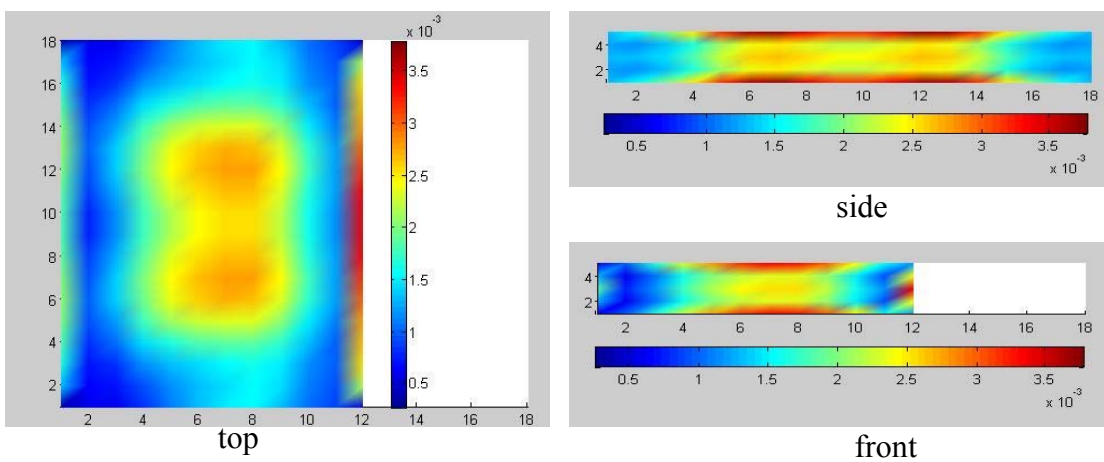
(c) EM distribution (W/m^3) inside a meshed potato in case-5 with 1.0% salt content.
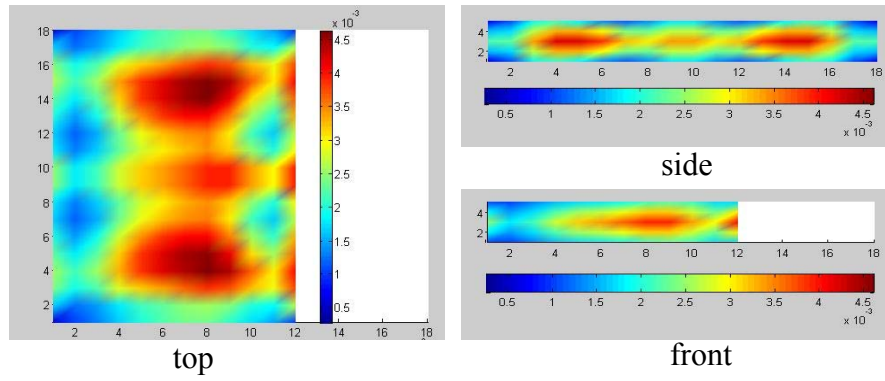
(d) EM distribution (W/m^3) inside a meshed potato in case-6 with 0% salt content.
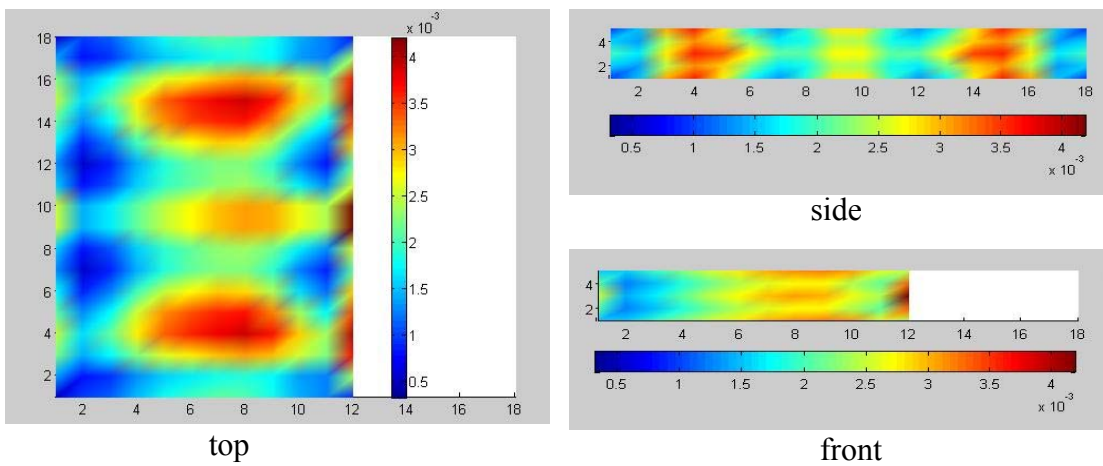
(e) EM distribution (W/m^3) inside a food package in case-6 with 0.5% salt content.
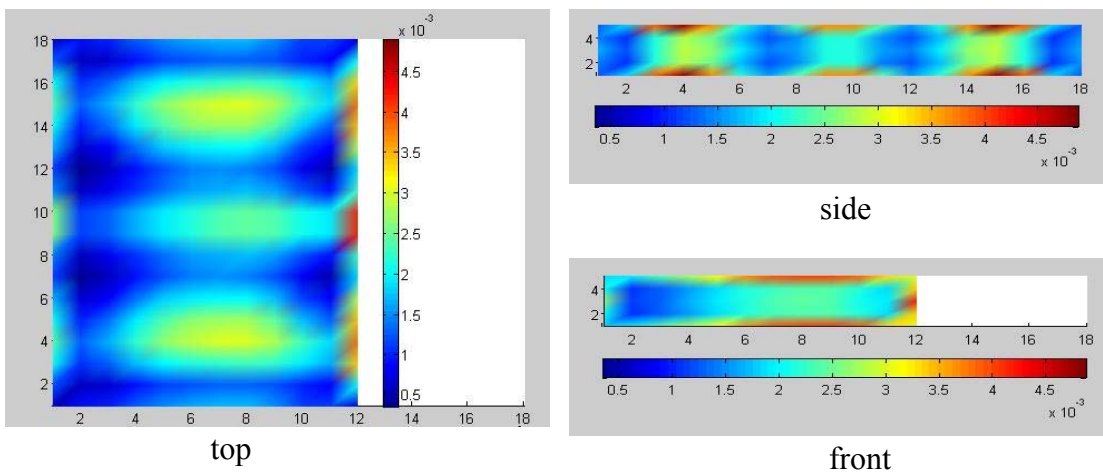
(f) EM distribution (W/m^3) inside a food package in case-6 with 1.0% salt content.

Fig 6.9 3-D heating patterns (top, front, and side) inside a food package

Fig 6.9(a)-(f) show that the EM distribution inside a food package that was selected as the third one from the left shown in Fig 6.7 does not change with the salt content at each of the three directions.

Temperature sensitivity analysis

Another important factor in developing the novel technology of MW sterilization is that the temperature at any point inside food packages can be accurately tracked. Usually in practice, a temperature sensor probe is secured at a pre-selected point to record the temperature evolution during the process. However, due to the unique nature of the solid food as well as the human operation error, it is almost impossible to maintain the probe at the exact same location in every process even if the pre-selected point is fixed. This phenomenon was also shown in Fig 5.8, where simulated temperature profile and two measured temperature profiles at pre-determined cold spot were compared for validation purpose. Though the final temperatures from two repeated tests and that of simulation follow a similar trend, several deviations were observed in the intermediate stages (Fig 5.8). In this section, the numeric model will be utilized to assess the temperature sensitivity by examining the temperatures at the points around a selected cold spot at different time steps. Firstly, we investigated the same case as the one used for validation in Chapter5 (case 5 and case 6), plotting the temperature distributions over distinct planes at different simulation times. Secondly, some cases with four MW cavities are analyzed to provide the temperature sensitivity for the industrial extension of the MW sterilization techniques.

Case1:

In case 1, we investigated the MW sterilization with two MW cavities involved. The details of the system were described in Chapter 5. In this case, the food packages were heated from an initial temperature of 60˚C. The simulated temperature at the cold spot was recorded along with the temperature at its adjacent point that was one cell (8mm) to the left of cold spot.
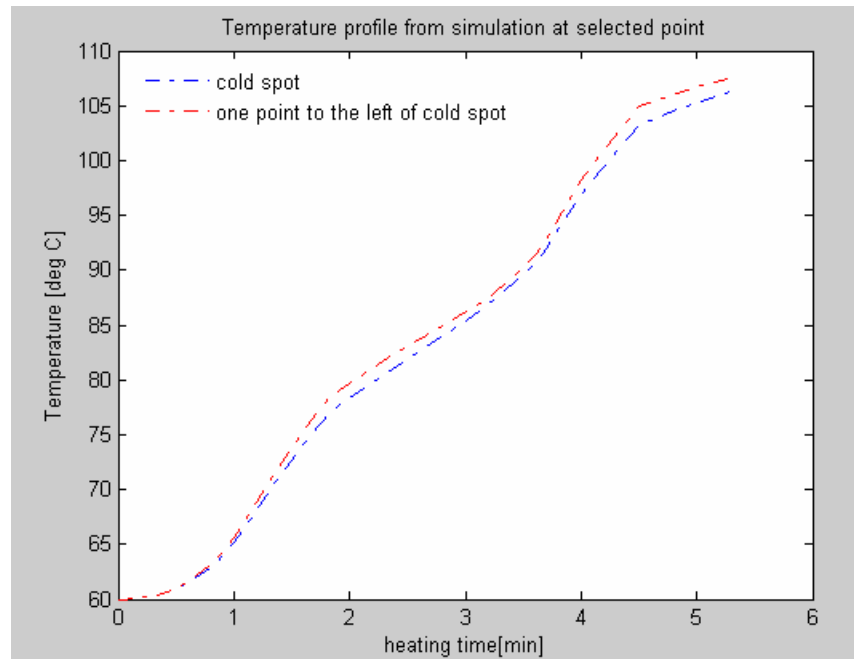
Fig 6.10 Temperature profile at neighbouring points (8 mm apart)

Fig 6.10 shows that the temperature was slightly larger when the temperature probe was accidentally placed 8 mm away from the actual pre-determined cold spot. The index of pre-selected cold spot was at $xc = 10$, $yc = 5$, $zc = 3$. To be able to determine the temperature sensitivity, one neighbouring point is not enough. Therefore, the surface plots over the vertical y-z plane ($x = xc$) were obtained to show temperature changing rate. Besides the final temperature distribution, the intermediate ones were also explored at several different simulation times. These simulation times were selected to represent four

distinct stages, i.e. pre-heating cavity, the first MW cavity, the second MW cavity, and final recorded temperature.

Fig 6.11 Temperature distribution (°C) at a vertical plane x=10 at different simulation time, for two MW heating sections

Fig 6.11 shows the temperature distributions on vertical plane x=10 at simulation time t=100sec, t=150sec, t=270sec, and t=320sec, respectively. With time approaching, more uniform heating was observed in both y and z directions. What is the coordinates for the cold spot? More abrupt changes were presented in z direction (i.e. food thickness), indicating that the temperature measurement is more sensitive to the vertical placement of the probe.

Case 2:

In this case, we assessed the temperature sensitivity in the industrial-extended system with four MW cavities. The combination was case5-case6-case3-case5, with input power to each cavity 16.5KW, 7KW, 5KW, 5KW, respectively. Results were obtained to show the temperature distributions over y-z plane where cold spot was located. As in case 1, the temperature distributions were selected to represent the intermediate statuses during the process, which were the time steps when the food packages received the most MW energy inside each cavity.
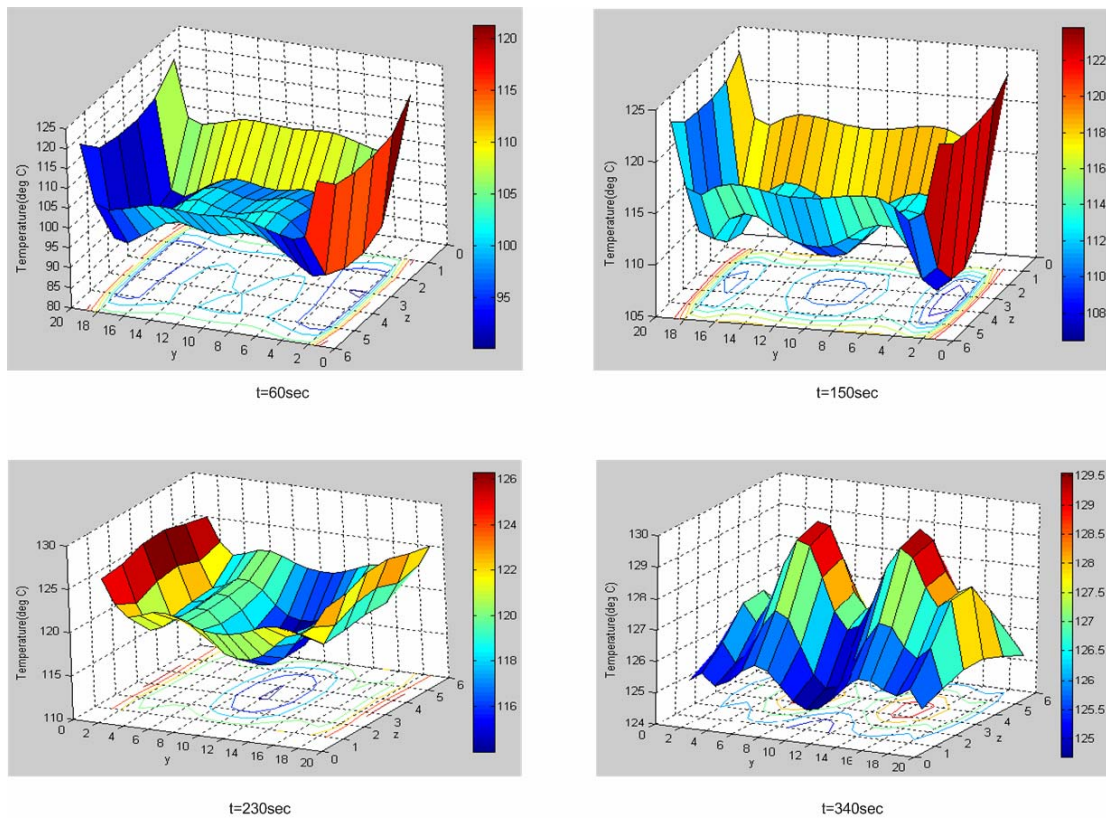
Fig 6.12 Temperature distribution (°C) at a vertical plane x=10 at different simulation time for four MW heating sections

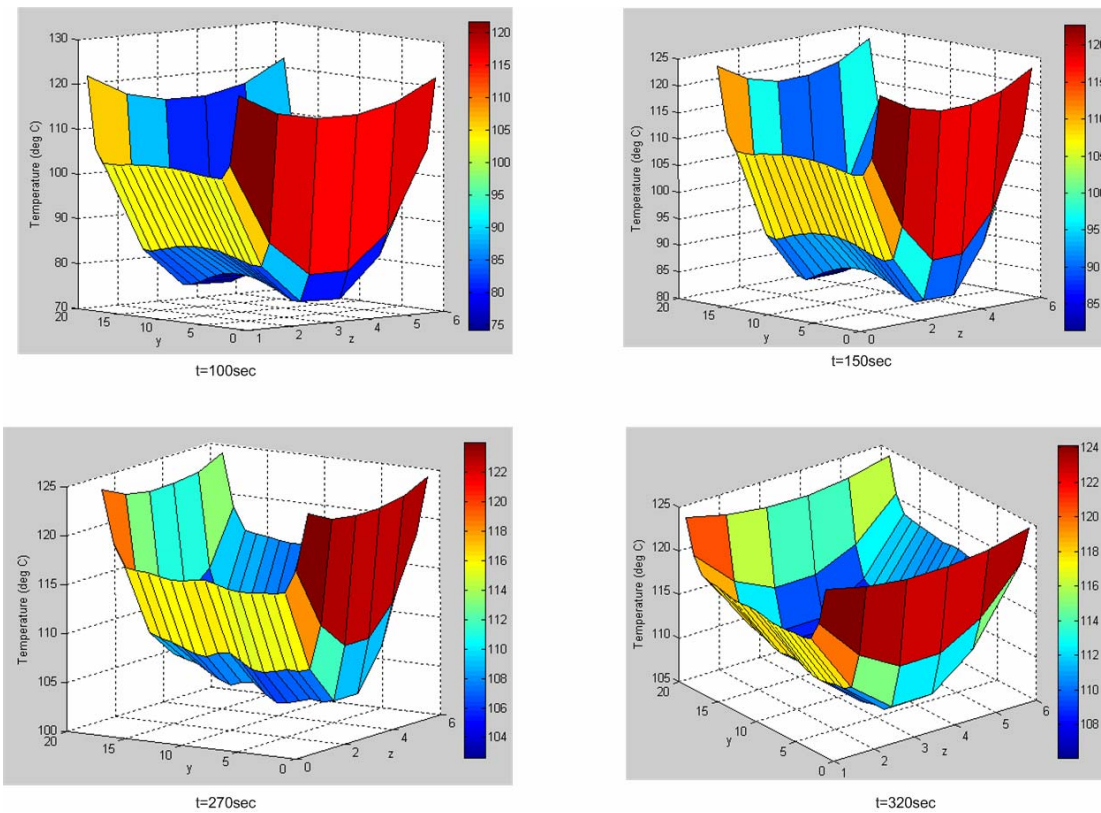Fig 6.12 shows the temperature distributions over the y-z plane when the food package moved to the center of each MW cavity. Steeper change was found along z direction than that found in y direction. It should be noted that the final temperature

174

distribution presented at t=340sec was much smoother than those at previous time steps since the temperature value at any point varied only within small range (<5°C). In this section, the temperature distributions over the vertical surface of y-z plane where the cold spot found to be were obtained to assess the temperature sensitivity to facilitate the validity of optical sensor measurement of temperature value during MW sterilization process. Though not presented here, smooth patterns after MW heating were also found in the x-direction. As a result, there were more abrupt changes along the vertical plane of the food package than the horizontal plane. Because of the difficulty in fixing the measure points for distinct experiments and simulations, the divergence of these recorded values were anticipated especially in intermediate statuses as shown in the model validation in the last chapter.

Conclusions

In this chapter, we investigated several applications using proposed model in previous chapters, including examination of EM patterns under different physical configurations and with different food properties. An optimization algorithm was developed to ensure the temperature of the food package within a specific temperature range required for food safety after process since Food and Drug Association (FDA) requires that the temperature at cold spot be over 121°C. In addition, to facilitate the FDA approval of this novel technology, we have to make sure that the measured temperature at each point inside food package truly reflects the real temperature. This indicates the necessity to investigate the temperature sensitivity inside the package. The temperature sensitivities over the vertical planes where cold spot was located were studied at different simulation times. It was concluded that the temperature gradients are

presented in each of the three coordinator directions, which justifies the observation in the validation process. Since the temperature gradients are smaller in x and y directions than that in z direction, more deviation between experiment and simulation results are expected when the temperature probe was placed higher or lower than the desired location even with a small error. But this error is can not be easily avoidable, because the temperature probe inside the food package is short and the surrounding water makes packages very unstable during the process. In the simulation model, for the sake of simplification, we also assumed the symmetry of the considered geometry, which, however, has small difference from real one. For example, in our simulation , the food package was assumed cuboids with identical surface on the top and bottom. But in practice food packages had a plastic cover on the top and polymetric material on the bottom, which allowed filling pre-selected food followed by a vacuum process. The relatively rigid and thick tray bottom imposed high thermal resistance compare to that of the top thin and flexible lid film. This resulted in the asymmetric heat transfer from surrounding hot water and consequently leads to the deviation between experiment and simulation results.

Only preliminary results about temperature sensitivity were obtained in the current studies. However, because of the importance of temperature sensitivity and the difficulty of accurate measurements and calculation of temperature, —Comprehensive analysis for temperature sensitivity are necessary for future studies.

References

Ayoub, J., Berkowitz, D., Kenyon, E., & Wadsworth, C. (1974). Continuous microwave sterilization of meat in flexible pouches. *Journal of food science* 39, 303-313.

Balanis, C. A. (1982). *Antenna theory: analysis and design*, Wiley, New York,

Balanis, C. A. (1989). *Advanced engineering electromagnetics*, John Wiley & Sons,

Barratt, L., & Simons, D. (1992). Experimental validation of a computer simulation of microwave heating. *in Proc. 27th Microwave Power Symp*, 118-122.

Bows, J., Patrick, M. L., Dibben, D. C., & Metaxas, A. C. (1997). Computer simulation and experimental validation of phase controlled microwave heating. *presented at the 6th Microwave and High Frequency Heating Conference*, Fermo, Italy.

Buffler, C. R. (1993). *Microwave cooking and processing*, Van Nostrand Reinhold, NY. USA.

Burfoot, D., Griffin, W., & James, S. (1988). Microwave pasteurization of prepared meals. *Journal of Food Engineering*, 8, 145-156.

Burfoot, D., Railton, C. J., Foster, A. M., & Reavell, R. (1996). Modelling the pasteurization of prepared meal with microwave at 896MHz. *Journal of Food Engineering*, 30, 117-133.

Campbell, G. S., Calissendorff, C., & Williams, J. H. (1991). Probe for Measuring Soil Specific-Heat Using a Heat-Pulse Method. *Soil Science Society of America Journal*, 55(1), 291-293.

Carson, J. R. (1929). Reciprocal theorems in radio communication. *Proc. IRE*, 17, 952-956.

Chen, H., Tang, J., & Liu, F. (2007a). Coupled simulation of an electromagnetic heating process using the Finite Difference Time Domain method *Journal. of Microwave Power and Electromagnetic Energy*, 41(3), 50-68.

Chen, H., Tang, J., & Liu, F. (2007b). Simulation model for moving food packages in microwave heating processes using conformal FDTD method. *submitted to Journal of Food Engineering*.

Clemens, J., & Saltiel, G. (1995). Numerical modeling of materials processing in microwave furnaces. *International Journal of Heat and Mass Transfer*, 39(8), 1665-1675.

Cook, H. F. (1952). A physical investigation of heat production in human tissues when exposed to microwaves. *Brit. J. Appl. Phys.*, 3, 1-6.

Curtis, J. M. (1999). Experimental verification for microwave processing of materials in a single mode rectangular resonant cavity., Virginia Polytechnic Institute and State University, USA.

DeCareau, R. (1985). *Microwaves in the food processing industry*, Academic press, Inc. NY. USA.

Desmarais, R., & Breuereis, J. (2001). How to select and use the right temperature sensor. *Sensor*, 18(1).

Dibben, D. C., & Metaxas, A. C. (1994a). Experimental verification of a finite element solution to heating problems in a multi-mode cavity. *in Proc. 2nd Int. Conf. Computation in Electromagnetics*, Nottingham, 135-137.

Dibben, D. C., & Metaxas, A. C. (1994b). Finite-Element Time-Domain Analysis of Multimode Applicators Using Edge Elements. *Journal of Microwave Power and Electromagnetic Energy*, 29(4), 242-251.

Eves, E. E., Kopyt, P., & Yakovlev, Y. Y. (2004). Determination of complex permittivity with neural networks and FDTD modeling. *Microwave and Optical Technology Letters*, 40(3), 183-188.

Giese, J. (1992). Advances in microwave food processing. *Food Technol.*, 46, 118-123.

Guan, D. (2003). Thermal processing of hermetically packaged low-acid foods using microwave-circulated water combination (MCWC) heating technology. Ph. D. Dissertation: Washington State University, Pullman, WA, USA. 2003.

Guan, D., Cheng, M., Wang, Y., & Tang, J. (2004). Dielectric properties of mashed potatoes relevant to microwave and radio-frequency pasteurization and sterilization processes. *Journal of Food Science*, 69(1), E30-E37.

Guan, D., Gray, P., Kang, D. H., Tang, J., Shafer, B., Ito, K., Younce, F., & Yang, C. S. (2003). Microbiological validation of microwave-circulated water combination heating technology by inoculated pack studies. *J. Food Sci.*, 68(4), 1428-1432.

Guan, D., Plotka, V., Clark, S., & Tang, J. (2002). Sensory evaluation of microwave treated macaroni and cheese. *Journal of Food Process. Preserv.*, 26, 307-322.

Guru, B. S., & Chen, K. M. (1976). A computer program for calculating the induced EM field inside an irradiated body. *Dept. of Electrical Engineering and System Science*, Michigan State Univ., East Lansing, MI 48824.

Guy, A. W., Lin, J. C., Kramar, P., & Emery, A. F. (1974). Measurement of absorbed power patterns in the head and eyes of rabbits exposed to typical microwave sources. *Proc. 1974 Conf. Precision Electromagnetic Measurements (London, England)*, 255-257.

Gwarek, W. K., Celuch-Marcysiak, M., Sypniewski, M., & Wieckowski, A. (1999). *QuickWave-3D Software Manual*, QWED, Porland.

Harlfinger, L. (1992). Microwave sterilization. *Food Technol.*, 46(12), 57-60.

Harms, P. H., Chen, Y., Mittra, R., & Shimony, Y. (1996). Numerical modeling of microwave heating systems. *Journal of Microwave Power and Electromagnetic Energy*, 31(2), 114-121.

Harms, P. H., Lee, J. F., & Mittra, R. (1992). A Study of the Nonorthogonal Fdtd Method Versus the Conventional Fdtd Technique for Computing Resonant Frequencies of Cylindrical Cavities. *Ieee Transactions on Microwave Theory and Techniques*, 40(4), 741-746.

Harrington, R. F. (1959). On Scattering by large conducting bodies. *IRE Trans. Antennas Propagat*, AP-7(2), 150-153.

Harrington, R. F. (1961). *Time-Harmonic Electromagnetic Fields*, McGraw-Hill, New York.

Harrington, R. F. (1967). Matrix methods for field problems. *Proc. IEEE*, 55(2), 136-149.

Harrington, R. F. (1968). *Field Computation By Moment Methods* Macmillan, New York.

Harrington, R. F. (1992). *Origin and development of the method moments for field computation*, Computational electromagnetics, New York: IEEE Press.

Hayt, W. H., & Kimmerly, J. E. (1978). *Engineering Circuit Analysis*, 3rd ed., McGraw-Hill, New York,

Hilderbrand, F. B. (1962). *Advanced Calculus for Applications*, Prentice-Hall, Englewood Cliffs, N. J.

Holland, R. (1993). Pitfalls of Staircase Meshing. *Ieee Transactions on Electromagnetic Compatibility*, 35(4), 434-439.

Huygens, C. (1690). Traite de la lumiere. Translated into English by Thompson, S. P., London, 1919 and reprinted by the University of Chicago press.

Incropera, F. P., & DeWitt, D. P. (2001). *Introduction to heat transfer, 4th*, John Wiley & Sons, NY, USA.

Jones, D. S. (1964). *The theory of electromagnetism*, New York: Macmillan, pp. 450-452.

Jurgens, T. G., Taflove, A., Umashankar, K., & Moore, T. G. (1992). Finite-Difference Time-Domain Modeling of Curved Surfaces. *IEEE Transactions on Antennas and Propagation*, 40(4), 357-366.

Kalhori, S., Elander, N., Svennebrink, J., & Stone-Elander, S. (2003). A re-entrant cavity for microwave-enhanced chemistry. *J. Microwave Power & Electromagnetic Energy*, 38(2), 125-135.

Kastner, R., & Mittra, R. (1983). A new stacked two-dimensional spectral iterative technique (SIT) for analyzing microwave power deposition in biological media. *IEEE Trans Micro. Theo. Tech.*, MTT-31(1), 898-904.

Kim, H. J., & Taub, I. A. (1993). Intrinsic chemical markers for Aseptic processing of particulate foods. *Food Technol*, 47(1), 91-97.

Kim, H. J., Taub, I. A., Choi, Y. M., & Prakash, A. (1996). Principles and applications of chemical markers of sterility in high-temperature-short-time processing of particular foods, Washington, D.C. 54-69.

Komarov, V. V., & Yakovlev, Y. Y. (2003). Modeling control over determination of dielectric properties by the perturbation technique. *Microwave and Optical Technology Letters*, 39(6), 443-446.

Kong, J. A. (1981). *Research Topics in Electromagnetic Theory*, New York: John Wiley. pp: 290-355.

Kopyt, P., & Celuch-Marcysiak, M. (2003). Coupled electromagnetic and thermal simulation of microwave heating process. *Proc. 2nd Intern. Workshop on Information Technologies and Computing Techniques for the Agro-Food Sector*, Barcelona, November-December, 2003, 51-54.

Kraus, J. D., & Carver, K. R. (1973). Electromagnetics. 464-467. McGraw-Hill, New York.

Kunz, K. S., & Lee, K. M. (1978). A Three-Dimensional Finite-Difference solution of the external response of an aircraft to a complex transient EM environment: part I – the method and its implementation. *IEEE Trans. Electromagnetic Compatibility*, EMC-20(2).

Lau, M. H. (2000). Microwave heating uniformity in model food systems. From *Microwave pasteurization and sterilization of food products*. Ph.D. Dissertation: 2000.

Lau, M. H., Tang, J., Taub, I. A., Yang, T. C. S., Edwards, C. G., & Mao, R. (2003). Kinetics of chemical marker formation in whey protein gels for studying microwave sterilization. *Journal of Food Engineering*, 60(4), 397-405.

Lau, R. W. M., & Sheppard, R. J. (1986). The modelling of biological systems in three dimensions using the time domain finite-difference method: part I. The implementation of the model. *Phys. Med. Biol*, 31(11), 1247-1256.

Leo, R. D., Cerri, G., & Mariani, V. (1991). TLM techniques in microwave ovens analysis: Numerical and experimental results. *in Proc. 1st Int. Conf. Computation in Electromagnetics*, London, 361-364.

Livesay, D. E., & Chen, K. M. (1974). Electromagnetic fields induced inside arbitrary shaped biological bodies. *IEEE Trans Micro. Theo. Tech.*, MTT-22(12), 1273-1280.

Lorenson, C. (1990). The why's and how's of math modeling for microwave heating. *Microwave World*, 11(1), 14-23.

Ma, L. H., Paul, D. L., Pothecary, N., Railton, C., Bows, J., Barratt, L., Mullin, J., & Simons, D. (1995). Experimental Validation of a Combined Electromagnetic and Thermal Fdtd Model of a Microwave-Heating Process. *IEEE Transactions on Microwave Theory and Techniques*, 43(11), 2565-2572.

Madsen, N. K., & Ziolkowski, R. W. (1988). Numeric solution of maxwell's equations in the time domain using irregular nonorthogonal grids. *Wave Motion*, 10, 583-596.

McDonald, B. H., & Wexler, A. (1972). Finite-element solution of unbounded field problems. *IEEE Trans Micro. Theo. Tech.(1972 Symp, Issue)*, MTT-20, 841-847.

Mechenova, V. A., & Yakovlev, Y. Y. (2004). Efficiency optimization for systems and components in microwave power engineering. *J. Microwave Power & Electromagnetic Energy*, 39(1), 46-60.

Meredith, R. (1998). *Engineer's handbook of industrial microwave heating*, The institution of Electrical Engineers, London, UK.

Metaxas, A. C., & Meredith, R. J. (1993). *Industrial Microwave Heating*, London, UK.

Michaelson, S. M. (1969). Biological effects of microwave exposure. *Proc. Biological Effects and Health Implications of Microwave Radiation Symp*, Med. College Virginia (Richmond), Rep. BRH/DBE 70(2), 35-58.

Mittra(Ed.), R. (1973). *Computer Techniques for Electromagnetics*, Pergamon, New York.

Moore, J., & Pizer, R. (1984). *Moment Methods in Electromagnetics*, Wiley, New York.

Mudgett, R., & Schwartzberg, H. G. (1982). Microwave food processing: Pasteurization and sterilization: A review. *AIChe Symposium Series*, 78(218), 1-11.

O'Meara, J., Farkas, D., & Wadsworth, C. (1977). Flexible pouch sterilization using combined microwave-hot water hold simulator. *Contact No. (PN) DRXNM 77-120*, U.S. Army Natick Research & Development Laboratories, Natick, MA.

Ohlsson, T. (1987). Sterilization of foods by microwaves. *International Seminar on New Trends in Aseptic Processing and Packaging of Food stuffs*, 22 Oct. 1987;Munich. SLK Report nr 564. Goteborg, Sweden: The Swedish Institute for Food and Biotechnology.

Ohlsson, T. (1990). Controlling heating uniformity - The key to successful microwave products. *Euro. Food Drink Rev.*, 2, 7-11.

Ohlsson, T. (1991). Microwave heating uniformity. *AICHE Conference on Food Engineering*, Chicago. March 11-12.

Ohlsson, T. (1992). Development and evaluation of microwave sterilization process for plastic pouches. *Paper presented at the AICHE Conference on Food Engineering*, March 11-12, Chicago.

Okoniewski, M. (1993). Vector wave equation 2D-FDTD method for guided wave equation. *IEEE Micro. Guided Wave Lett.*, 3(9), 307-309.

Osepchuck, J. M. (1984). A history of microwave heating applications. *IEEE Trans. Microwave Theory Tech*, MTT-32, 1200-1224.

Palombizio, P., & Yakovlev, Y. Y. (1999). Parallel worlds of microwave modeling and industry: a time to cross? *Microwave World.*, 20(2), 14-19.

Pandit, R. B., Tang, J., Liu, F., & Mikhaylenko, M. (2007a). A computer vision method to locate cold spots in foods in microwave sterilization processes. *Pattern Recognition*, 40, 3667-3676.

Pandit, R. B., Tang, J., Liu, F., & Pitts, M. (2007b). Development of a novel approach to determine heating pattern using computer vision and chemical marker (M-2) yield. *Journal of Food Engineering*, 78(2), 522-528.

Pandit, R. B., Tang, J., Mikhaylenko, G., & Liu, F. (2006). Kinetics of chemical marker M-2 formation in mashed potato - A tool to locate cold spots under microwave sterilization. *Journal of Food Engineering*, 76(3), 353-361.

Paoloni, F. (1989). Calculation of power deposition in a highly overmoded rectangular cavity with dielectric loss. *Journal of Microwave Power and Electromagn. Energy*, 24(1), 21-32.

Pathak, S., Liu, F., & Tang, J. (2003). Finite difference time domain(FDTD) characterization of a single mode applicator. *J. Microwave Power EE*, 38(1), 37-48.

Prakash, A., Kim, H. J., & Taub, I. A. (1997). Assessment of microwave sterilization of foods using intrinsic chemical markers. *Journal of Microwave Power and Electromagnetic Energy*, 32(1), 50-57.

Richmond, J. H. (1965). Digital computer solutions of the rigorous equations for scattering problems. *Proc. IEEE*, 53, 796-804.

Ruello, J. H. (1987). Seafood and microwaves: some preliminary observations. *Food Technol.in Australia.*, 39, 527-530.

Ryynanen, S., & Ohlsson, T. (1996). Microwave heating uniformity of ready meals as affected by placement, composition, and geometry. *Journal of Food Science*, 61(3), 620-624.

Sadiku, M. N. O. (2000). *Numerical Techniques in Electromagnetics*, 2 ed., CRC, NYC.

Sadiku, M. N. O. (2001). *Elements of Electromagnetics*, 3 ed., Oxford University Press, New York.

Schelkunoff, S. A. (1936). Some equivalence theorems of electromagnetics and their application to radiation problems. *Bell System Tech. J.*, 15, 92-112.

Schiffmann, R. (1990). Problems in standardizing microwave over performance. *Microwave World.*, 11(3), 20-24.

Schwan, H. P. (1972). Microwave radiation: biophysical considerations and standards criteria. *IEEE Trans. Biomed. Eng.*, BME-19, 304-312.

Smyth, N. F. (1990). Microwave-Heating of Bodies with Temperature-Dependent Properties. *Wave Motion*, 12(2), 171-186.

Speigel, R. J. (1984). A review of numerical models for predicting the energy deposition and resultant thermal response of humans exposed to electromagnetic fields. *IEEE Trans. Microwave Theory and Techn*, MTT-32, 730-746.

Spiegel, R. J. (1984). A review of numerical models for predicting the energy deposition and resultant thermal response of humans exposed to electromagnetic fields. *IEEE Trans. Microwave Theory and Techn*, MTT-32, 730-746.

Stanford, M. (1990). Microwave oven characterization and implications for food safety in product development. *Microwave World.*, 11(3), 7-9.

Stenstrom, L. (1972). Taming microwaves for solid food sterilization. *IMPI symposium*, Ottawa, Ganada. May 24-26.

Stenstrom, L. (1974). US Patents 3,809,845; 3,814,889.

Taflove, A. (1980). Application of the finite-difference time-domain method to sinusoidal steady-state electromagnetic-penetration problems. *IEEE Trans. EM Comp.*, EMC-22(3), 191-202.

Taflove, A. (1998). Computational electrodynamics : the finite-difference time-domain method, Artech House, Boston.

Taflove, A., & Brodwin, M. E. (1975a). Computation of the Electromagnetic Fields and Induced Temperatures Within a Model of the Microwave-Irradiated Human Eye. *IEEE Trans Micro. Theo. Tech.*, MTT-23(11), 888-896.

Taflove, A., & Brodwin, M. E. (1975b). Numerical solution of steady-state electromagnetic scattering problems using the time-dependent Maxwell's equations. *IEEE Micro. Theo. Tech.*, MTT-23(8), 623-630.

Taflove, A., & Umashankar, K. (1980). A hybrid moment method/finite-difference time-domain approach to electromagnetic coupling and aperture penetration into complex geometries. *IEEE Trans. Ant. Prop.*, AP-30(4), 617-627.

Taflove, A., & Umashankar, K. (1981). Solution of complex electromagnetic penetration and scattering problems in unbounded regions. *Computational methods for infinite domain media-structure interaction*, Washington, D.C: ASME, 46, 83-113.

Taflove, A., & Umashankar, K. (1990). The finite-difference time-domain method for numerical modeling of electromagnetic wave interactions. *Electromagnetics*, 10, 105-126.

Tang, J., Liu, F., Pathak, S., & Eves, G. (2006). Apparatus and method for heating objectives with microwaves. U.S. patent 7,119,313.

Thom, A., & Apelt, C. J. (1961). *Field Computations in Engineering and Physics*, D.Van Nostrand, London.

Torres, F., & Jecko, B. (1997). Complete FDTD analysis of microwave heating processes in frequency-dependent and temperature-dependent media. *IEEE Transactions on Microwave Theory and Techniques*, 45(1), 108-117.

Tsai, L. L. (1978). Moment methods in electromagnetics for undergraduates. *IEEE Trans. on Education*, E-21(1), 14-22.

Umashankar, K., & Taflove, A. (1982). A novel method to analyze electromagnetic scattering of complex objects. *IEEE Trans. EM Comp.*, EMC-24(4), 397-405.

Veronesi, P., Leonelli, C., De Marchi, G., & De Marchi, U. (2003). Microwave assisted drying of water-based paints for wood. In: *Proc. 9th AMPERE Conf. on Microwave and High Frequency Heating, 169-172. Loughborough, U.K.*

Watanabe, W., & Ohkawa, S. (1978). Analysis of power density distribution in microwave ovens. *Journal of Microwave Power and Electromagn. Engergy*, 13(2), 173-182.

Webb, J. P., Maile, G. L., & Ferrari, R. L. (1983). Finite element solution of three dimensional electromagnetic problems. *IEE Proceedings*, 130(2), 153-159.

Wu, T. K., & Tai, L. L. (1974). Numerical analysis of electromagnetic fields in biological tissues. *Proc. IEEE(Lett.)*, 62, 1167-1168.

Wylie, C. R. (1960). *Advanced Engineering Mathematics*, McGraw-Hill, New York.

Yakovlev, Y. Y. (2001). Improving quality of microwave heating by packaging - analytical approach. *The 2001 ASAE Annual Meeting, Sacramento, CA, Paper 01-6149*.

Yakovlev, Y. Y. (2004). Optimization of reflection and transmission characteristics of a waveguide window. In: *Proc. 4th World Congress on Microwave & Radio Frequency Applications, 172-174. Austin, TX.*

Yakovlev, Y. Y., & Murphy, E. K. (2004). FDTD-backed reconstruction of complex permittivity with neural networks. In: *Proc. 6th Seminar "Computer Modeling & Microwave Power Industry", 40-46. Austin, TX.*

Yee, K. S. (1966). Numerical solution of initial boundary-value problems involving Maxwell's equations in isotropic media. *IEEE Trans. Ant. Prop.*, AP-14, 302-307.

Z.Shou-Zheng, & C.Han-Kui (1988). Power distribution analysis in rectangular microwave heating applicator with stratified load. *Journal of Microwave Power and Electromagn. Energy*, 23(3), 139-143.

Zhang, H., & Datta, A. K. (2000). Coupled electromagnetic and termal modeling of microwave oven heating of foods. *Journal of Microwave Power and Electromagnetic Energy*, 35(2), 71-85.

Chapter 7 Conclusions and Future Improvement

MW sterilization technology as an emerging novel technology has a significant improvement over the conventional methods. It sharply reduces the processing time to reach the required temperature level so as to largely retain the quality of the heated food package. The 915 MHz single-mode sterilization technology developed at Washington State University (WSU) uses a combination of hot water and MW heating that improves heating uniformity as well. With this technology, single-mode EM wave is produced and propagated inside the rectangular cavity, which makes it possible to track the heating patterns between processes. However, this High Temperature Short Time (HTST) method suffers from a major difficulty. That is, EM energy is not be evenly distributed inside the food package within a short time, leading to possible sever non-uniform heating without a carefully system design. Though proper physical configurations are desired, it is extremely difficult to make an efficient and reliable system by only conducting experiments, especially for industrial applications. This is because numerous variables influence heating patterns in a microwave system, leading to a large number of combinations need to be considered in the design. The high labor and equipment costs keep industrial companies from making adequate investment in research and development effects.

Owing to the rapid growth of computer industry, high performance computers with affordable prices are available along with the advance computational techniques. In this research, a comprehensive model was developed to simulate the coupled electrodynamic and thermodynamic phenomena using the state-of-art conformal FDTD method. The model was built to simulate heating processes from MW energy and

190

surrounding hot water for stationary and moving packages inside the single-mode MW system composed of a rectangular cavity and two horn waveguides. First of all, the fundamental principles of Maxwell's equations were investigated in analytical approaches. Due to its complexity, the analytical methods can only applied to simple and standard systems. However, it provided justification for pursuing more elaborate numeric approach to obtain the solutions. Following the analytical discussion, several numeric approaches were studied such as FDTD, FEM, and MoM. We then focused on the FDTD method because of its explicit solution approaching, relative simple construction of numeric grids, and elimination of matrix operations. Compared with FEM and MoM, the FDTD technique significantly reduces the simulation time and memory consumption by using an explicit differential equation to solve Maxwell's equations and heat transfer equations with appropriate boundary conditions. In spite of these merit of FDTD method, its application is limited to regular geometries at the time it is initially proposed. The reason is that it is lack of a sophisticate algorithm to correctly model the irregularities. Its application is significantly increased after the conformal FDTD method is developed. The conformal FDTD method solves the integration form of Maxwell's equations over the irregular boundary while keep the traditional FDTD approach valid inside the geometry. Since the discretization of the integration form intrinsically utilizes the Amper's and Gauss's law along the interface, the conformal method adapts to the irregular surface to a large accuracy while the increased computing time and memory usage over the traditional method can be neglected. With the merits of conformal FDTD technique, we applied this method in our study to calculate the EM field components while employing traditional FDTD method to solve the thermal equations. The reason

that we only apply original FDTD algorithm in solving thermal equations is the finite grids used in thermal field inherits from those generated in EM solver, i.e. the mesh generated by conformal FDTD technique. This makes the data transportation between EM solver and thermal solver more straightforward and less computation burdens.

A numeric model is meaningless if it is validated by hard evidence. Usually, the most effective and reliable way to verify a numeric model for industrial application is to compare the simulated results with measured results. In this study, validation was performed by comparing simulated temperature profiles and distributions with measured temperature and heating patterns. The experiment temperatures were measured by placing fiber optical sensors to the hot and cold spots inside the food package during the sterilization process; the heating patterns were obtained from computer vision method which employed chemical marker M-2 to correlate the temperature distribution with color intensity. The model was validated with food packages in both stationary and moving modes.

After validation, several applications were explored by using the model. The applications included evaluating the effects of input powers of each MW cavity on heating uniformities, assessing the influence of the distance between neighboring trays, and studying the effects of different physical configurations and salt contents on EM field patterns. In addition, an optimization scheme was developed to provide proper schedules for MW heating processes. With a reliable simulation platform, numerous schedules could be investigated for system optimization and requirement satisfaction. As an example, the numeric model along with the optimization algorithm was used for a four-cavity system, which was an industrial extension of a two-cavity system. It greatly

benefited in obtaining required schedules and conducting corresponding improvements. Another important application was to use the developed platform to examine the temperature sensitivity around the location where the cold spot was located. Two sets of temperature sensitivity check were presented in Chapter 6, indicating its validity in analyzing the temperature sensitivity for MW heating processes.

For future studies, detailed analysis of temperature sensitivity after process is necessary to facilitate its pursuit of FDA approval. This requires more sophisticate algorithms to study the temperature sensitivity with more constrained criteria. For instance, the temperature at the cold spot is required to be 120˚C with 1˚C accuracy and the temperature sensor allows for ±0.5˚C measured errors. These conditions put more constraints into the follow-up researches. The current model simulates the movement of food packages by taking snapshots at different simulation time. A drawback is that the number of snapshots is limited by the dimension of the cavity in the moving direction (6 here), which essentially provides a lower bound of moving speed that sometimes narrows down its applications. A possible improvement is to dynamically upgrade each cell in the numeric grids and exchange information between data structures in each time step. This would, however, significantly increase its complexity and computing time especially when dealing with thousands of cells. Up to now, a constant velocity of moving packages was assumed, therefore, the model can be improved to adapt to more advanced strategy of having variable speed during the MW heating process. There are two options to set the variable speeds. The first option is to pre-select various speeds based on previous simulation results, which deliberately change the speed at different positions along the moving direction to improve the uniformity with high possibility. The second

option makes the model more automatic. It adopts a strategy that adaptively selects the moving speed based on the latest temperature information. This strategy obviously needs more sophisticate algorithm and hard ware interaction that allows real time information exchange and online monitor.